Variability of Be stars

JASSYR A. SALAS MARTINEZ

Supervisor: Dr. Catalina Arcos (UV)
Internal reviewer: Dr. Maja Vučković (UV)
External reviewer: Dr. Jonathan Labadie-Bartz (PSL)

Tesis para optar al grado de Magíster en Astrofísica
Instituto de Física y Astronomía
Facultad de Ciencias
Universidad de Valparaíso

March 2025
Valparaíso, Chile.

The Night Has A Thousand Eyes

The night has a thousand eyes,
And the day but one;
Yet the light of the bright world dies
With the dying sun.

The mind has a thousand eyes,
And the heart but one:
Yet the light of a whole life dies
When love is done.

Francis William Bourdillon
(22 March 1852 – 13 January 1921)

This thesis is solely my own composition,
except where specifically indicated in the text.

Jassyr Salas Martínez
March 2025
Valparaíso, Chile.

Acknowledgements

The journey I have been through from the beginning of my master's degree to the end has been turbulent, which has taken me through a roller coaster of emotions, a difficult but satisfying journey. Finally, after so many ups and downs, joys and sorrows, I have managed to get to where I wanted to be, culminating my master's degree in astrophysics. To endure this journey would not have been possible without the support of many important people during these years. I want to thank and dedicate this achievement and thesis to all the people who accompanied me during the process.

First of all, I would like to thank my family—my parents, Juan and Sandra and my sister, Maria Camila—for their unconditional support, emotional accompaniment, and motivation to continue. The first year in Chile would not have been possible without them. I also want to thank my pets, Michu and Gotica, who fill me with love and joy.

Thanks to Professor PhD Catalina Arcos for supervising this degree project, for her patience with me, for her motivation, and for trusting me. Besides being an exceptional mentor, Professor Cata has been a personal inspiration. During the process of this thesis, she went through the process of motherhood for the first time, demonstrating to me and increasing my admiration for her ability to balance her responsibilities as a researcher, mentor, and mother with excellence.

Thanks to Prof. Maja Vučković for her support during the frequency analysis section of this thesis. In addition, she provided us with her key ideas, thanks to her experience, which led us to clarify our doubts. She has been a great mentor during this process, being understanding and patient. Her positive attitude, constant willingness to help, and confidence in my ability motivated me to persevere.

Finally, I would like to thank my friends Daysi and Diego, with whom I shared the experience of living for the first time in a different country. They taught me about their passion for research, which motivated me not to give up. They also supported me when I felt alone as a foreigner and far away from my family. I would also like to thank to José Tobias and Nicole Iglesias for being such close friends, you have helped me a lot with your support, home, food and office, among other things, and most important companionship during these months of work, you don't know how special it has been for me.

Finally, thanks Cat for being by my side during the long hours of work, for your sweet words and talks in the late nights and offer me your support and affection, thank you for being there ¡Te quiero!.

This work received financial support from FONDECYT No. 1211941 and is in the frame of FONDECYT N1230131. This thesis was possible thanks to the financial support of the IP Postgraduate Fellowship in Astrophysics. We would also like to thank PhD Jonathan Labadie-Bartz for extending his Be star list from TESS at the start of this research.

Abstract

This study explores the interplay between non-radial pulsations (NRPs) and the formation and variability of circumstellar discs in Be stars through a combined photometric and spectroscopic analysis. NRPs are hypothesized to play a critical role in the ejection of stellar mass during outbursts, significantly influencing disc formation and variability, particularly in emission lines such as Hα and in photometric behaviour. By integrating photometric data from the TESS space telescope with spectroscopic data from the BeSS database, this thesis investigates the hypothesized correlations between NRPs and circumstellar disc dynamics. While no clear correlation was found between NRP influencing the creation and dissipation of the disc (as probed by Hα emission), on the other hand, we found that stars with higher NRP amplitude do not necessarily relate to host stronger discs. Highlighting the complexity of Be star systems and the need for multi-wavelength studies to unravel their variability.

The analysis encompassed 134 Be stars, with over 220 TESS light curves and 560 Hα spectra collected. Spectroscopic data were synchronized with TESS observations to enable simultaneous analysis of light curves and spectral variability. Stellar parameters, including effective temperature (T_{eff}), surface gravity ($\log g$), and rotational velocity ($v \sin i$), among others, were catalogued. Light curves were extracted and processed using the Python package `lightkurve`.

Frequency analysis was conducted using the Lomb-Scargle method, producing periodograms for each star to identify characteristic frequencies. A focused study on six Be stars (f01 Cyg, HD 45314, HD 110432, HD 120991, HD 174237, and ζ Tauri) was performed due to their pronounced circumstellar disc features, variability in light curves and spectra, and their classification as γ Cassiopeiae analogues.

These stars, primarily early-type Be stars (B0-B2), exhibited g-mode pulsations with frequencies ranging between 0.8 and 4 d^{-1}, alongside complex pulsational behaviour. Notably, HD 110432 demonstrated a unique single p-mode pulsation, while HD 45314, an Oe star, displayed distinctive characteristics. Orbital periods were recovered for the two binary systems f01 Cyg and HD 174237. For f01 Cyg, the disc's radial extent was estimated at $\sim 15, R_{\odot}$, well within the Roche limit ($\sim 40, R_{\odot}$). HD 120991 exhibited high-intensity emission, which was

attributed to an outburst, with periodic V/R ratio variations detected during emission peaks. In HD 110432, amplitude variations in pulsational frequencies were interpreted as early signs of a future outburst. However, no definitive correlation was found between NRPs and Hα line variability (formation or dissipation of the Be star disc), highlighting the need for high-resolution, high-cadence spectroscopic observations, and also the highly complex nature of these kinds of stars.

The results contribute to a broader understanding of Be star variability and disc dynamics. It highlights the potential of combining photometric and spectroscopic datasets to unravel short-term variability patterns, thereby advancing the study of disc formation and dissipation processes.

Contents

CHAPTER 1

Introduction

1.1 Be stars

Classical Be stars are the main sequence B-type stars that have or have had emission lines (”e” stands for emission) in their spectrum. They were discovered when Father A. Secchi (Secchi, 1866) made an observation of γ Cas and noted that Hβ was brighter than the rest of the spectrum. It was not until 1931 that a clear definition and a first mechanism were proposed for the origin of the emission lines: ”... a nebulous ring revolving around the star” (Struve, 1931). Later on, the now widely used classical definition of Be stars was suggested: The emission lines present in the Be stars spectrum are formed due to material ejected from the central star, which is in fast rotation. This material creates a geometrically thin Keplerian rotation decretion disc made of gas that lies along the equator (Rivinius et al., 2013).

The central stars are some of the fastest rotating non-degenerate stars, spinning at or near the critical (break-up) velocity (Townsend et al., 2004). Fast rotation impacts several key aspects of physical properties. It causes geometric deformation and gravity darkening and alters the stellar internal structure and pulsational characteristics. Moreover, it plays an important role in the formation of circumstellar discs and significantly influences the structure of stellar winds. The origin of their rapid rotation remains unclear, and it is not yet definitively known how close classical Be stars actually come to reaching their critical rotational speed. It is believed that Be stars are products of binary evolution, where the secondary transfer angular momentum to the *future* Be star, thus causing its fast rotation (Gies et al., 2000). Recent studies suggest that all Be

stars may belong to binary systems, although there is still insufficient evidence to confirm this hypothesis (Oudmaijer & Parr, 2010; Klement et al., 2019).

As it has been introduced, Be stars are known by their emission lines originating from their disc. So far, they are the only stars known to contain decretion discs. The mechanism by which these discs are formed is still under discussion, and it is the main question regarding Be stars. In the following, the main observational features will be described, as well as the hypothesis that supports the study of this thesis.

1.2 Observational features of Be stars

1.2.1 Spectral Energy Distribution

The spectral energy distribution (SED) shows the energy as a function of light frequency or wavelength. Figure 1.1, taken from Touhami et al. (2010), shows the SED observations from 0.4 to 4.2 μm of the Be star η Tau. The figure plots observations taken in 2006 (black points) and 2008 (grey points), and the best Kurucz model reproducing the SED (solid line). An increase in the flux at shorter wavelengths can be spotted, which is consistent with the variability of η Tau. The SED helps to identify the excess infrared emission, which indicates the presence of a cold material surrounding the host star. Typically, it is a technique used in young stars, which are surrounded by protoplanetary discs (accretion discs). For Be stars, the SED also permits the identification of the decretion material ejected by the star.

The contribution of the disc to the continuum is the result of the inner and outer regions of the disc. The inner region is considered radially opaque to radiation in the continuum, while the outer region is optically thin.

The size of the inner region called the pseudo-photosphere, is dependent on wavelength and the gas density (Carciofi & Bjorkman, 2008). The effect on the SED of the inner or outer region will depend on the disc viewing angle:

- From pole-on angles, the SED will be the superposition of the stellar continuum with an excess in the near-infrared
- From edge-on angles, the disc may absorb and scatter the light coming from the star. Leading to an IR excess dominated by cooler outer layers.

The size at different wavelengths of the pseudo-photosphere, as mentioned, is dependent on the wavelength and the gas density. For a low gas density (10^{-11} g cm^{-3}) 80% of the total flux is formed at $\sim 2R_*$ (bands V, H, and K) and for the $60\mu m$ is formed at $\sim 5R_*$. In the dense

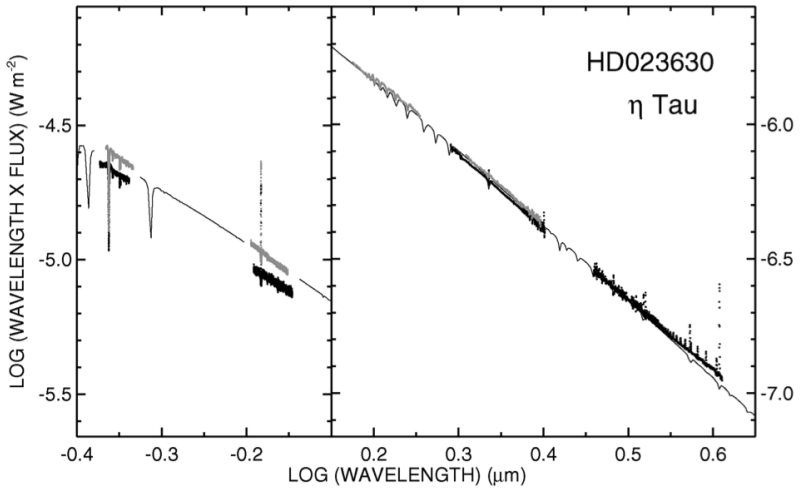

Figure 1.1: Observational change in the SED of η Tau from Touhami et al. (2010). Data are taken in 2006 (black points) and 2008 (grey points). The solid line represents the best Kurucz model that predicted the stellar SED.

case ($10^{-10}\,\mathrm{g\,cm^{-3}}$), the values grow to $4R_*$ (bands V, H, and K), and for the $60\,\mu m$ band to $15R_*$ (Rivinius et al., 2013). In other words, the pseudo-photosphere in the continuum is larger at longer wavelengths.

1.2.2 Spectral Lines

Observations of Be stars have shown different shapes of Balmer emission lines. The features presented in each emission line can help describe the disc or give information about the inclination angle of the system. Figure 1.2 helps to demonstrate this idea. When the star is seen from the pole (pole-on), Hα has a single peak, whereas for higher inclination angles (edge-on), the representative double peak emission for Be star discs starts to appear. Line formation in Be stars envelopes was well studied by Hummel (1994). Generating synthetic Hα line profiles based on 3D simulations of radiate transfer calculations in an optically thin gas ($10^{-12}\,\mathrm{g\,cm^{-3}}$), they conclude that the so-called "wine-bottle" (A type example in the figure) and the shell profiles (D type example in the figure) can be explained by the same Keplerian disc viewed from different inclination angles *i* (see Table 1.1).

The majority of information about Be stars comes from spectroscopic analysis. Spectral lines that characterize Be stars can form in the stellar atmosphere (absorption) and in the disc (emission).

If the Be star is in an active phase (disc), the spectrum will present Balmer lines in emission

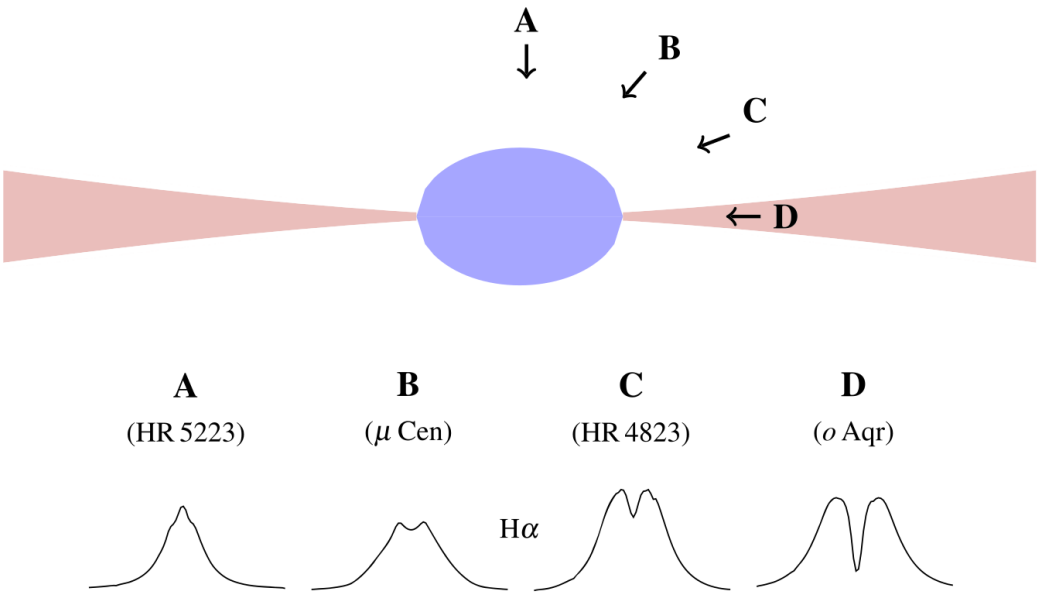

Figure 1.2: Schematic view of Hα emission lines from different sights of view (Rivinius et al., 2013).

[1]. These lines are used to derive several properties of the disc, such as disc mass and size and disc variability. From absorption lines (star), the stellar mass, effective temperature, stellar rotation and radial velocities are usually obtained. Typical measurements from spectral lines are: equivalent width (EW), double peak separation (DPS), violet-to-red (V/R) variations, intensity of the line and radial velocity (RV)

EW measures the strength of a spectral line, representing the area the line covers relative to the continuum. A more negative EW in emission lines indicates a larger disc. The DPS measures the velocity difference between these peaks and is related to the disk's rotation and size. V/R variations describe asymmetries in the two peaks of a double-peaked emission line, often linked to disk density variations. The intensity of the emission line refers to its peak height above the continuum, reflecting the amount of emitted radiation. Lastly, the radial velocity indicates the motion of the emitting material along the line of sight, disk dynamics and binarity.

These measurements help characterize the properties and behaviour of Be star discs, offering insights into their dynamics and interactions:

- Equivalent Width (EW): For emission lines, it is related to the mass of the disc. Larger values of EW indicate a more massive disc. By convention, negative signs are used for emission.

[1] Sometimes, even metallic lines are also in the emission, since it will depend on temperature and place of the line formation.

- Double-Peak Separation (DPS): Emission lines in the spectrum could be split into two peaks. The separation of the peaks is related to the disc rotation. The DPS is correlated with the projected stellar rotational velocity, $v \sin i$. This separation can vary depending on the size of the disc. Specifically, larger, well-developed discs, as well as those that are more evolved, typically exhibit smaller separations compared to smaller, newly-formed discs, which tend to have larger separations.

- Violet to Red peak intensity variation (V/R): When the disc suffers some kind of perturbation, the DPS becomes asymmetric, because there exists an over-density in one part of the disc. Some of these asymmetries are cyclic and could be the product of density waves due to tidal forces of an orbiting companion (Miroshnichenko et al., 2023) or they follow a one-armed density wave which does not require a companion (Okazaki, 1997).

- Intensity of the line (I): It is normally related to disc formation/dissipation, occurring in the order of months or years.

- Radial velocity (RV) variation: The RV variation is the result of a possible companion. The shift between the wavelength of the spectral line and the theoretical value measures it.

Studying the emission lines of Be stars can provide good information about the orbital parameters of the disc, and hence the star. As studied by Sigut et al. (2020), the inclination angle can be determined by fitting the Hα line profile. In their work, a sample of 11 Be stars with interferometric data was studied. The authors simulated their Hα emission lines by implementing the `Bedisk` and `Beray` codes Sigut (2018). Comparing observation with synthetic data, they reliably obtained inclination angles within $\pm 10^{\circ}$.

These kinds of studies continue to this day. The work of Lailey & Sigut (2024) uses machine learning algorithms trained with synthetic Hα emission lines generated via `Bedisk` and `Beray` suite codes to precisely estimate inclination angles. The method was tested on 92 Be stars, obtaining an error of $\pm 7.6^{\circ}$, which is comparable with line profile fitting. The best algorithm of this study was a neural network with regression, surpassing neural networks with classification and support vector regression.

1.2.3 Stellar wind

Stellar winds in Be stars are fundamental for understanding their mass-loss mechanisms and the formation and evolution of their circumstellar discs. These stars exhibit rapid rotation and are

	Optically thin gas ($10^{-12}\,\mathrm{g\,cm^{-3}}$)	Optically thick gas ($10^{-10}\,\mathrm{g\,cm^{-3}}$)
$i = 0°$		One peak
$i < 5°$	Double peak (NSB)	
$5° < i < 30°$	Wine-bottle shape	
$10° < i < 75°$		Double-peak
$i < 75°$	double-peaked+central depression	Shell

Table 1.1: Features observed at different inclination angles Hummel (1994).

characterized by line-driven winds, where radiation pressure acting on metal ions accelerates the wind. This mechanism distinguishes them from normal B-type stars and significantly influences their circumstellar environments.

The most widely accepted explanation for the line-driven wind phenomenon is the CAK theory (Castor et al., 1975), later extended to the mCAK theory (Friend & Abbott, 1986) to incorporate the effects of stellar rotation. This refinement is particularly useful for Be stars, as rotation introduces deviations from spherical symmetry.

Rotation impacts the physics and diagnostics of line-driven winds in three significant ways: (i) it modifies the dynamics of the wind, (ii) it alters the interpretation of mass-loss rates ($\dot{M}$), and (iii) it induces line-profile variability due to interactions between photospheric disturbances (e.g., stellar spots or non-radial pulsations), rotation, and wind dynamics.

Observationally, Be star winds display velocities ranging from 500 to 2000 km s^{-1}, as demonstrated by interferometric studies of Achernar (Kervella & de Souza, 2006; Meilland et al., 2007). The regions above and below the circumstellar disc (polar latitudes) resemble the winds of non-emission B-type stars governed by the same radiative processes.

The relationship between rotational velocity $v \sin i$ and stellar wind features was explored by Grady et al. (1987, 1989) using archival data from the International Ultraviolet Explorer (IUE). Their findings indicate:

- Low $v \sin i$ Be stars (≤ 150 km s^{-1}) exhibit winds similar to non-Be stars.
- Intermediate to high $v \sin i$ Be stars exhibit stronger winds, particularly during active Be phases.

The interaction between stellar winds and circumstellar discs in Be stars has been extensively studied, both observationally and theoretically. The Wind-Compressed disc (WCD) model (Bjorkman & Cassinelli, 1993) proposed that rapid stellar rotation compresses stellar winds into the equatorial plane, facilitating disc formation. However, a more in-depth theoretical analysis

revealed that the WCD model is likely not a feasible explanation for Be disk formation (Owocki et al., 1996). This model was later surpassed by the Viscous Decretion disc (VDD) theory (Lee et al., 1991), which attributes the persistence and evolution of Be star discs to viscous forces and mass ejection mechanisms.

One notable example of such theoretical and observational advances is the Be star ζ Tauri. Štefl et al. (2009) compiled observational data spanning 1991 to 2007, concluding that its disc parameters remained largely unchanged over time. Further modelling by Carciofi et al. (2009), using disc density and inclination angle, successfully reproduced the star's SED across the visible to the far-infrared range, its linear polarization, and the spectral line profiles of hydrogen lines. This study provides strong evidence that the VDD scenario is the mechanism responsible for the formation of ζ Tau's circumstellar disc.

This body of research underscores the importance of integrating theoretical frameworks with multi-wavelength observations to unravel the complex interplay between stellar winds and discs in Be stars.

1.2.4 Variability

Variability in Be stars is a defining characteristic of this class of stars, arising from the dynamic and complex interactions between the star and its circumstellar disc. These variations manifest across a wide range of timescales, from days to months and even years, each linked to distinct physical phenomena. Observationally, these changes are most commonly detected through photometric fluctuations, which reveal changes in brightness or colour, and spectroscopic studies, which highlight variations in emission and absorption line profiles.

When a Be star is observed during different epochs, the variability will be present in the photometry through flux changes due to the appearance or disappearance of the disc, the appearance of a sudden and temporary increase in a star's brightness, called outburst, often accompanied by enhanced mass loss or structural changes in its surrounding material; the passage of a binary companion, or the presence of non-radial pulsations. In spectroscopy, the variability is visible in the changes of V/R intensity peaks, intensity of the emission line, and/or the shape of the line profile, etc. Figure 1.3 shows an example of long-term variation in the Be star ψ^{09} Aur, where the disc almost dissipates in around 3 years, from 2020 to 2023. Long-term variability is primarily associated with changes in the circumstellar disc, such as its formation and dissipation, which significantly impact the total light emitted by the star. Short-term variability ($\sim$ hours to days) often arises from phenomena such as outbursts or mass ejections from the star, which temporarily strengthen emission lines as material is expelled into

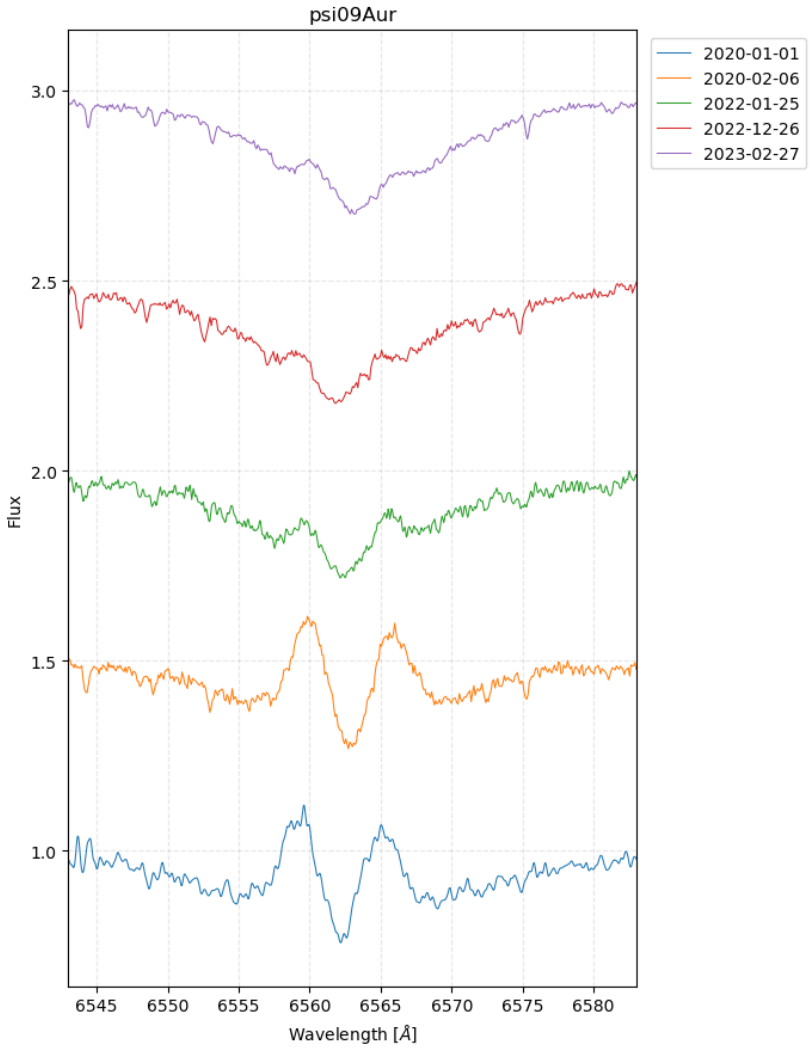

Figure 1.3: Example of a long-term variation. Spectroscopic observations of the Be star ψ^{09} Aur (B8IIIe) from 2020 to 2023. The gradual dissipation of the shell profile suggests the dispersal or reconfiguration of the circumstellar disc.

the circumstellar environment.

Additionally, the disc can exhibit warping or tilting due to external torques, such as gravitational interactions with a binary companion, further influencing its observable properties over extended periods. Table 1.2 summarizes the information about the variability of Be stars and also includes the most common method of observation.

Variability provides clues about the physical phenomena occurring in the star and in the surrounding material. Since Be stars are highly variable stars, they are the subject of active research. Their possible variable origins are in the stellar wind and mass-loss mechanisms, disc dynamics and interactions in binary systems, and non-radial pulsations. Be stars are of

Variation Type	Timescale	Observation Method	Possible Origin
Non-radial pulsations	Hours to days	Photometry, spectroscopy	Surface oscillations
Rotational modulation	Days	Photometry, spectroscopy	Surface spots or inhomogeneities
Outbursts	Days to weeks	Photometry, spectroscopy	Sudden mass ejection
disc formation/dissipation	Months to years	Spectroscopy, photometry, polarimetry	Episodic mass-loss events
Density waves in the disc	Months to years	Spectroscopy	disc instabilities
Binary-induced variations	Days to years	Radial velocity, photometry, X-ray	Gravitational or mass transfer effects
disc precession	Months to years	Polarimetry, spectroscopy	disc warping due to torques
Long-term brightness changes	Years	Photometry	disc density or inclination angle changes

Table 1.2: Different types of variability in Be stars, with their corresponding timescale and possible origins

complex variability nature, highlighting the need for diverse observational techniques that examine different aspects of the star (e.g. photometry for stellar pulsation, and spectroscopy for disk activity, among others).

1.3 Motivation

Several studies have focused on identifying binarity in individual Be stars (Juza et al., 1991; Koubskỳ et al., 2000), a group of Be stars (Miroshnichenko et al., 2023), line formation in Be stars (Hummel, 1994; Arias et al., 2006), the dynamics or characterization of the disc (Carciofi, 2010; Klement et al., 2017), catalogue or classification (Arcos et al., 2017, 2018; Jagadeesh

et al., 2021; Labadie-Bartz et al., 2022; Naze & Robrade, 2023) and line profiles (Apparao & Tarafdar, 1989; Dachs et al., 1992; Hummel & Dachs, 1992). However, as of the date this document is being written, no published studies have done a statistical correlation between pulsations and disc formation on a sample of Be stars.

The motivation for this study stems from a lack of investigations into correlations between the two characteristic phenomena of Be stars: disc formation/dissipation and non-radial pulsations. Previous efforts have already been made to analyze these observations individually. On the one hand, spectroscopic observations provide information about the structure and composition of the disc (disc dynamics as a key factor in the formation and evolution of the characteristic Be star environment), while on the other hand, photometric observations give information about the light variations of the star+disc (pulsations as a driver of variability and mass ejection). Understanding the relationship between these two phenomena is intended to further our understanding of the variability and disc formation/dissipation surrounding Be stars.

By exploring this intersection of knowledge and studies, this work bridges the gap between stellar interior physics and circumstellar environment studies by presenting the study of light curves and spectra of Be stars with the objective of obtaining a possible correlation between the variability in the light curves and the presence of discs, which is determined by the spectrum of the star. The organization of this thesis is as follows: Chapter 2 contains the theory about pulsations and the VDD model. Chapter 3 describes the origin of the sample, the specifications of the telescope with which they were observed, and also the selection of the targets that will later be analyzed. Chapter 4 consists of a theoretical description of the generalized Lomb-Scargle periodogram and the selection criteria of the predominant frequencies in the mentioned periodogram. In addition, the implementation of the methods code is detailed. Chapter 5 presents the results of a sub-sample of 6 stars, representative of our whole sample, while in Chapter 6, the results are discussed. Finally, in Chapter 7, the conclusions of this work are presented.

CHAPTER 2

Theoretical Framework

Having already discussed the context of Be stars and their observables, this Chapter will describe the stellar pulsations that give rise to the mass transport in the stellar interior, which might lead to the characteristic disc of Be stars. The physical dynamics between the disc and stellar pulsations is a complex phenomenon. Pulsations may enhance or suppress mass ejection episodes, influencing the disc's evolution over time.

This chapter will describe the observations and theoretical description of the non-radial pulsations in Be stars. It will also provide a theoretical explanation of the disc's density and structure and how they relate to current observations.

2.1 Pulsations in Be stars

Stellar pulsations are periodic expansions and contractions of a star's outer layers, driven by instabilities between internal forces such as pressure and gravity. These oscillations provide valuable insight into the internal structure and dynamics of stars, revealing details about their composition, temperature, and evolutionary state. Stellar pulsations are often studied in spherical coordinates (r, θ, ϕ), with the oscillatory modes mathematically described by spherical harmonics. These modes are characterized by three quantum numbers: the radial order (n), which denotes the number of nodes in the radial direction; the degree of the node (l), representing the number of nodes on the stellar surface; and the azimuthal order (m), indicating the number of nodes in the azimuthal direction.

Stellar pulsations can be broadly categorized into two types: radial pulsations (RP) and non-radial pulsations (NRP). Radial pulsations involve a spherically symmetric expansion and contraction, where the entire star oscillates uniformly, maintaining its spherical shape $(l = 0)$. This is the most straightforward pulsation mode and is commonly observed in classical variable stars such as Cepheid variables and RR Lyrae stars. In contrast, NRP occurs when $l \neq 0$, leading to more complex oscillation patterns. The simplest non-radial mode is the axisymmetric dipole mode $(l = 1, m = 0)$, where one hemisphere of the star contracts while the other expands, with the node located along the equator. The most frequently observed modes in Be stars are sectoral NRP, where $l = |m|$ (Rivinius et al., 2001), (Rivinius et al., 2003). These modes, often referred to as "sectoral", can be visualized by imagining a peeled orange: an $m = 1$ sectoral mode would resemble an orange divided into two slices, while an $m = 2$ mode would have four slices, and so on.

The oscillatory behaviour of stars can be described by two primary solutions to the equation of motion: pressure modes (p-modes) and gravity modes (g-modes). For p-modes, pressure is the restoring force for perturbations, dominating at higher frequencies and involving oscillations primarily in the outer stellar layers. In contrast, g-modes are driven by buoyancy, which serves as the restoring force and are prominent at lower frequencies. In Be stars, gravity modes typically dominate within the frequency range of 0.5 to 2 d^{-1} (Rivinius et al., 2013).

The first evidence of NRPs in Be stars was reported by Baade (1982a,b), who observed complex line profile variations in the star ω CMa. Subsequent studies, such as Rivinius et al. (2003), identified that most early-type Be stars exhibit low-order g-mode pulsations, which are responsible for much of the observed variability. More recently, Labadie-Bartz et al. (2022) analyzed a sample of ~ 400 Be stars and confirmed the prevalence of non-radial pulsations in this class. Nearly every system studied displayed multiple periodic signals within the frequency range of 0.5 to 4 d^{-1}, emphasizing the widespread presence of g-modes in Be stars.

During outbursts in Be stars, additional frequencies emerge alongside the persistent g-mode frequencies. These new frequencies are broader and less defined, while the original g-modes weaken. Studies by Huat et al. (2009) and Balona (2012) suggest that these transient frequencies may have a circumstellar origin, potentially arising from short-lived cyclic events.

Stellar pulsations in Be stars provide a window to study the mass transport in the stellar interior. Stellar oscillations can give us a hint at the origin of the Be phenomenon. Since the advent of satellite photometry, this area has continuously advanced, generating new questions that will deepen our understanding of star structures.

2.2 Viscous Decretion Discs

The Viscous Decretion disc (VDD) model is the most accepted theory of disc growth. While fast stellar rotation lowers the effective gravity near the stellar equator, a second mechanism, likely stellar pulsation, is responsible for pushing the near-equatorial matter into orbit in the inner disc. Once in orbit, a viscous mechanism occurs, diffusing matter and angular momentum outwards, making the disc grow.

The geometry of the decretion disc in Be stars is typically considered as an elongated and thin disc in hydrostatic equilibrium (Figure 2.1). It is described in a cylindrical reference frame (r, ϕ, z), where r is the radial distance from the rotation axis, ϕ is the azimuthal angle, and z is the height above the equatorial plane of the disc. Theoretically, the structure of a geometrically thin disc follows from considering the vertical force equilibrium at a height z above the midplane in a disc orbiting at cylindrical radius r around a star of mass M.

The gravitational potential for a thin disc $(r \ll z)$ is approximated as

$$\phi \approx -\frac{GM}{r^2} + \frac{1}{2}\Omega_k^2 z, \tag{2.1}$$

where $\Omega_k = \sqrt{\frac{GM}{r^3}}$ is Keplerian angular velocity. The first term is the dominant gravitational potential generated by the central star. At the same time, the second approximates the gravitational potential contribution outside the equatorial plane, i.e., in the vertical direction (z).

The disc is in hydrostatic equilibrium in the vertical direction. The gravitational force of the disc must balance the pressure generated by the gas. The hydrostatic equilibrium equation is

$$\frac{1}{\rho}\frac{dP}{dz} = -\frac{d\phi}{dz}$$

Assuming an isothermal gas, the pressure is given by $P = c_s^2 \rho$, where c_s is the sound velocity of the medium and ρ is the density of the gas. Replacing the pressure and the gravitational potential in the hydrostatic equation, we get

$$\frac{c_s^2}{\rho}\frac{d\rho}{dz} = -\Omega_k^2 z, \tag{2.2}$$

which has the solution

$$\rho(r,z) = \rho_0 r^{-n} \exp\left[-\frac{z^2}{2H^2}\right], \tag{2.3}$$

where H is the scale height of the disc given by $H(r) = \frac{c_s}{\Omega_k} = \frac{c_s}{\sqrt{GM}} r^{3/2}$ and ρ_0 is the density at $z = 0$. This is the density profile of the disc, which decreases outwards due to mass and angular momentum transport, being denser in inner regions. The scale height H grows with the

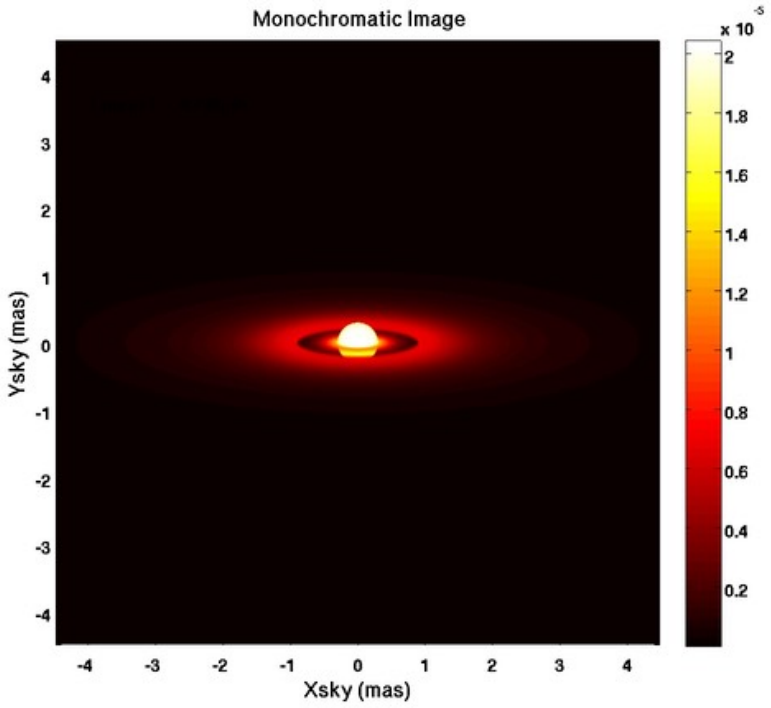

Figure 2.1: Be star representation. A theoretical image is seen at a wavelength of about 5 μm. (Image taken from from `http://astro.uwo.ca/ asigut/`. Generated using `BEDISK/BERAY` codes.

distance, creating what is known as a "flaring disc" with an opening angle. This equation shows that the density in the disk equatorial plane falls with the power law. In the vertical direction, the density distribution is controlled only by gas pressure and the gravity of the star.

Touhami et al. (2011) used this parametric model for the density distribution in Be discs, reproducing accurately the statistical properties of the colour excesses observed in a sample of 130 stars. Table 2.1 summarised by Arcos, C. PhD thesis presents disc density parameters reported by various authors. The base density (ρ_0) ranges from 10^{-12} to 10^{-10} g cm^{-3}, while the power-law exponent (n) varies between 1.5 and 3.5.

Author	Sample	Line/SED	n	ρ_0 (g cm^{-3})
Arcos et al. (2017)	63	Hα	2.0-3.5	$(4.00-6.30)\times10^{-11}$
Vieira et al. (2017)	80	Near-IR	1.5-3.5	$10^{-12}-10^{-10}$
Silaj et al. (2014)	8	Hα	2.5-3.5	$10^{-12}-10^{-10}$
Silaj et al. (2010)	56	Hα	3.5	$10^{-11}-10^{-10}$
Touhami et al. (2011)	130	Near-IR	3.0	$10^{-12}-2.0\times10^{-10}$

Table 2.1: Table from Arcos, C. PhD thesis detailing the main disc density distribution parameters.

The structure of the disc of Be stars may seem to result from a set of equations. However, this is not the case. The thin structure of the disc has been demonstrated observationally on many occasions. The study by Quirrenbach et al. (1997) pioneered the use of interferometry to map the disc structure. They carried out a detailed analysis of the circumstellar disc of the star ζ Tauri. One of their major key results was to reconstruct the structure of the disc of ζ Tauri by applying the maximum-entropy method to generate a map of the disc emission in the Hα line. Their results confirmed the thin geometry and supported the standard model that Be star discs are gaseous discs in Keplerian rotation. Figure 2.2 shows the density profile and also the temperature structure of a Be star disc. It can be noticed that in the plot on the right, the temperature of the disc in the equatorial plane and close to the star is much lower than in the farther regions. This may seem strange, but it is a reflection of the high density of the disc (left panel). The concentration of a large amount of material in this region creates a high opacity to the radiation, which causes a temperature decrease.

As for the scale height, there is also observational evidence supporting the flaring disc. For a disc with a temperature slightly lower than the photosphere, the scale height begins at 0.04 R_*, corresponding to an opening angle of approximately 2°. It gradually expands to 3.5 R_* (or 10°) at a distance of 20 R_* from the star. Usually, the opening angles of the disc in Be stars are small. Yudin (2001) compiles data from 627 classical Be stars and performs a statistical analysis to obtain information about the geometry of the circumstellar envelopes surrounding these stars. One of their conclusion is that most Be stars are surrounded by optically thin discs with a half-opening angle between 10° and 40°.

The size of the disc is obtained from observations of spectra or by analyzing the SED (Klement et al., 2017). The extent of the disc depends on the wavelength at which it is observed. This is known as the emitting region. Longer wavelengths correspond to cooler regions and, hence, to larger radii (valid only for the continuum). For example, observations of the γ Cas disc extension give values of 7 R_*, 1.54 R_*, 1.66 R_*, and 2.50 R_* in Hα, R band, H band, and K band, respectively. Table 2.2 lists Hα observations from Optical Large Baseline Interferometry (OLBI). The emitting region is only estimated from Gaussian fittings and is listed. We note that the size of the emitting region for Hα is usually less than 25R_*.

Star	Sp. Type	R_* [$R_\odot$]	Measured FWHM [mas]	Diameter [AU]	Radius [R_*]	Refs
Hα						
γ Cas	B0.5IVe	10	3.47 ± 0.02	0.652 ± 0.004	7.01 ± 0.04	a
γ Cas	B0.5IVe	10	3.59 ± 0.04	0.675 ± 0.008	7.25 ± 0.08	b
ϕ Per	B2Vsh	7.0	2.67 ± 0.20	0.588 ± 0.044	9.03 ± 0.68	a
ϕ Per	B2Vsh	7.0	2.89 ± 0.09	0.637 ± 0.020	9.77 ± 0.30	b
χ Oph	B2Ve	5.7	3.46 ± 0.07	0.557 ± 0.011	10.5 ± 0.2	c
ν Cyg	B2Ve	4.7	1.0 ± 0.2	0.20 ± 0.04	4.5 ± 0.9	d
ζ Tau	B2IVsh	7.7	4.53 ± 0.52	0.618 ± 0.071	8.63 ± 0.99	a
ζ Tau	B2IVsh	7.7	3.14 ± 0.21	0.428 ± 0.029	5.98 ± 0.40	e
48 Per	B3Ve	6.0	2.77 ± 0.56	0.41 ± 0.08	7.3 ± 1.5	a
48 Per	B3Ve	6.0	2.10 ± 0.2	0.31 ± 0.03	5.5 ± 0.5	f
ψ Per	B5Vsh	4.7	3.26 ± 0.23	0.583 ± 0.041	13.34 ± 0.94	a
ψ Per	B5Vsh	4.7	4.00 ± 0.2	0.716 ± 0.036	16.36 ± 0.82	f
o Cas	B5IIIe	7.7	1.90 ± 0.10	0.409 ± 0.022	5.71 ± 0.30	g
β Psc	B6Ve	3.5	2.4 ± 0.2	0.30 ± 0.03	9.3 ± 0.8	d
κ Dra	B6IIIe	6.4	2.0 ± 0.3	0.30 ± 0.05	5.1 ± 0.76	d
η Tau	B7IIIe	8.5	2.65 ± 0.14	0.328 ± 0.017	4.15 ± 0.22	a
η Tau	B7IIIe	8.5	2.08 ± 0.18	0.257 ± 0.022	3.26 ± 0.28	h
β CMi	B8Ve	3.5	2.65 ± 0.10	0.131 ± 0.005	4.03 ± 0.15	a
β CMi	B8Ve	3.5	2.13 ± 0.15	0.106 ± 0.007	3.24 ± 0.23	h

Table 2.2: Size of the emitting region estimated from Gaussian fits, for Hα. Taken from Rivinius et al. (2013). [a] Quirrenbach et al. (1997), [b] Tycner et al. (2006), [c] Tycner et al. (2008), [d] Touhami et al. (2013), [e] Tycner et al. (2004), [f] Delaa et al. (2011), [g] Koubskỳ et al. (2010), [h] Tycner et al. (2005)

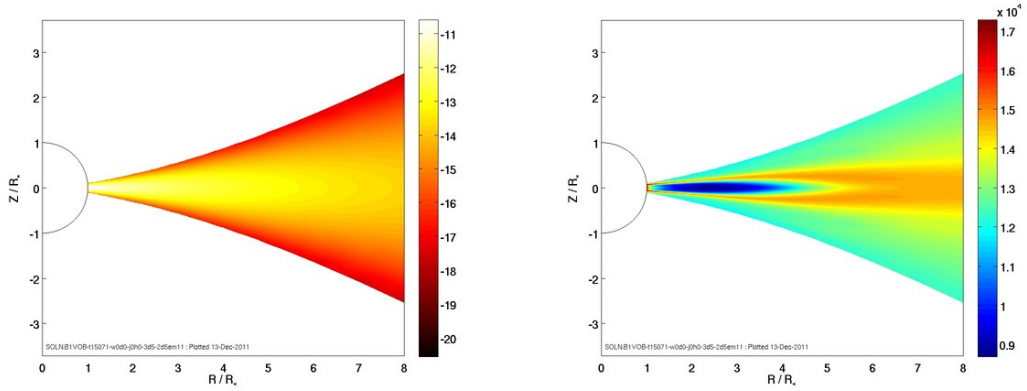

Figure 2.2: Density profile (*left*) and temperature structure (*right*) of the disc. Disc density profile: the colour bar shows how dense the gas is (g cm^{-3}); white means high-dense gas regions, while black colours are for lower-density gas regions. Temperature structure: blue colours indicate cooler regions. Images taken from from `http://astro.uwo.ca/ asigut/`. Generated using `BEDISK/BERAY` codes.

CHAPTER 3

Observations

3.1 Sample

The initial sample of stars was provided by Ph.d. Jonathan Labadie Bartz, an expert in the field of light curve variability in Be stars. The sample came from the Transiting Exoplanet Survey Satellite (TESS) observations. This section will outline the origin of the initial star sample, provide a brief overview of the telescope and its observations, and detail the selection of stars (or targets) that will be processed and analyzed in this thesis.

3.2 The Transiting Exoplanet Survey Satellite and Photometric Observations

The Transiting Exoplanet Survey Satellite (TESS) space telescope, is a NASA mission launched in April 2018 to search for transiting exoplanets around 200000 bright main sequence stars, with a bright limit magnitude of 4 or even brighter (Ricker et al. (2015)). Stars in the southern hemisphere were observed during the first-year mission. In contrast, the northern stars were observed during the second-year mission, leaving subsequent observations of the same portions of the sky until the primary mission was completed.

TESS consists of four identical cameras that come with specially designed f/1.4 lenses. This offers each camera an extensive field of view measuring 24×24 degrees. The four cameras

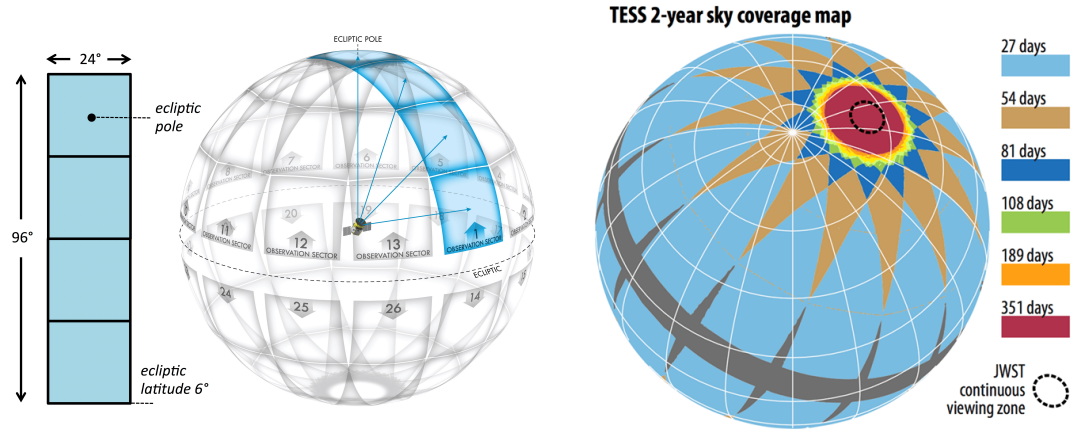

Figure 3.1: Illustrations showing how the TESS array of lenses observe the sky and the observing sector with the corresponding time duration for each viewing zone. Credits: TESS Website (2023)

are organized into an array providing a combined field of view of 24×96, allowing a complete monitoring of a whole hemisphere in one year. Details of the instrument are in Table 3.1.

Since TESS cameras act as a 1×4 array, the scanning strategy consists of dividing the hemisphere into continuously observed sectors for 27.4 days. After the observation is completed the FOV is shifted eastward by about 27 deg to observe the next sector. An illustration exemplifying this is shown in Figure 3.1

TESS provides multiple observing cadences, including 30-minute, 2-minute, and 20-second exposures. For this analysis, the 2-minute cadence data is used to ensure a balance between time resolution and signal quality. the telescope achieves high photometric precision, with a noise floor of approximately 60 ppm per hour for optimal targets (Ricker et al., 2015). Additionally, TESS has a pixel scale of about 21 arcseconds per pixel, meaning that each pixel covers a relatively large region of the sky, which can lead to the blending of nearby sources and requires careful contamination checks.

During years 1 and 2 of the mission (July 2018 - July 2020), the southern hemisphere and northern hemisphere were observed, respectively. During Year 3 of the mission (July 2020-July 2021), the southern ecliptic hemisphere was re-observed. During Year 4 (July 2021-September 2022; 16 sectors), parts of the northern ecliptic hemisphere were re-observed, and a 240° swath of the ecliptic was observed for the first time. During Year 5, the northern hemisphere survey was completed and a new southern survey began (TESS Website, 2023).

Field of view of each lens	24 deg $\times$ 24 deg
Combined field of view	24 deg $\times$ 96 deg = 2300 deg^2
Entrance pupil diameter	10.5 cm
Focal ratio (f/#)	f/1.4
Wavelength range	600 to 1000 nm
Ensquared energy	50% within 15 $\times$ 15 μm (1px, or 0.35 $\times$ 0.35 arc min)
	90% within 60 $\times$ 60 μm (4 $\times$ 4 pixels
	or 1.4 $\times$ 1.4 arc min)

Table 3.1: Specifications of TESS lenses. Ensquared energy is the fraction of the total energy of the point-spread function that is within a square of the given dimensions centred on the peak.

3.3 The Be Star Spectra (BeSS) Database and Spectroscopic Observation

The BeSS (Be Stars Spectra) Database[1] (Neiner et al., 2011) is an online database that focuses on collecting and sharing spectra of Be stars. In this database, which is used by professionals and amateur astronomers, spectra of Be stars are collected to analyze and share further.

The idea of creating a database for Be-type stars arose because the data was scattered, unorganized and inhomogeneously classified. The database contains and strives to collect spectra of Be stars from professional and amateur astronomers, compiling a comprehensive collection of the available data.

As of January 2024, BeSS contains a total of 282288 spectra.

Users can query in the BeSS. A query can be performed by completing the form seen in figure 3.2. As shown, the form can be filled to search a star by stellar parameters, spectral parameters, instrument or instrument specification, observers, and wavelength domain, among others. When a query is performed, BeSS lists all the spectra found for the specified criteria. It also displays information related to the instrument, author and related to the spectra. The data can be downloaded file by file or by selecting several spectra. A quick look at the spectra can be accessed before download as well.

As an example for the Be star QR Vul, Figure 3.3 shows how BeSS data can be used to study changes in the disc, such as the changes observed during the outburst of QR Vul between 2007 and 2009. Amateurs and professional astronomers registered this event in the BeSS Database. The outburst was logged before, during, and after its presence, allowing studies to measure the

[1] `http://basebe.obspm.fr/basebe/`

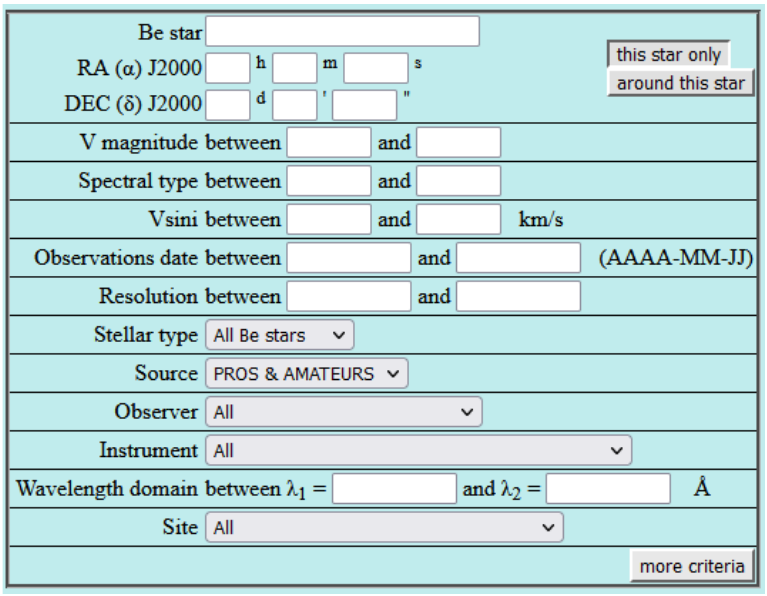

Figure 3.2: BeSS query. Screenshot from the BeSS Database website. Queries can be performed by stellar parameters, instruments, observers, etc.

change in the equivalent width of the spectra.

This database has proven to be a great tool when searching for Be stars. It contains a very large catalogue of spectra, useful for studies of long-term phenomena in Be stars, variations in spectra, and Be star statistics, all with a high-quality degree.

3.4 Target Selection

The classification process begins after obtaining the complete sample of Be southern stars, observed with TESS. In order to follow the variability of these stars, only targets observed in more than one cycle were selected.

Cycles 1, 2, and 3 are included in Dataset 1, cycle 4 in Dataset 2, and cycle 5 in Dataset 3. To ensure a continuous analysis of the stars' variability, all cycles have been carefully matched.

Since the comparison between the datasets is commutative, only 3 combined dataset groups are obtained, creating what we call datasets 1+2, datasets 1+3, and datasets 2+3. The final values are shown in Table 3.2, with a total of 506 matched stars.

The pre-classification is done. In order to obtain a correlation between the phenomena occurring in the stellar photosphere (e.g., pulsations, outflows, etc.) and their connection with the disc (e.g., formation, dissipation, etc.), it is necessary to have simultaneous observations with both spectroscopy and photometry data. Therefore, the next step was to create a cross-match list

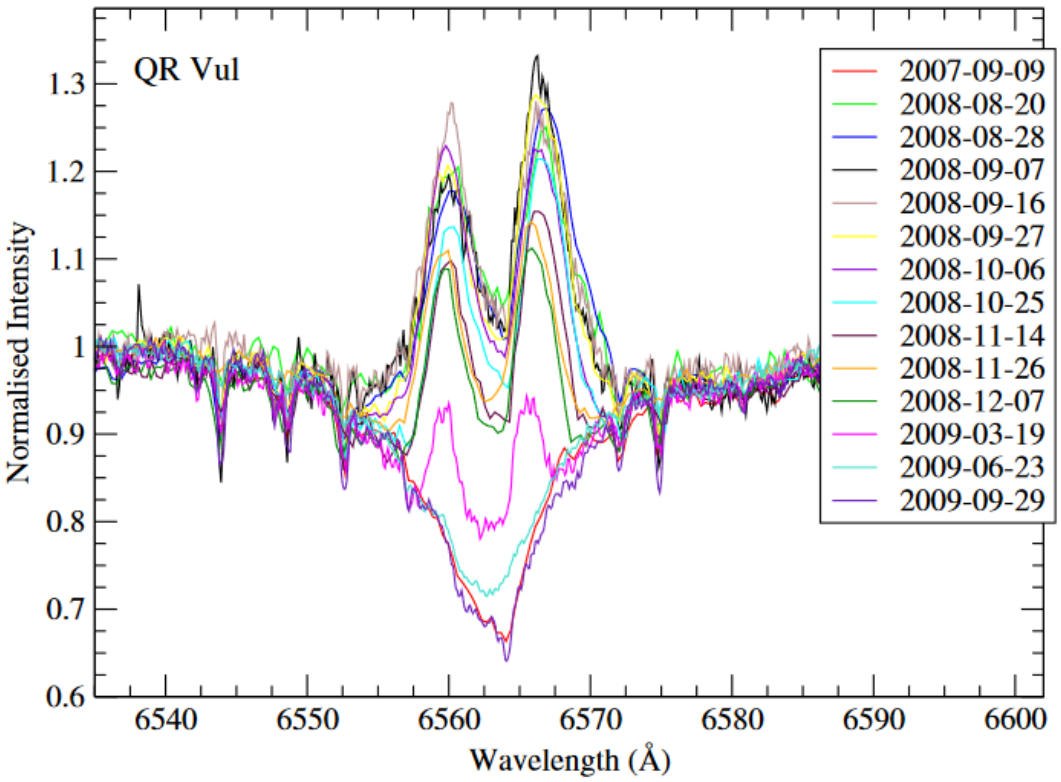

Figure 3.3: Observations of QR Vul at Hα before, during, and after the outburst which occurred in 2008 and was detected thanks to BeSS (Credits C. Buil, V. Desnoux, J. Guarro, M. Pujol, and O. Thizy, Neiner et al. (2011)).

	Dataset 1+2	Dataset 1+3	Dataset 2+3	Total
No. of stars.	40	400	66	506

Table 3.2: Number of targets after performing a matching set. This is a pre-selection of Be star from the original sample.

between the sample's TESS and spectroscopic data.

Before searching in the Bess Database, the Web TESS Viewing Tool (WTV)[2] was used to obtain the sectors and dates for each target.

The search in the BeSS Database webpage was based on using the data provided by WTV, but with an interval of ± 1 month, since the variations on the stellar photosphere affecting the disc are not reflected instantaneously (see Section 5).

With this search of photometric and spectrometric data, the sample was reduced from ~ 500

[2] `https://heasarc.gsfc.nasa.gov/wsgi-scripts/TESS/TESS-point_Web_Tool/TESS-point_Web_Tool/wtv_v2.0.py/`

	Dataset 1+2	Dataset 1+3	Dataset 2+3	Total
No. of stars.	12	75	49	134

Table 3.3: Final target selection

to 134 stars which have observations in the BeSS Database and observations with TESS taken at about the same time (Table 3.3).

CHAPTER 4

Methods

The final goal of this chapter is to obtain the periodogram plots for each star, which encode information about the photometric signals in the TESS data. In the first subsection, the Lomb-Scargle algorithm is described. Then, in order to discern the most relevant frequencies from noise, the False Alarm Probab ilities (FAP) theory is detailed. Finally, the code implementation of both techniques is described in detail.

4.1 The Generalized Lomb-Scargle Periodogram

The Lomb-Scargle algorithm is a technique used to analyze irregular time series and look for periodicities in the data. It was developed by Lomb in 1976 (Lomb (1976)) and then generalized by Scargle in 1982 (Scargle (1982)). It is particularly useful in the investigation of periodic signals in noisy or non-uniformly spaced data.

The Lomb-Scargle algorithm was developed as an alternative to Fourier analysis in situations where the data are not equally spaced in time, which is common in astronomical observations. This technique is especially valuable for analyzing short, irregularly spaced time series data.

However, in the process of obtaining periodograms, there are a number of problems that must be considered when using real data with the Lomb-Scargle algorithm. The most relevant are:

- Noisy data: Data with prominent noise could result in false-positive frequencies and

problems in finding periodicity.

- Non-periodic signal: If the signal has a variable frequency, Lomb-Scargle could have difficulties finding these variations.

- Frequency aliasing: Overlapping of frequencies if the sample rate is not high enough to detect the true periodicity.

In addition, we have to consider the frequency grid, maximum or minimum frequency, Nyquist limit, and the origin of the largest peak in the periodogram, among other things.

The Lomb-Scargle periodogram is the least-squared interpretation of the Fourier transform method. This method involves fitting a model to the data at each frequency and selecting the frequency that maximizes the likelihood.

In the least-squared interpretation, a sinusoidal model is proposed for each frequency f,

$$y(t,f) = A_f \sin(2\pi f t - \phi_f), \tag{4.1}$$

where the amplitude and phase, A_f and ϕ_f, respectively, depend on the frequency. These models are fitted in the least-squared view to a χ^2 statistic at each frequency,

$$\chi^2(f) = \sum_n \left(\frac{y_n - y_{\text{model}}(t_n, f)}{\sigma_n} \right)^2, \tag{4.2}$$

where σ_n corresponds to the uncertainties associated to each frequency, y_n the data and y_{model} the computed model.

The best model $\hat{y}(t,f)$ can be found in the χ^2 is minimized at each frequency with respect to A_f and ϕ_f, this minimum value is denoted as $\hat{\chi}^2$. The Lomb-Scargle periodogram can be rewritten in terms of the χ^2 (Scargle (1982)) as

$$P(f) = \frac{1}{2}\left[\hat{\chi}_0^2 - \hat{\chi}(f)\right], \tag{4.3}$$

where $\hat{\chi}_0^2$ is the non-varying reference model. It is key to note that the Lomb-Scargle periodogram assumes a sinusoidal model for the data (VanderPlas (2018)).

4.1.1 Periodogram Normalization

In the context of least-squared, the periodogram is interpreted as the goodness of fit for a model. Since the periodogram can be expressed in χ^2 models, it has to be bounded. From Eq. 4.3, if the model fits perfectly at some frequency f_0 then $\hat{\chi}_0^2(f_0) = 0$, and $P(f) = \hat{\chi}_0^2/2$. Also, the

best fit can not perform worse than a simple constant. Therefore, the minimum value is zero (VanderPlas (2018)). The normalized periodogram corresponding to these conditions is

$$P_{\text{norm}}(f) = 1 - \frac{\hat{\chi}^2(f)}{\hat{\chi}_0^2}. \tag{4.4}$$

This is the 'standard' normalization. The resulting quantity is a unitless periodogram that lies in the range $0 \leq P_{\text{norm}}(f) \leq 1$

4.2 Lightcurves and Code Implementation

This section presents the computational implementation for cleaning light curves and the Lomb-Scargle periodogram. Here we describe how the light curves were obtained and cleaned, and the tools used in the Python programming language and Jupyter Notebooks.

With the `lightkurve` Python package, aperture photometry was performed semi-automatically. Then, a contaminant search in the field is performed with the help of Gaia, and finally, detrending and denoising are performed with the statistical method of Principal Component Analysis (PCA).

4.2.1 The `lightkurve` package pipeline

As a means to describe the method for obtaining the lightcurves, the star HD 126693, with TESS Input Catalog code 389217256 (TIC 389217256) is used. It is worth mentioning that this procedure was applied to all the 136 targets selected in Section 3.4.

Most spatial telescopes, or even those on the ground, include movement from the telescope (or the earth) or noise from the background in their observations. These little effects add errors to the final results at the time of analysis. In the case of the lightcurves observed with TESS, the observed curve is noisy with an uncorrected trend (see Figure 4.4).

That is why a clean and detrended light curve is needed for a proper and professional analysis.

For this purpose, the package `lightkurve`, from the TESS website[1], was used. This package offers key tools for cleaning and correcting the light curves.

In addition to the `lightkurve` package, we made use of the file `LCExtrac.py`. This is a Python script that contains a set of functions that facilitate downloads, manipulation, and cleaning of light curves files.

[1] `https://heasarc.gsfc.nasa.gov/docs/tess/`

The most relevant functions are: `query_lc`, `change_aperture`, `contaminants`, `tpf_to_lc`, `detrended_tpf_to_lc`, `sig_clip_lc`. The input parameters are shown in Figure 4.1.

Each function fulfils a particular task. For example, the `contaminats` function finds targets near the zone of the star concerned (Figure 4.3).

```
def query_lc(ID, method, mission, author, cadence, sec, cutout_size, quarter, campaign):
  '''Function to get the lightcurve of a target source by using the lightkurve
    package.'''

def change_aperture(tpf, ini_mask, method, star_cut, sky_cut, ref_pixel):
  '''Function to visually change the TargetPixelFile mask.'''

def contaminants(tpf, mask, dmag, dist_cont):
  '''Function to visually locate potential contaminants from Gaia EDR3 and export the
    closest ones to an output txt file.'''

def tpf_to_lc(tpf, mask, flux_err_cut):
  '''Function to convert a TargetPixelFile object to its lightcurve.'''

def detrended_tpf_to_lc(lc, tpf, mask_background, npcs):
  '''Function to perform the detrending by Principal Component Analysis (PCA)
  given an input lightcurve.'''

def sig_clip_lc(lc, sigma):
  '''Function to perform a sigma clipping to the input lightcurve.'''
```

Figure 4.1: Functions from `LCExtrac.py`. A short description of their functionality is included

For a long description of each input parameter of the `LCExtrac.py` functions, see Appendix A. The input values used to query each target were:

- `query_lc(ID, method='tpf', author='TESS-SPOC', sec=id_sectors)`
  - `ID`: ID of the source to query.
  - `method='tpf'`: Method which query the TargetPixelFile object.
  - `author='SPOC'`: Observations from TESS Science Processing Operations Center (SPOC)
  - `sec=id_sector`: TESS sector in which the target was observed
- `change_aperture(tpf, sky_cut=0.01)`
  - `'tpf'`: The input TargetPixelFile obtained with the previous function.
  - `'sky_cut=0.01'`: Input cut value to select the background. Default 0.01 $e^{-} s^{-1}$ was used.
- `contaminants(tpf, mask='new', dmag=5, dist_cont=100)`

  - `'tpf'`: Same as before
  - `mask='new'`: Initial mask used to plot the aperture. `'new'` takes the mask crested with the previous function.
  - `dmag=5`: Gaia G magnitude difference used to limit the contaminants. Default 5 was used.
  - `dist_count=100`: Maximum distance in arsecs of the contaminant sources to be exported to a `txt` file.

- `tpf_to_lc(tpf, mask='new')`
  - `'tpf'`: Same as before
  - `mask='new'`: `'new'` takes the new mask created before.

- `detrended_tpf_to_lc(lc, tpf, tpf.mask_background, npcs=5)`
  - `lc`: Input light curve created with the function `tpf_to_lc`
  - `tpf`: Same as before
  - `tpf.mask_background`: Mask used to consider the background. Created with the `change_aperture` function.
  - `npcs=5`: Define the initial number of principal components to inspect. Default 5 was used.

- `sig_clip_lc(lc, sigma=lc.std)`
  - `lc`: Same as the `lc` from before.
  - `sigma=5`: Sigma clipping factor applied to the light curve.

The process to obtain a clean and detrended lightcurve begins by making a query to the TESS data with the `query_lc` function, which returns a list of observations in different TESS sectors, i.e., dates. This information comes in the form of a `TargetPixelFile` (TPF) Python object, which is a format that the `lightkurve` package has to codify a flux map.

Then the `change_aperture` function is applied to the TPF in order to select the background mask and target (Figure 4.2). This selection will be used during the process of cleaning and detrending. Some stars are bright enough to saturate the sensors of TESS, creating a bloom that can extend until the CCD boundary. This should not be a problem, precision photometry can still be achieved since TESS pixels conserve flux. Accurate light curves can be obtained even

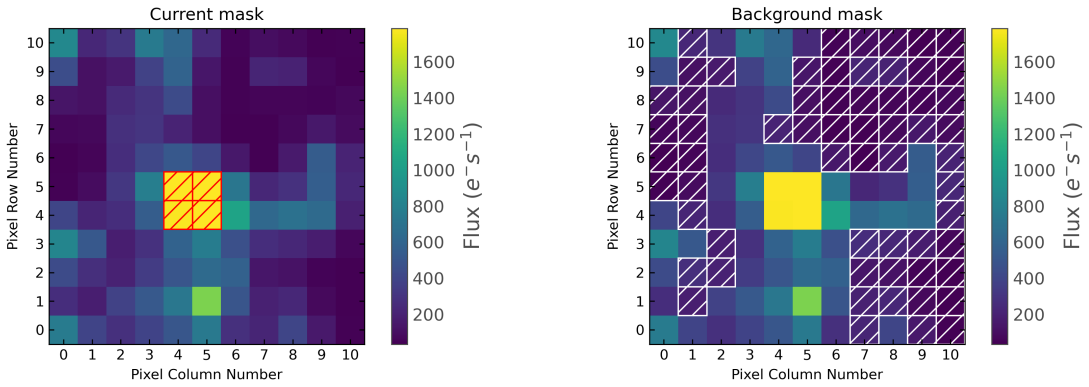

Figure 4.2: TargetPixelFile during the change aperture step.

for highly saturated sources (Labadie-Bartz et al. (2021) is a perfect example study), ensuring high-quality data for even the brightest stars in our sample.

The next step is to identify potential contaminants near the target, ensuring that no nearby stars introduce variability into the extracted light curve, so the analysis remains focused on the Be star's intrinsic variations. This is done by calling the `contaminants` function to the previous TPF (Figure 4.3). In this step, it is important to properly use the previously selected mask for the target and the background.

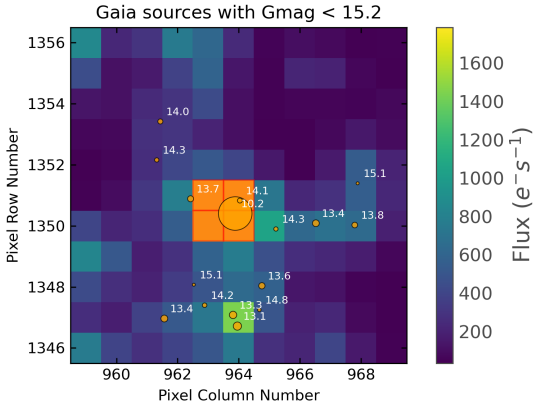

Figure 4.3: Contaminant surrounding HD 126693. For this example, the star is alone in the field of view.

The following steps make use of the already created mask from the TPF and convert it into a lightcurve, then a detrending with the `detrended_tpf_to_lc` is performed, and finally, a sigma clipping is done by calling the function `sig_clip_lc`. The sigma clipping is done until 5σ. The visual procedure is presented in the Figures 4.4

Finally, once the final light curve is obtained, the search for dominant frequencies with the Lomb-Scargle periodogram starts. These next steps consist of the description of the code

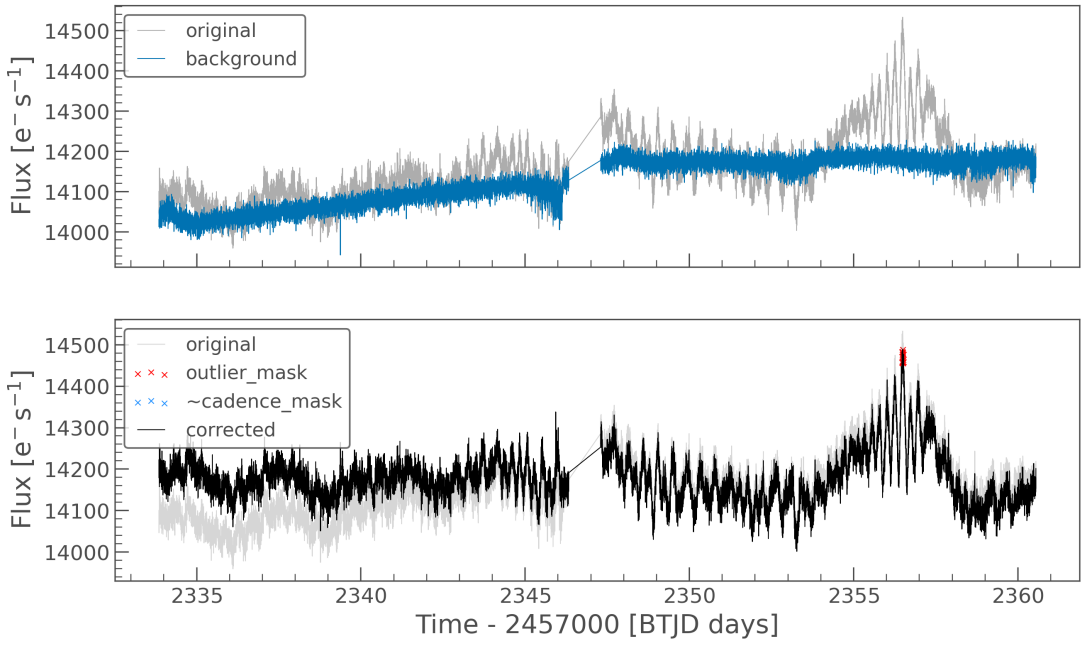

Figure 4.4: Top: original lightcurve (grey) and regressors (blue) to perform the detrend. Bottom: detrended lightcurve. The label also denotes the outliers in red asterisks

implementation to obtain the frequency/period, peaks of the periodogram, and phase plots of the corresponding star. It starts by taking the lightcurve's time and flux and passing it into the function `LombScagle` from the `astropy` package, creating an object that will return a grid of frequency when specified. The parameters of the grid are maximum and minimum frequency, Nyquist limit and samples per peak. The minimum frequency corresponds to $\delta f = 1/5T$, where $T = t_{\max} - t_{\min}$, the maximum limit correspond to the Nyquist limit $f_{\mathrm{Ny}} = 1/2T$, and 20 samples per peak.

4.3 Stochastic Low Frequency and PyWhiten

In the study of photometric variability in Be-stars, the identification of significant signals is crucial. However, the presence of noise can make this task difficult, especially the one located in the low-frequency part of the power spectra. The Stochastic Low Frequency (SLF) is the observed phenomenon in the light curves where the brightness fluctuates randomly in the long timescales (days to weeks) (Figure 4.5).

With the advent of new space telescopes, a new window in asteroseismology has opened to understand the internal structure of stars. One of these new understandings was the SLF. Since it is a recent topic, the origin of SLF is still being debated. It could be caused by subsurface

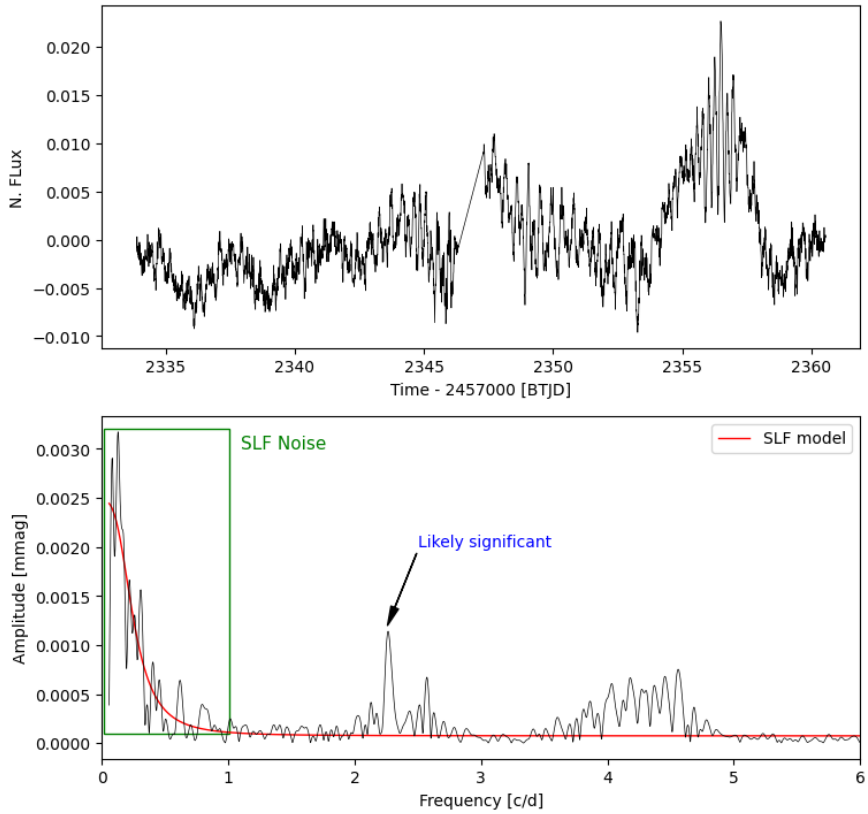

Figure 4.5: Light curve of HD 126693 during Sector 38 of TESS observations. The SLF noise is enclosed within a green box. This stochastic noise may pose challenges in accurately identifying potentially significant peaks.

convection zones or by internal gravity waves launched by turbulent core convection. This phenomenon adds to several stellar surface and stellar winds phenomena observed in hot stars of spectral type O, B, or A, such as surface velocity variations or line profile variability.

The SLF Model, developed by Dominic Bowman and collaborators in 2019, is used to characterize stochastic variability, particularly in the low-frequency range of their power spectra. This model fits the power excess observed in stars, which is thought to arise from stochastic oscillations driven by convective processes in their outer envelopes. The model is represented by the equation:

$$\alpha = \frac{\alpha_0}{1 + \left(\frac{f}{f_{char}}\right)^{\gamma}} + C_w, \tag{4.5}$$

where α_0 indicates the amplitude at zero frequency, f_{char} is the characteristic frequency ($1/(2\pi\tau)$; τ being the timescale of the light curve). Finally, γ is the gradient of the linear part of the profile, and C_w is the white noise term.

To address the challenge of identifying significant signals, usually in the range $f < 0.5$ c/d (as is the case for Be-stars), Stacey (2022) developed a Python program for Pre-Whitening (PyPW. PyWhiten as Python package), an iterative frequency analysis tool based on the pre-whitening technique. PyPW aims to identify and characterize periodic components in stellar light curves, even in the presence of significant SLF noise. This program addresses the difficulties of analyzing complex light curves, such as simultaneously optimizing multiple frequency components and managing SLF noise. Table 4.1 compares the frequencies found by Period04 and PyPw in Plaskett's star. We note that values are almost equal, proving that both methods can be used for this analysis. Therefore in this thesis, we will implement the PyPW method.

The work of Stacey (2022) focused on the photometric variability of Plaskett's star (HD 47129). Using observations from TESS, the CoRoT satellite, Hipparcos, and ASAS, the work expands the knowledge of this star by providing an asteroseismological perspective on Plaskett's star and new interpretations of the frequency spectra.

The Plaskett's star is a spectroscopic binary system (O8 III/I + O7.5 III) identified by John Plaskett in 1922 (Plaskett, 1922). The system caught the interest of the scientific community due to its high mass ($M \sin^3 i = 138.9\ \mathrm{M}_\odot$). The orbital period has been observed to be 14.39 days in a nearly circular orbit (Linder et al., 2008). The two spectral components appear blended, however, the O7.5 component presents rotational broadening in its spectral lines ($v_{\sin i} = 360 \pm 40$ km/s; (Grunhut et al., 2022)), and the O8 component presents narrow lines ($v_{\sin i} = 60 - 75$ km/s; (Linder et al., 2008)).

	PyPW			Period04		
I	Frequency [c/d]	Amplitude [mmag]	Phase	Frequency [c/d]	Amplitude [mmag]	Phase
1	1.64542(33)	17.56(22)	0.634(13)	1.64542(94)	17.575(65)	0.63432(59)
2	0.80884(51)	11.34(22)	0.847(20)	0.80880(14)	11.358(65)	0.84726(91)
3	0.63524(97)	6.05(23)	0.023(38)	0.63523(27)	6.065(65)	0.0230(17)
4	0.1387(10)	5.77(23)	0.652(40)	0.13867(29)	5.773(65)	0.6525(18)
5	1.1041(12)	4.65(23)	0.190(49)	1.10404(36)	4.651(65)	0.1909(22)
6	0.7129(11)	5.00(23)	0.958(46)	0.71298(33)	5.017(65)	0.9576(21)
7	0.2858(15)	3.88(23)	0.845(59)	0.28581(43)	3.878(65)	0.8450(27)
8	0.3907(16)	3.59(23)	0.861(64)	0.39060(46)	3.580(65)	0.8610(29)
9	0.4416(19)	3.10(23)	0.494(74)	0.86993(55)	3.034(65)	0.0471(34)
10	0.8700(19)	3.03(23)	0.045(76)	0.44145(54)	3.087(65)	0.4959(34)

Table 4.1: Table 4.1 from Stacey (2022). These are the comparative frequencies results found for the Plaskett's star using PyPW (left) and Period04 (right). The I column indicates the iteration in which the corresponding frequency was detected.

CHAPTER 5

Results

The analysis for the 134 Be stars resulted from over 220 TESS light curves and 560 Hα spectra collected. Spectroscopic data were synchronized with TESS observations to enable simultaneous analysis of light curves and spectral variability. Stellar parameters, including effective temperature (T_{eff}), surface gravity ($\log g$), and rotational velocity ($v \sin i$), among others, were catalogued. Light curves were extracted and processed using the Python package `lightkurve`. Frequency analysis was conducted using the Lomb-Scargle method, producing periodograms for each star to identify characteristic frequencies. Because of the huge amount of plots generated in this analysis ($\sim$53 GB in total), the reader is encouraged to contact the author[1] for access to all the results for the 134 Be stars or access the drive where the plots generated in this thesis for all the stars are located[2]. Moreover, in this thesis six stars were analyzed and discussed in detail: f01 Cygni, HD 45314, HD 110432, HD 120991, HD 174237, and ζ Tauri. These stars were selected among the full sample based on their distinct characteristics of prominent circumstellar disks, variability in their light curves, number of spectra associated with changes in the light curves, and, in some cases, information about X-ray emissions in the literature.

For each star, we examine the spectroscopic variability based on the Hα line, which provides insight into the structure and dynamics of the circumstellar disc. We also obtain the frequencies associated with photometric variability and compare these results with changes observed in the

[1] jassyr.salas@postgrado.uv.cl

[2] Plots Drive

Hα line. Additionally, we seek information in the literature indicating binary systems, e.g., with any X-ray emissions, which suggest the presence of a compact companion.

An analysis of the full sample of 134 stars revealed widespread photometric variability. All the stars exhibited detectable signals in their TESS light curves. This high detection rate suggests a significant level of activity within our target population. The distribution of the strongest detected TESS frequencies spanned from 0.001 c/d to 20.0 c/d, with a median frequency of 1.42 c/d. This broad range highlights the diverse range of pulsations a Be star can have, such as g-mode or p-mode pulsations. Most of the highest frequencies fall within the range of $< 1.0\ \mathrm{d}^{-1}$, this suggests a SLF intrinsic to the variability of Be stars, although some stars were SLF-free and had easily detectable signals, these were not the majority.

Out of the 134 stars analyzed, a significant portion, specifically 77, showed no correlation between the variations detected in TESS data and those observed in their spectra. Regarding spectroscopic variability, most stars had limited data, with low-resolution spectra or spectra taken with long time intervals, hindering the detection of variations. However, ψ^{09} Aur was identified as a notable case, showing variability in spectra and light curves. This star is of interest because in the span of three years, the Hα emission line decreases, indicating a dissipation of the disc. It is important to note that ψ^{09} Aur had widely spaced intervals between observations, which may bias this commentary. These systems warrant further investigation, and future studies involving spectrometric and photometric observations could provide valuable insights into their nature. While a detailed analysis of all 134 stars is beyond the scope of this thesis, these preliminary findings provide a broader context and highlight the potential for future research.

5.1 f01 Cygni

f01 Cygni is a well-known Be star with spectral type BI.5Vnne (Lesh, 1968), also known as HD 200120 and 59 Cygni, located in the Cygnus constellation. It is relatively bright, V = 4.75^{mag} Ducati (2002), and can be observed with the naked eye under good conditions.

f01 Cyg was classified as such in the catalogue of Be stars (Jaschek & Egret, 1982), where also assigned with a projected rotational speed of $v \sin i = 100$ km s^{-1}. Abt et al. (2002), by fitting the lines 4471 Åand 4481 Å, with Lorentzian or Gaussian profiles to yield the equivalent width and Full-Width-Half-Maximum of the line, and then calibrating against the standards by Slettebak et al. (1975), obtained a higher value of $v \sin i = 325$ km s^{-1}.

As a typical Be star, f01 Cyg presents variability in its brightness. The General Catalogue

of Variable Stars (Samus' et al., 2017) presents f01 Cyg as a Gamma Cassiopeiae (GCAS) variable star, however, this designation is based solely on its photometric variability and does not imply the presence of the strong and hard X-ray flux characteristic of γ Cas analogues, which are defined explicitly by their X-ray properties. f01 Cyg is confirmed to be a binary system Be+sdO (also called ϕ Per-type binaries) with an orbital period of 28.2 days (Maintz et al., 2005). Studies from UBV photometry and spectroscopy (Harmanec et al., 2002) have identified long-term variations of the V/R peak intensity (with a period of 2 years per cycle) by studying the line HeI 6678 Å.

In this study, we present 4 light curves with a cadence of 2 minutes, taken by the TESS telescope, for the star f01 Cyg. The light curves were observed during sectors 15 – 16 (August - September 2019) and sectors 55 – 56 (August - September 2022).

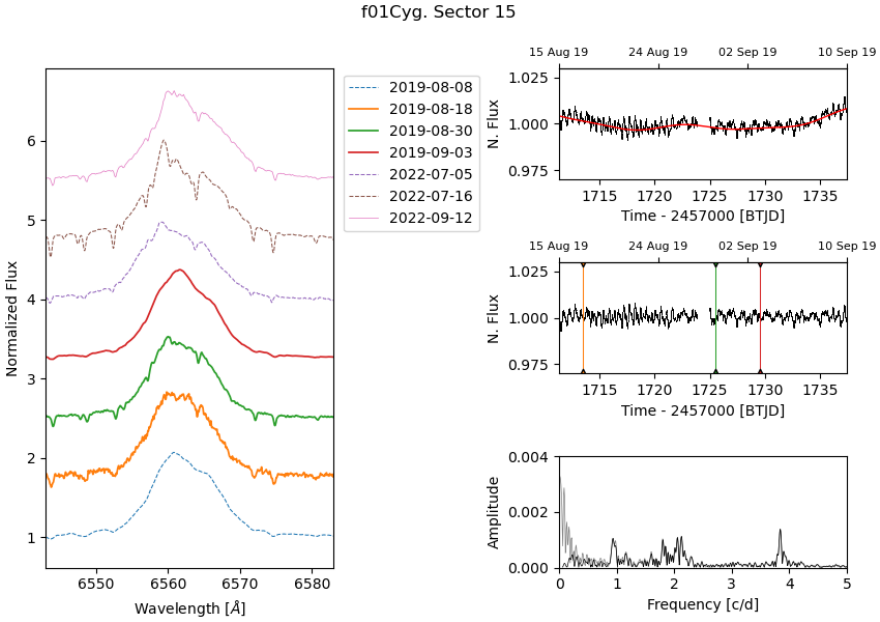

Figure 5.1: Results for the TESS sector 15 for the Be star f01 Cyg. The light curve was taken during Aug-Sep 2019. Three spectra coincide with the TESS observations window (solid colours).

To begin describing the light curves of f01 Cyg, it is necessary to remember the high variability in the brightness of Be stars, as is the case here. In Figure 5.1, two important characteristics can be observed: 1. the decrease ($\sim$ 1725 BTJD) and increase of brightness (long-term trend) and 2. short variations in brightness. These two features are typical of this Be star and also of those that will be described later.

In the light curve figures, we have also superimposed, in coloured lines, the spectra that coincided with TESS's observation time. Three coincident spectra for sector 15 will be described

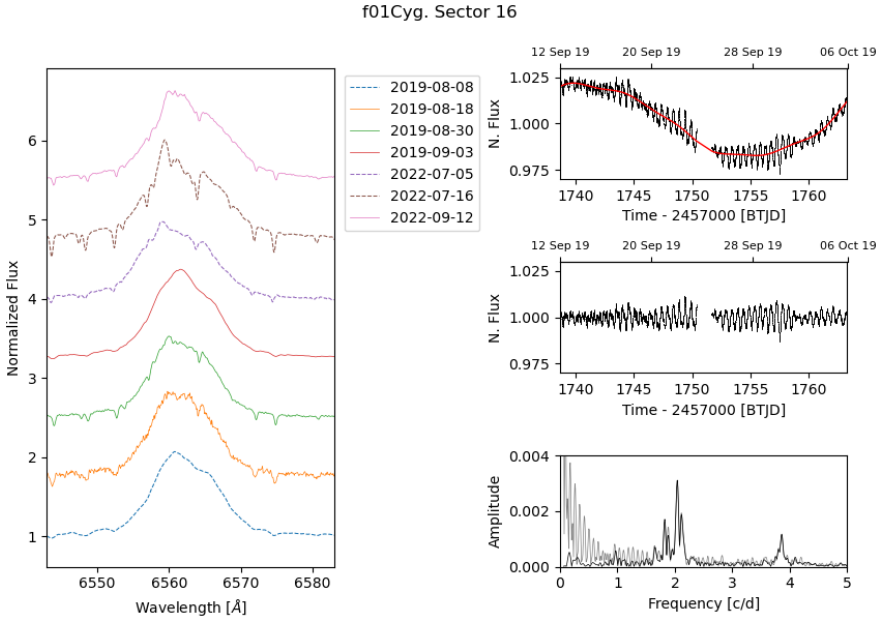

Figure 5.2: Results for the TESS sector 16 for the Be star f01 Cyg. The light curve was taken during Sep-Oct 2019. No spectra coincide with the TESS observations window.

later.

Continuing with the Figure 5.1 of f01 Cyg, we see again how the brightness decreases and then resumes an increasing trend. If this figure is analyzed together with that of sector 16, we can see that the variation in brightness is about 1 month, and this trend is repeated periodically (also observable in sectors 55-56). For sector 16, there are no matching spectra.

The overall analysis of sectors 55 - 56 shows the periodicity mentioned above. The brightness peaks around 2814 BTJD and peaks again approximately 30 days later, at 2844 BTJD. Some kind of ”beats” can also be seen in sector 56.

The periodograms of each light curve are also shown here. The final periodograms is shown in Figures 5.1, 5.2, 5.3, 5.4.

It can be seen how in all the periodograms, for each sector, many frequencies are presented with very high amplitudes close to zero. This is known as Stochastic Low-Frequency (SLF). The SLF can affect the identification of significant peaks, such as the group frequencies around $\sim$2.0 d^{-1} and $\sim$3.8 d^{-1}. However, the approximately 1-month trend must be carefully identified since we saw in the light curves that it is a trend and is not noise from the light curves.

Table 5.1 shows all frequencies found for f01 Cyg. Each column represents a TESS sector. The frequencies are listed in ascending order. The middle line represents the separation of the SLFs ($f < 0.5$ d^{-1}) from significant frequencies.

In addition to the SLF, as mentioned, the group of frequencies around $\sim$2.0 d^{-1} and $\sim$3.8

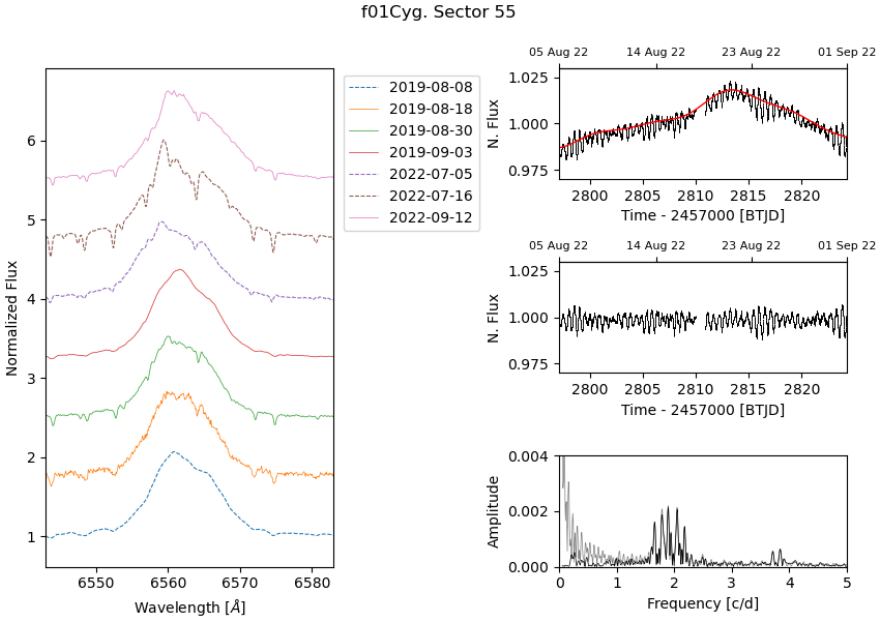

Figure 5.3: Results for the TESS sector 55 for the Be star f01 Cyg. The light curve was taken during Aug-Sep 2022. No spectra coincide with the TESS observations window.

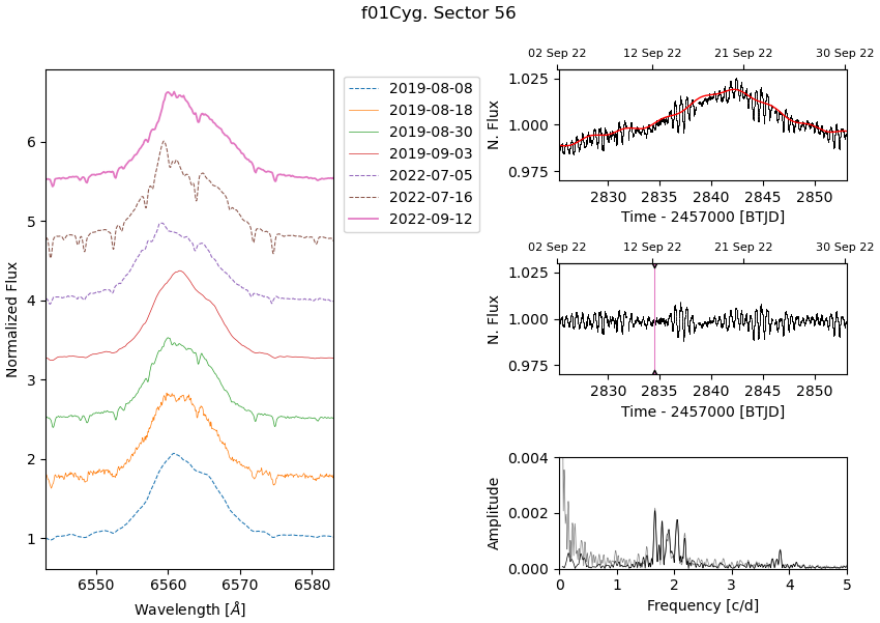

Figure 5.4: Results for the TESS sector 56 for the Be star f01 Cyg. The light curve was taken in Sep 2022. Only one spectrum coincides with the TESS observations window.

d^{-1} are repeated in all sectors, implying that these are important frequencies to identify. These are two groups of frequencies, classified as mid-range frequencies associated with g-mode pulsations.

The f01 Cyg spectra were taken from BeSS. A total of 7 spectra were obtained covering the dates from August to September 2019 and 2022, coinciding with TESS observations. In the figure of the spectra, on the left are all the spectra downloaded from BeSS, recalling that a time of $\pm$30 days concerning the light curves, since the changes in brightness in the light curves are not immediately observed in the spectra and on the right only the spectra that coincided with the TESS observations (4 in this case).

It is important to note that in the spectra plots, the y-axis is not separated by a uniform time spacing; the separation is only a visual aid and does not represent the time between them.

The 2019 spectra look quite similar, highlighting that the third one has a lower resolution than the first two. Between them, there is a gap of approximately 15 days, during which no changes in line intensity, shape, or equivalent width are noticeable. The V/R ratio is greater than 1.

There is a considerable V/R variation in the 2022 spectra. The intensity of the line changed during July and September 2022. The left peak increases from July 05 to July 16 and decreases again from July to September, meaning that some process must have occurred during this time.

Sector 15	Sector 16	Sector 55	Sector 56
0.0392392	0.04003573	0.03600455	0.03241738
0.05543826	0.07527533	0.04468027	0.07850845
0.13128107	0.09325587	0.09082685	0.28040268
	0.20700631	0.15429411	
0.93289134			
0.97389414	0.9708969		
	1.66176859	1.65752339	**1.66272261**
			1.74891461
		1.792769	1.78668224
1.80020559	1.82072682	1.83086467	1.85289695
	1.88527463	**1.90004877**	1.90219383
	1.94032491	1.91364159	1.97498473
			1.99528506
2.03419689	2.01217161	2.0459416	2.06106966

2.03942058	**2.05784763**	2.08037682	2.07417357
2.12687964	2.10055462	2.18272635	2.1844197
	2.14556966		
3.80185388	3.73716404	3.711611	3.70824549
3.84234373	3.84403227	3.8427736	3.84131397
3.93417588	3.85982563		
	3.93079005		
7.78530189		8.71600338	8.7143283
10.6394239		9.08750959	8.85574377
10.8003126		10.6252742	10.6799137
10.9097754		10.7592415	10.7632073
11.567632		10.8080588	10.8203975
12.8647105		12.8650084	12.8715066
15.0253574		14.9932812	14.9945487

Table 5.1: List of frequencies [d^{-1}] found in the periodograms of f01 Cyg in Sectors 15, 16, 55 and 56. Bold numbers represent the highest amplitude frequency in each sector. Above the horizontal line are the frequencies $< 0.5\,d^{-1}$ (SLF).

5.2 HD 45314

HD 45314, also known as PZ Gem, is a particular star in this study. It is a Be star with a spectral type O9e (Burssens et al., 2020), making it the only Oe-type star in this section. Oe stars are O-type stars with Be-star characteristics. This classification is considered an extension of the Be phenomenon into the range of temperature of O-type stars. Common features of Be stars' light curves and spectra are present in this star.

The Oe stars exhibit emission lines in H I, He I, and Fe II but lack some emission features typically seen in earlier-type O stars. The Small Magellanic Cloud (SMC), which has a lower metallicity than the Milky Way, contains a higher fraction of Oe stars (0.26 ± 0.04) compared to the Milky Way (0.03 ± 0.01) (Golden-Marx et al., 2016), suggesting that metallicity may play a role in their formation or prevalence.

HD 45314 has been also found to be a γ Cas star (Samus' et al., 2017), like the other stars in this section. As γ Cas type stars, it undergoes X-ray emissions and possibly might be a binary system. However, no companion has been detected, and it is not likely to be responsible for the X-ray spectra similar to γ Cas stars (Rauw et al., 2013).

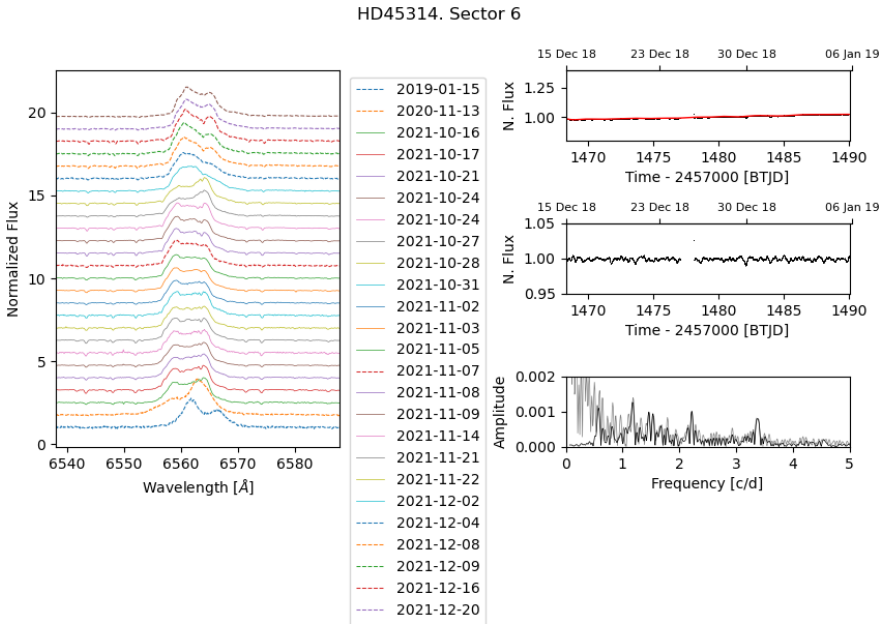

Figure 5.5: Results for the TESS sector 6 for the Be star HD 45314. The light curve was taken from Dec 2018 until Jan 2019. No spectra coincide with the TESS observations window. The spectroscopic observations cover Jan 2019, Nov 2020, and, Oct-Dec 2021.

The results for HD 45314 are presented here. It was observed by TESS in sectors 6 (December 2018), 33 (December 2020), 43, 44 and 45 (September - November 2021), making a

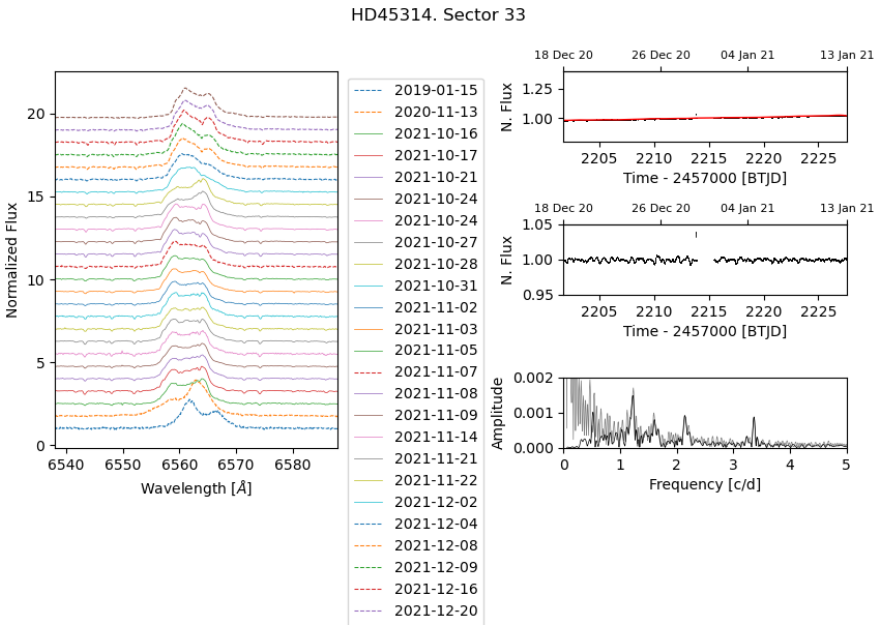

Figure 5.6: Results for the TESS sector 33 for the Be star HD 45314. The light curve was taken from Dec 2020 until Jan 2021. No spectra coincide with the TESS observations window.

total of 5 sectors, i.e., 5 light curves. The spectrometric observations comprise 26 spectra of Hα, of which 15 coincide with the TESS observations.

The light curves are characterized by high variability of short frequencies and increased brightness in sectors 6 and 33. Sectors 43 - 45 show this same increase in brightness. However, it settles down in Sector 44 and decreases during Sector 45.

An increase in amplitude in the reduced light curves in Figures 5.7, 5.8 and 5.9 (right-centre panel) can also be noticed; during sectors 43 - 45.

The periodograms of HD 45314, starting with sectors 6 and 33, show well-defined frequencies around $\sim$1.1, $\sim$1.2, and $\sim$3.3 d^{-1}, although with a very low amplitude. In sectors 43–45, the amplitude of the same frequency groups increases, which is expected given that the corresponding light curves also exhibit greater amplitude in these sectors. In sector 43, the frequency around $\sim$1.1 d^{-1} disappears, or possibly combined with the frequency of $\sim$1.2. Table 5.2 lists all frequencies found in the periodograms. The range of frequencies encountered suggests g-mode pulsations. In bold is the frequency (> 0.5 d^{-1}) with the highest amplitude.

The periodograms of sectors 43, 44 and 45 show a considerable increase in the amplitude of the frequency close to ~ 3.3 d^{-1} (Figures 5.8 and 5.9). In this sector, the spectrometric observations start to present some changes.

The spectra of HD 45314 are similar in shape and intensity with slow V/R variation and a DPS. A slight radial velocity change can be noticed. There are 25 spectra, and 16 of them fall

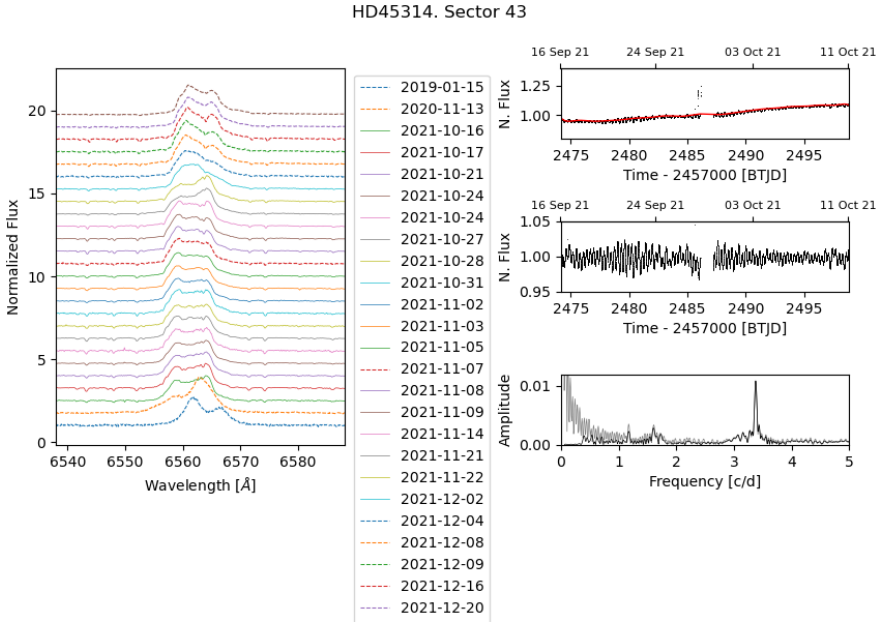

Figure 5.7: Results for the TESS sector 43 for the Be star HD 45314. The light curve was taken from Sep 2021 until Oct 2021. No spectra coincide with the TESS observations window.

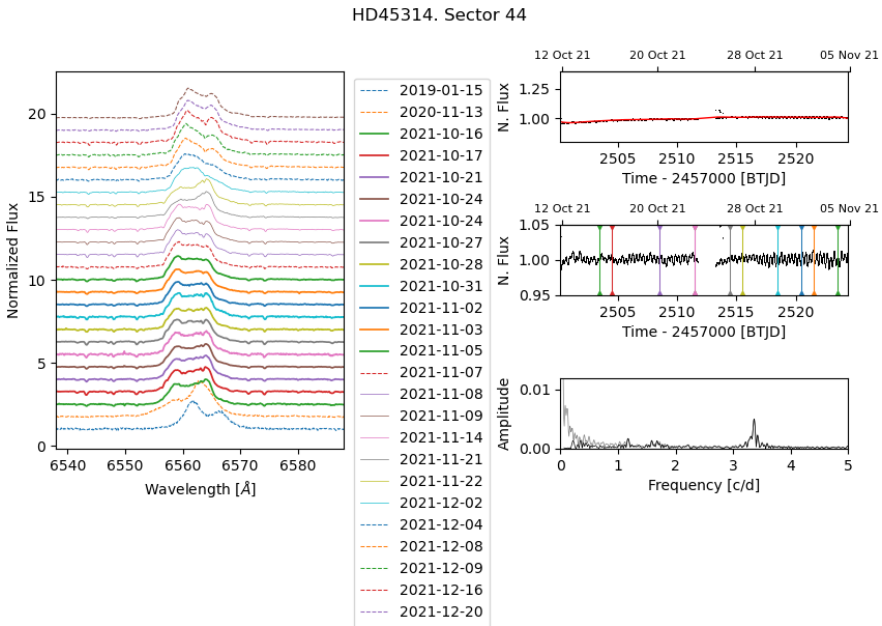

Figure 5.8: Results for the TESS sector 44 for the Be star HD 45314. The light curve was taken from Dec 2020 until Jan 2021. 10 spectra coincide with the TESS observations window (solid colours).

within the light curve observation time during sectors 44 and 45.

The spectrographic observation appears to be similar from 2021-Oct-16 until 2021-Nov-05, with little variation in the DPS. During sector 45, from 2021-Nov-08 until 2021-Nov-22, the

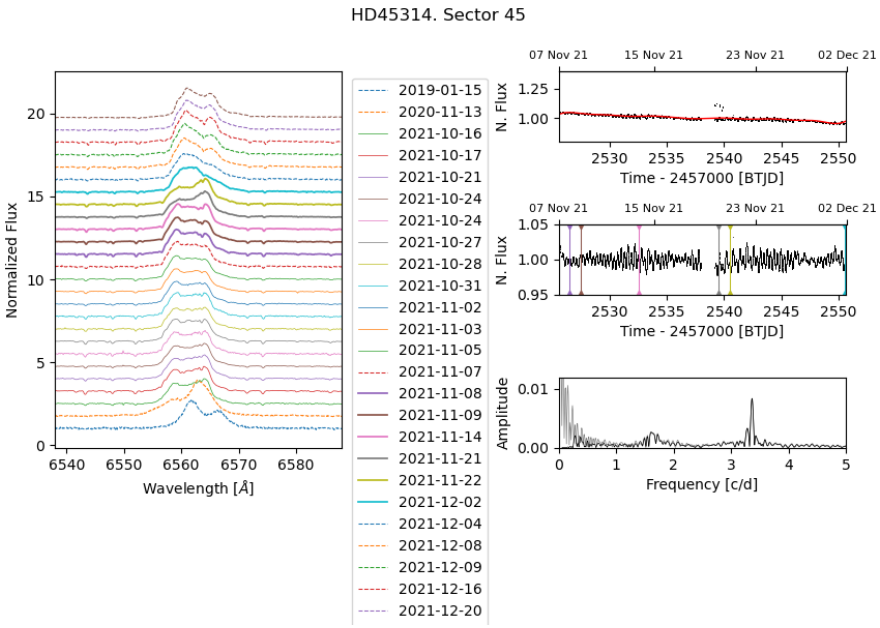

Figure 5.9: Results for the TESS sector 45 for the Be star HD 45314. The light curve was taken from Nov 2021 until Dec 2021. 5 spectra coincide with the TESS observations window (solid colours).

violet peak increases in intensity, which later will be inverse in 2021-Dec-02, being the red peak that starts and increases in intensity.

Sector 06	Sector 33	Sector 43	Sector 44	Sector 45
0.06920275	0.04909605	0.06787607	0.05199862	0.05322023
0.07136641	0.05619507	0.06796284	0.07864821	0.08108271
0.07383078	0.07664291	0.06911043	0.08523172	0.10819491
0.07894399	0.10304153	0.06942188	0.11133421	0.14588543
0.09254183	0.13762845	0.07509873	0.14459763	0.17695419
0.12337506	0.17041856	0.0798665	0.17574866	0.22124079
0.16694185	0.20458735	0.11335373	0.26739956	0.24373714
0.20383791	0.23336968	0.14717723		
0.24707016	0.24764398	0.18125369		
0.29776209	0.45860166	0.21601725		
0.33079041	0.51814739	0.25262829		
0.38751882		0.28864396		
0.41974388		0.32299717		

0.46147894		0.35535949		
0.57846187				
0.81151485	0.76847316			
1.06632922	1.12583821	1.17413383	1.1750682	1.60541498
1.14510843	1.17606208	1.60312394		1.65998386
1.17500662	**1.22509766**	1.65917795		
1.30140607	1.43665997			
1.46569424	1.61149862			
1.53508685	1.63785187			
1.66140229				
2.21900425	2.1310437			
	2.17353916			
	2.22156644			
3.35996779	3.25373783	3.2724958	3.33421432	3.27589967
3.40078185	3.36221329	**3.37402804**	**3.36174181**	**3.36734067**
		3.40747436	10.4839963	

Table 5.2: List of frequencies [d^{-1}] found in the periodograms of HD 45314 in Sectors 6, 33, 44, 43 and 45. Bold numbers represent the highest amplitude frequency in each sector. Above the horizontal line are the frequencies $< 0.5\,d^{-1}$ (SLF).

5.3 HD 110432

HD 110432 (BZ Cru) is a B-type star located in the constellation Centaurus, known for being a peculiar and intriguing object of study within the category of Be/X-ray binary stars, being the first proposed γ Cas type star (after γ Cas itself) Smith et al. (2012). It is classified as a B1e star (Arcos et al., 2018). HD 110432 is particularly interesting because its proximity to the Sun has been one of the most studied γ Cas-type stars.

The X-ray emissions from HD 110432 suggest the presence of a compact companion. However, no clear evidence of a companion star has been directly observed, making HD 110432 an enigmatic object and the subject of ongoing research. (de Oliveira et al., 2007a)

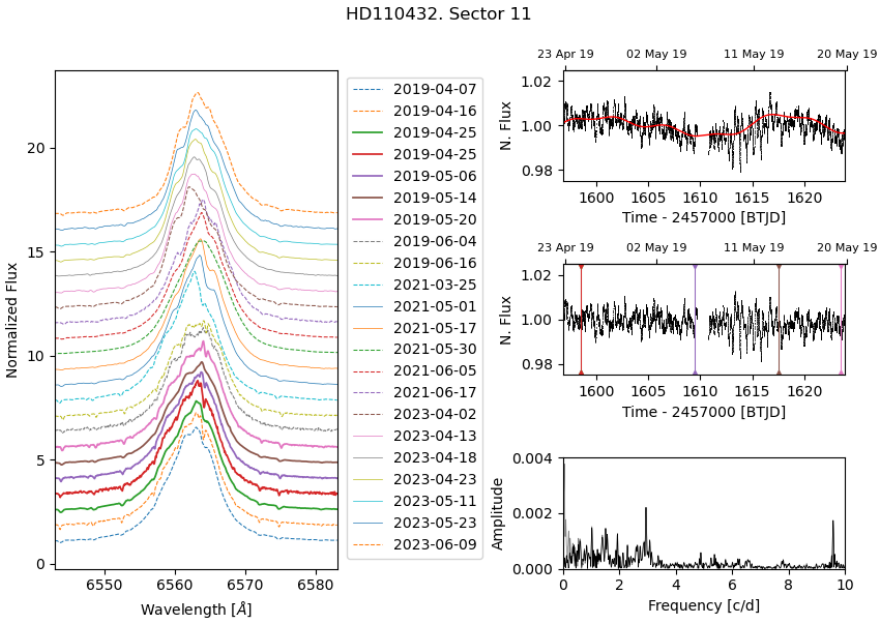

Figure 5.10: Results for the TESS sector 11 for the Be star HD 110432. The light curve was taken from Apr to May 2019. 4 spectra coincide with the TESS observations window (solid colours)

Jaschek & Egret (1982) proposed a $v_{\mathrm{sini}} = 213$ km s^{-1} for HD110432. Arcos et al. (2018) gave it a $v_{\mathrm{sini}} = 400$ km s^{-1}.

HD 110432 exhibits variability in both its optical and X-ray emissions, a characteristic feature of Be/X-ray binaries. The study of X-ray light curves suggests three types of variations: long cycles (months), intermediate variations (hours) and rapid flares (minutes). This kind of variability over different timescales is also present in the star γ Cas (Smith et al., 2012).

The optical light curves in this study are observed in TESS sectors 11 (May 2019), 37 - 38 (April - May 2021) and 64 - 65 (April - May 2023); making a total of 5 light curves. These are plotted in Figures 5.10, 5.11, 5.12, 5.13 and 5.14. As with most Be stars, the typical variability

of Be stars is also present here.

Looking at the light curves as a whole, there is no noticeable long-term trend, unlike the short-term variability that is present in all the sectors shown here. The short-duration variabilities are calculated to be around $\sim 2-20$ hours for each sector.

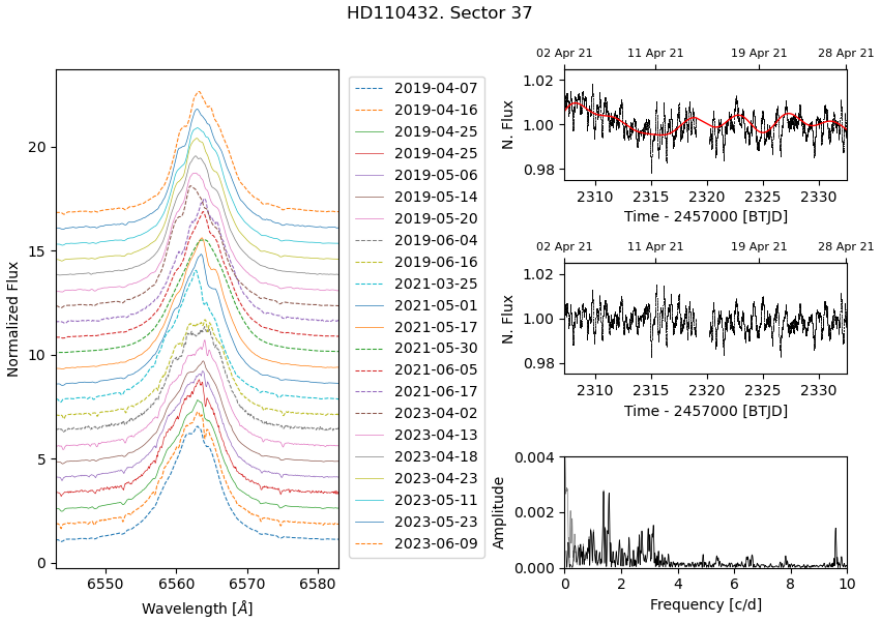

Figure 5.11: Results for the TESS sector 37 for the Be star HD 110432. The light curve was taken in Apr 2021. No spectra coincide with the TESS observations window.

If the adjoining sectors (37 - 38 and 64 - 65) are taken into account, a pattern can be recognized by observing the change in flux. First, sector 37 shows an almost constant brightness, just to slowly increase during sector 38. The same is repeated in sectors 64 - 65, a quasi-constant flux during the first sector that increases during the later sector.

The periodograms of HD 110432 are, in general, quite similar. All 5 periodograms present SLF and group frequencies around $\sim$1.25, $\sim$2.9 and $\sim$9.8 d^{-1}. Possible harmonics are the ones located around $\sim$5.0 - 7.5 d^{-1} and $\sim$11.0 - 12.5 d^{-1}. Table 5.3 lists all frequencies found in the periodograms.

A total of 22 spectra were downloaded from BeSS spanning the months of April - June 2019, March-May 2021 and April - May 2023 allowing us to observe several changes in the Hα line profile. 4 of the 5 light curves have simultaneous spectra in this study. All spectra of HD110432 show a subtle bottle-wine peak changing its radial velocity in a span of approximately 2 years. Just one hump can be seen, the left one during 2019 and 2021 and the right one during 2023.

Sector 11	Sector 37	Sector 38	Sector 64	Sector 65
0.05791825	0.08062329	0.05998613	0.06806761	0.03474435
0.10329341	0.0828132	0.06011612	0.10486632	0.05637624
0.21090832	0.208825	0.06550772	0.11251158	0.07991099
	0.25749841	0.06877638	0.335979	0.10239323
		0.07282852	0.41943583	0.21232516
		0.10211159	0.42602902	0.48074625
		0.17379005		
	0.92805261		0.94509881	0.94531836
1.03295861			1.0354534	1.03233304
1.4147515	**1.3782261**	1.3805808	1.38384633	**1.37477266**
1.51258562	1.57293109	**1.5736185**	1.52013885	1.57323082
1.57501345			**1.57795152**	
1.9388133				
2.9509285	2.73535099	2.68379999	2.94781261	
	2.95951887	2.85843857		
		2.94794023		
	3.1421537	3.08297185	3.14475679	3.08506756
		3.14138266		3.32244376
		4.89763905		
		5.37406152		
	6.44669891	6.4349322		
	6.47254158	6.50420157		
	6.63601033	6.63464946		
7.81533318	7.81688412	7.82010203	7.81008666	7.82454896
				7.87689981
			8.01515127	8.07553267
				8.20655249
9.5877097	9.58880355	9.58906455	9.58849994	9.58968774
9.7794373	9.78562228	9.78044856		9.77640362
11.1611678	11.1610452	11.1688171	11.1631391	11.1633566
11.5339526	11.9476943	11.9562191	12.7377904	12.7429425
11.9570163	12.1952875	12.1946139		
12.2020899				

13.5349275

Table 5.3: List of frequencies [d^{-1}] found in the periodograms of HD 110432 in Sectors 11, 37, 38, 64 and 65. Bold numbers represent the highest amplitude frequency in each sector. Above the horizontal line are the frequencies $< 0.5\,d^{-1}$ (SLF).

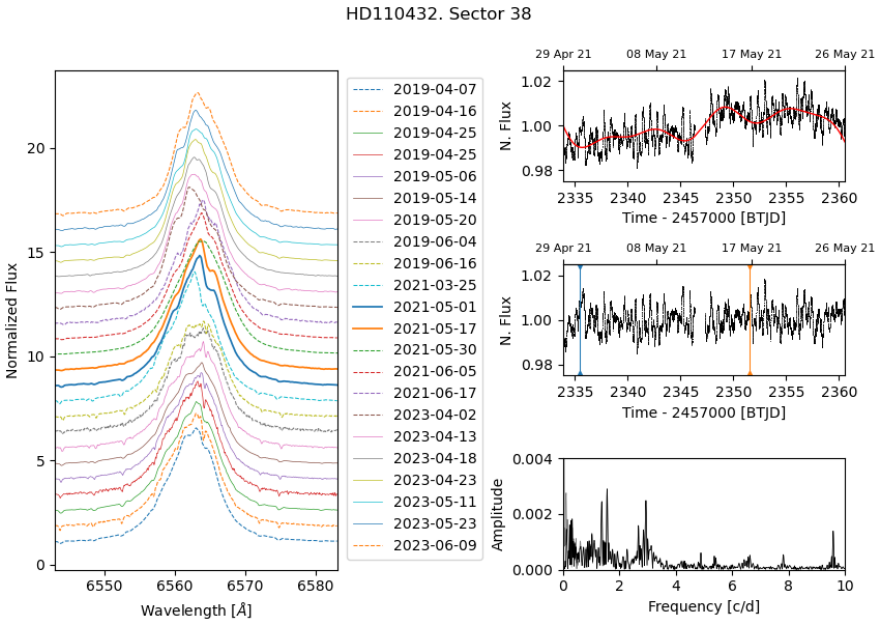

Figure 5.12: Results for the TESS sector 38 for the Be star HD 110432. The light curve was taken in May 2021. Two spectra coincide with the TESS observations window (solid colours).

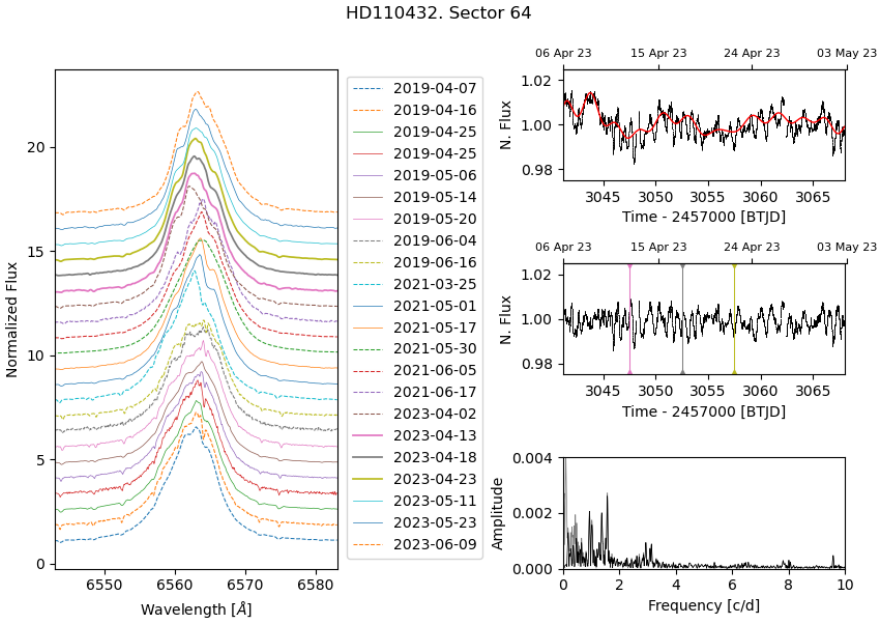

Figure 5.13: Results for the TESS sector 64 for the Be star HD 110432. The light curve was taken in Apr 2023. Three spectra coincide with the TESS observations window (solid colours).

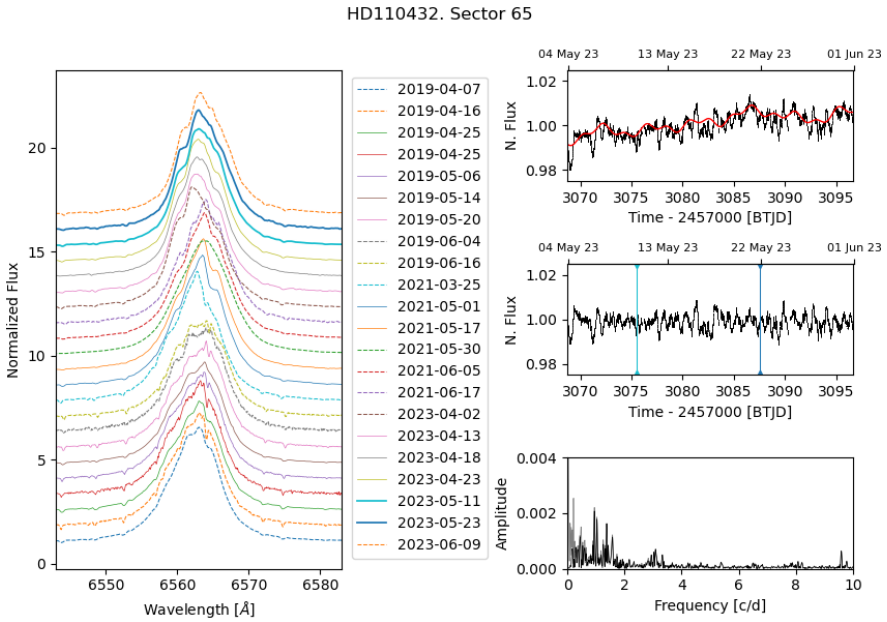

Figure 5.14: Results for the TESS sector 65 for the Be star HD 110432. The light curve was taken from May to Jun 2023. Two spectra coincide with the TESS observations window (solid colours).

5.4 HD 120991

HD 120991, also known as V767 Cen, is a Be star with a spectral type B2Ve (Levenhagen & Leister, 2006) located in the constellation of Centaurus. It has a magnitude of V 6.10 (Ducati, 2002), making it visible to the naked eye on dark nights. HD 120991 is known to have variability in both its brightness and spectral features.

In the General Catalogue of Variable Stars (Samus' et al., 2017), it is classified as a γ Cas type star (GCAS), a Be-star with strong X-ray emissions, possibly linked to binary companion (white dwarf) or alternative scenarios where they may originate closer to the Be star itself. Nazé et al. (2022a) study a large sample of γ Cas stars spectra to asses, via their radial velocity, the binarity status of the sample. While no signs of binarity were detected in HD 120991, the limited number of spectra prevents a definitive conclusion.

HD 120991 has a hard X-ray emissions variable on short timescales (Nazé, 2009), which reaffirms its γ Cas status. These variations in X-ray emissions and their relation to the disc creation of HD 120991 have been studied by Nazé et al. (2022b). However, optical and X-ray observations during a disc rebuilding, suggest no clear correlation between Hα EW and X-ray flux.

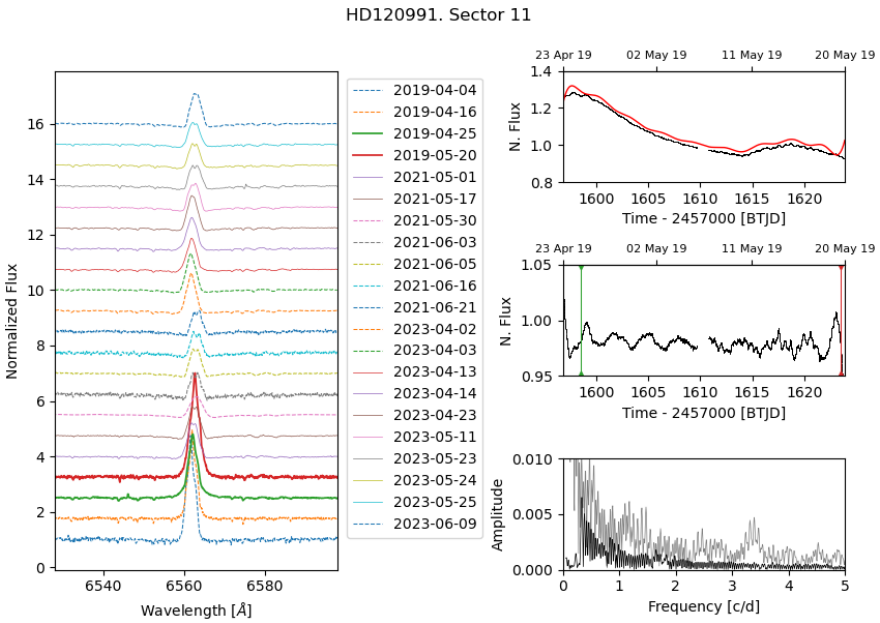

Figure 5.15: Results for the TESS sector 11 for the Be star HD 120991. The light curve was taken from Apr to May 2019. Two spectra coincide with the TESS observations window (solid colours).

The stellar parameter for HD 120991 are T_{eff} = 22000 K (Levenhagen & Leister, 2006), M = 6.02 $M_{\odot}$, R = 18.31 $R_{\odot}$ (Kervella et al., 2019) and a projected rotational velicity $v_{\rm sini}$ = 75

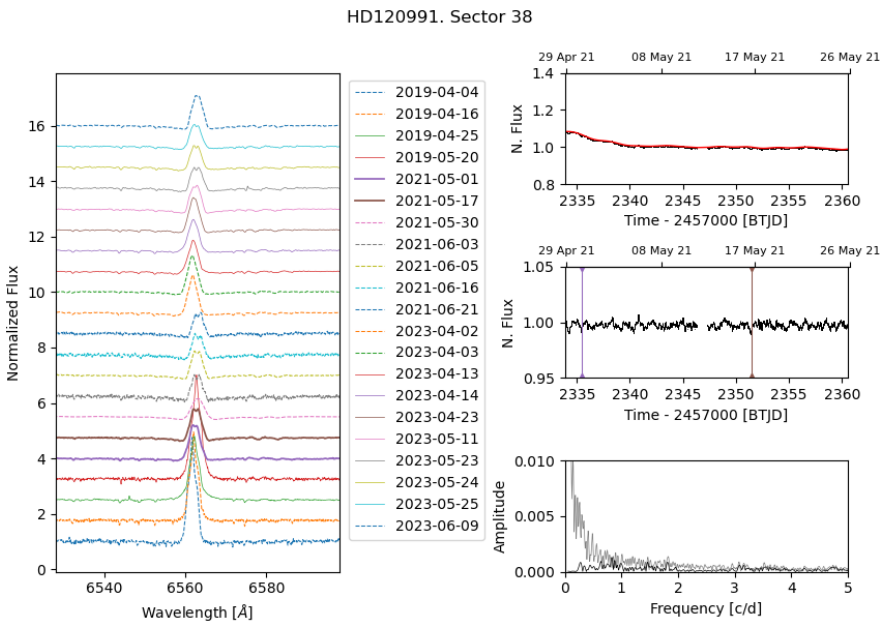

Figure 5.16: Results for the TESS sector 38 for the Be star HD 120991. The light curve was taken from Apr to May 2021. Two spectra coincide with the TESS observations window (solid colours).

km/s (Frémat et al., 2005).

HD 120991 shows high variability in brightness in its light curves. The TESS light curves were observed in sectors 11 (May 2019), 28 (May 2021), 64 and 65 (April - May 2023), showing long-trend variability. All results are presented in Figures 5.15, 5.16, 5.17 and 5.18.

During the first observation, i.e., sector 11 (Figure 5.15), HD120991 exhibits a large decrease in brightness during April - May 2019. The flux during this sector starts at a value of $\sim$1.3, that at the end of the month decreased to $\sim$0.9. This trend seems to hold for sector 38, although we have no other intermediate observations to say what could occurred during these two sectors.

Sector 38 starts with a high flux value that soon decreases to 1.0, which is maintained throughout the observation.

In sector 64 there are small bumps around $\sim$3047 and $\sim$3053 BTJD. The general trend in this sector is increased at the end of sector 65, around $\sim$3085 BTJD.

The periodogram for HD 120991 shows signals present in the TESS data, resembling those of other stars in the sample. However, their amplitudes are quite low, making them difficult to detect because of the dominant longer-term trends. The original periodogram of sector 11 seems to exhibit a group frequency around $\sim$3.5 d^{-1} that was removed during the cleaning. The majority of frequencies found for this star are low-frequency signals due to the high variability of its light curves. Table 5.4 lists all frequencies found in the periodograms.

This star has matching photometric and spectrometric observations. A total of 21 spectra

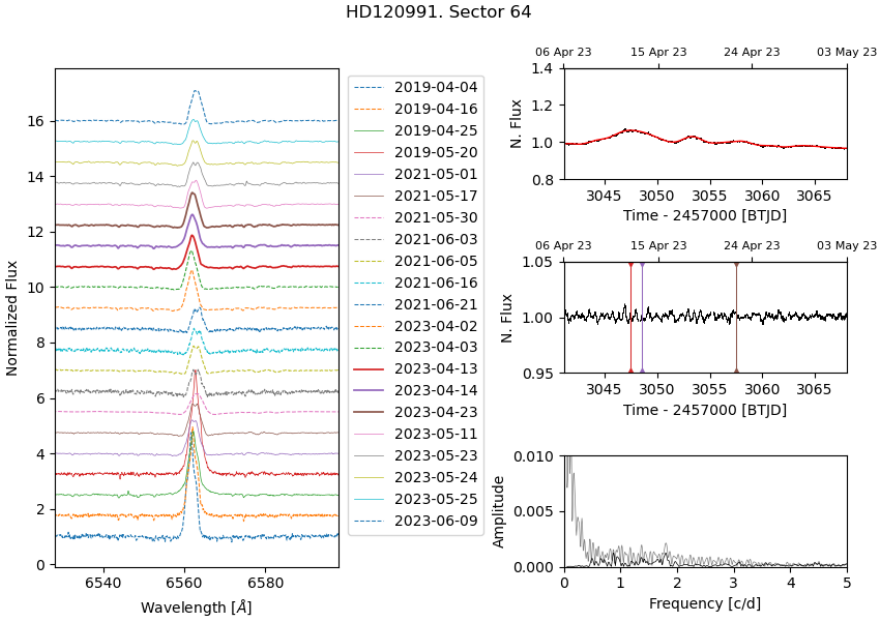

Figure 5.17: Results for the TESS sector 64 for the Be star HD 120991. The light curve was taken from Apr to May 2023. Three spectra coincide with the TESS observations window (solid colours).

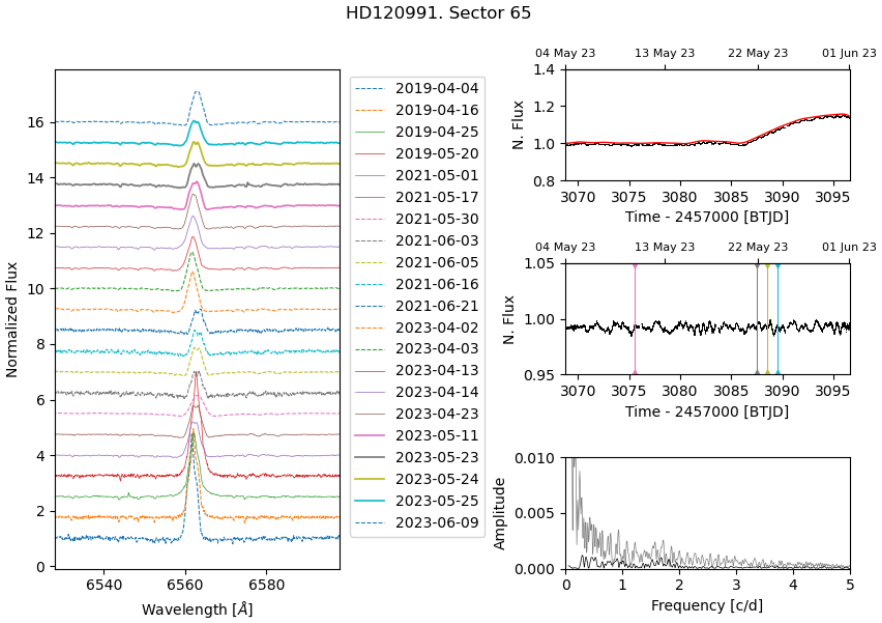

Figure 5.18: Results for the TESS sector 65 for the Be star HD 120991. The light curve was taken from May to Jun 2023. Four spectra coincide with the TESS observations window (solid colours).

were obtained from BeSS, 11 of them fall on the same dates as the TESS observations. Detailing the normalized light curves, which have the vertical lines of spectra dates, we can see in Figure 5.15 that two spectra fall within sector 11 dates.

The first spectrum (green one) shows a single-peak emission line for Hα; later, the same emission line (red one) has an increase in intensity. Since the changes in the light curve are seen later in the photosphere and disc (spectrography), this increase in line intensity could possibly be related to the start of the TESS light curve observation, where the brightness was higher. Suggesting a change in the disc approximately one month later.

All spectra of HD 120991, apart from the two mentioned before, seem to have the same intensity, shape and equivalent width. For sector 38, the line intensity decreased. This time a double peak is seen. Sectors 64 and 65 (Figure 5.17 and 5.18) have three and four spectra, respectively, that coincide with their dates. During sector 64 no changes are seen in the line. In sector 65, a double-apeak appears, and a small decrease in intensity seems to occur.

Sector 11	Sector 38	Sector 64	Sector 65
0.05646824	0.04581147	0.04544156	0.04446751
0.07446163	0.07082629	0.06513751	0.06613064
0.07545436	0.09399661		0.09523816
0.10352692	0.13002093	0.13133311	0.12242326
0.1366987	0.15981616	0.17088601	0.15317742
0.16910692	0.18914522		0.18581751
0.20290916	0.19545467		
0.23616209		0.23153718	0.22217531
0.27086409			0.24199584
0.30481736	0.31400853	0.29586776	
	0.38112561	0.35464239	0.33133374
		0.4208297	0.41001362
	0.83030166		
		0.87665837	
		1.80101378	

Table 5.4: List of frequencies [d^{-1}] found in the periodograms of HD 120991 in Sectors 11, 38, 64 and 65. Bold numbers represent the highest amplitude frequency in each sector. Above the horizontal line are the frequencies $< 0.5 d^{-1}$ (SLF).

5.5 HD 174237

HD 174237 (CX Draconis) is an interacting binary Be-type star located in the constellation of Draco and is classified as a B2Vne star. The system has an orbital period of 6.696 days, and it consists of HD 174237, a primary component and an F5III secondary, which fill the Roche lobe.

The classification indicates that the star is a hot, massive main-sequence star with a temperature ∼17500 K. The Be-star HD 174237 exhibits weak emission lines in its spectrum. The General Catalogue of Variable Stars (Samus' et al., 2017) classified this star as a GCAS+ELL, i.e., a γ Cas star which is a close binary system (although it is not considered as a γ Cas star due to their low X-ray emissions). The ELL classification comes from rotating ellipsoidal variables (b Per, Alpha Vir).

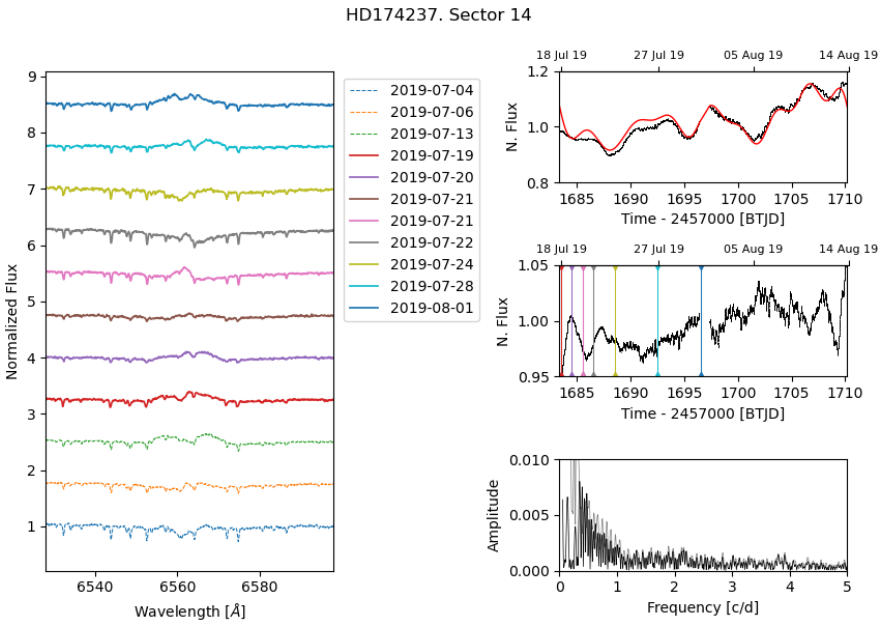

Figure 5.19: Results for the TESS sector 14 for the Be star HD 174237. The light curve was taken from Jul to Aug 2019. Eight spectra coincide with the TESS observations window (solid colours).

The source of the emission lines is a permanent accretion disc to the primary, which is highly variable (Richards et al., 2000). The companion is suggested to be an X-ray star that is phase-locked with the primary and is magnetically active due to rapid rotation (Guinan et al., 1984).

HD 174237 has a projected rotational velocity of $v_{\sin i} = 163$ km s^{-1}, a low velocity for its spectral type. Parameters such as mass (7.3 $M_{\odot}$), radius (4 $R_{\odot}$), temperature (17683 K), and radial velocity (-2.1 km s^{-1}), among others, were found Kervella et al. (2022).

The 13 light curves of HD 174237 in this study are highly variable, with low—and high-

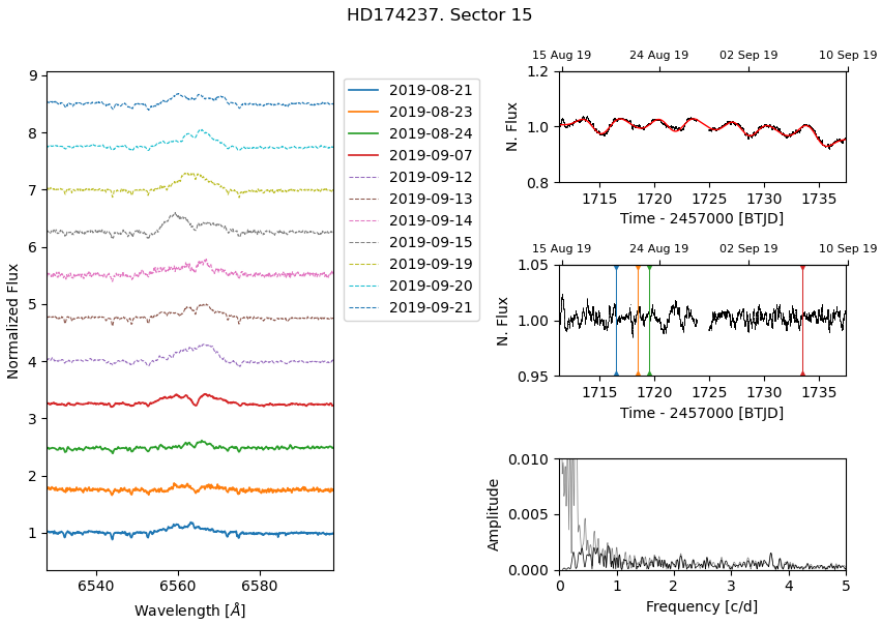

Figure 5.20: Results for the TESS sector 15 for the Be star HD 174237. The light curve was taken from Aug to Sep 2019. Four spectra coincide with the TESS observations window (solid colours).

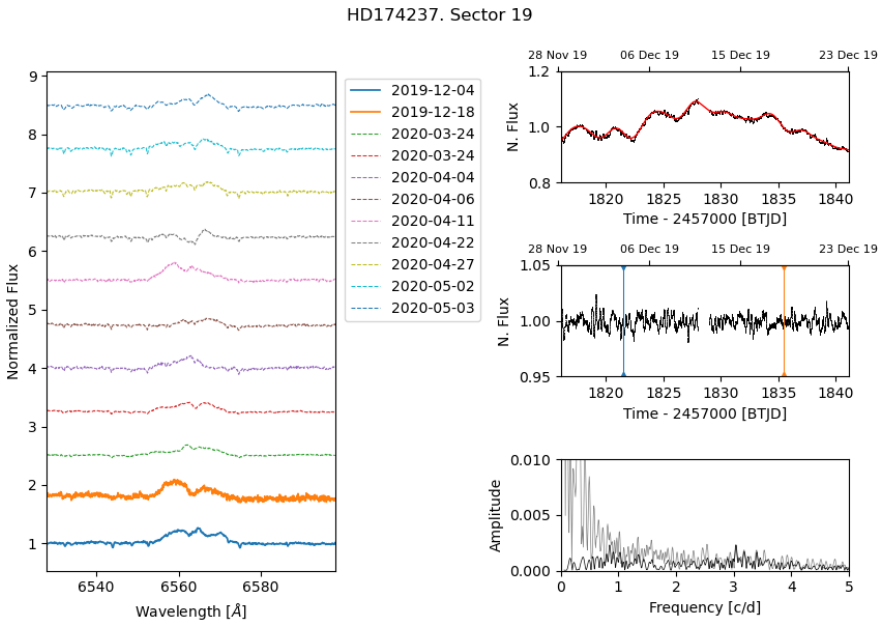

Figure 5.21: Results for the TESS sector 19 for the Be star HD 174237. The light curve was taken from Nov to Dec 2019. Two spectra coincide with the TESS observations window (solid colours).

frequency components throughout the sectors. Increasing and decreasing brightness and ellipsoidal variation appear and disappear throughout the observations.

The frequencies found mostly belong to SLFs, due to the high variability of the light curves,

for this reason, there is no intermediate line separating the SLFs and no bold frequencies. The period of the binary (6.69 days or 0.149 d^{-1}) was also recovered, especially in sectors 52, 53, 55 and 56 with the closest frequencies being 0.1447, 0.1503, 0.1512 and 0.1475 d^{-1}, respectively. Tables 5.5, 5.6, 5.7 and 5.8 contain all the frequencies found for this star.

From the beginning of the observations (Figure 5.19, 5.20), we can see the increase in brightness trend and the somehow hidden but noticeable ellipsoidal variations. The brightness starts to decrease by sector 15. From sectors 41 - 55, the changes in brightness stabilize, and the eclipses are more notorious.

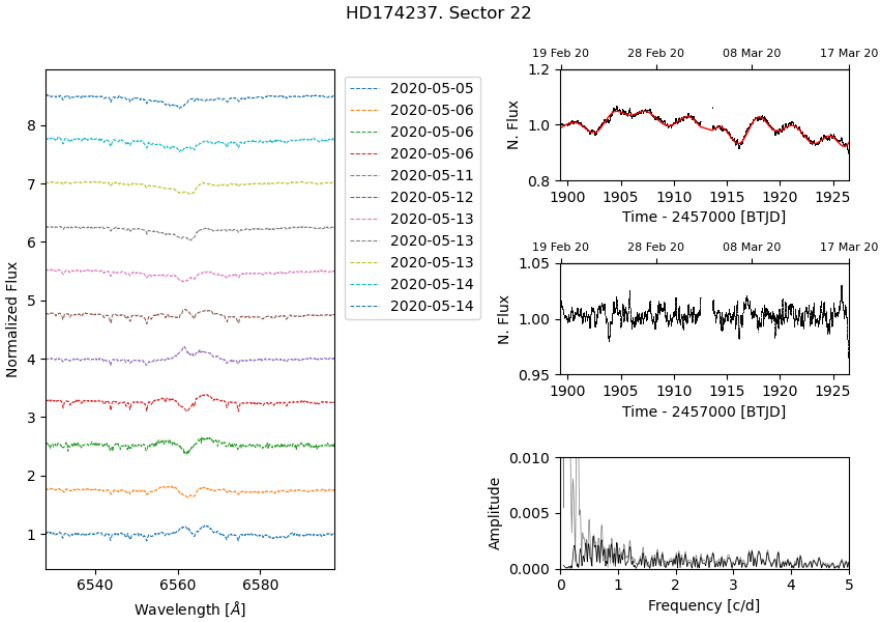

Figure 5.22: Results for the TESS sector 22 for the Be star HD 174237. The light curve was taken from Feb to Mar 2020. No spectra coincide with the TESS observation windows.

99 spectra were downloaded from BeSS, 54 of which fall within the period of the light curves from TESS. For better comprehension, the description will follow the spectra separation as in Figures 5.19 - 5.31.

During sector 13 (Figure 5.19), the Hα observations start in 2019-Jul-19 with wide wings. In the dates 2019-Jul-21 and 22, two days later, a left peak appeared and then disappeared two days later. The last observation in this sector is similar to the first one.

Sector 14 has a similar behaviour. The observations start in 2021-Aug-21 with a wide wing Hα that later, in 2021-Sep-07, shows a slight DPS appears. Following the observations in dashed lines in Figure 5.20, this DPS seem chaotic, in and out of the spectrum. In sector 19 (Figure 5.21), the spectra have a similar appearance. A DPS with erratic behaviour. During sector 22, there are no matching spectra, but it can be noticed that the DPS reappears this time

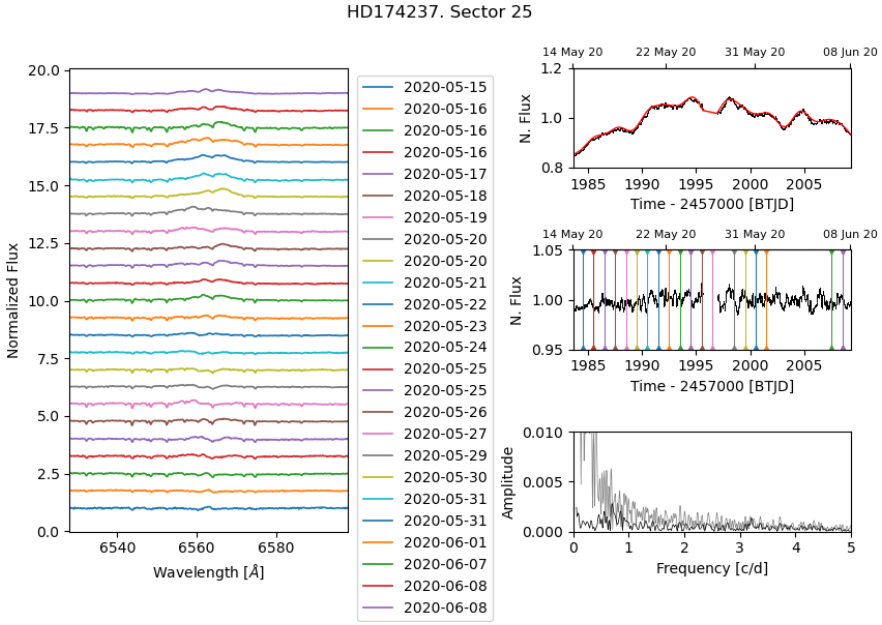

Figure 5.23: Results for the TESS sector 25 for the Be star HD 174237. The light curve was taken from May to Jun 2020. Twenty-five spectra coincide with the TESS observations window (solid colours).

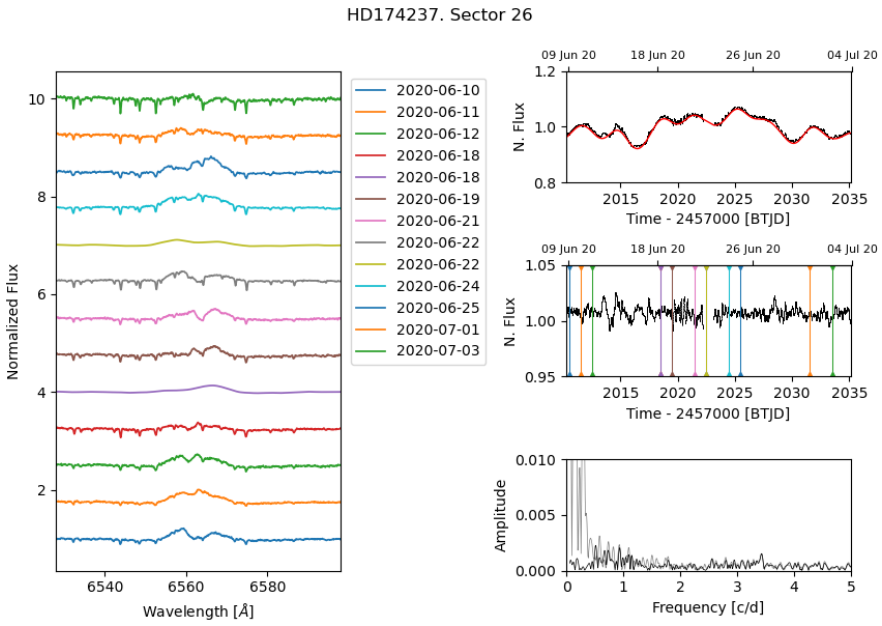

Figure 5.24: Results for the TESS sector 26 for the Be star HD 174237. The light curve was taken from Jun to Jul 2020. Thirteen spectra coincide with the TESS observations window (solid colours).

with a deeper valley.

Sector 25 (Figure 5.23) contains most of the spectra of this star. Low in intensity and with wide wings, Hα present no noticeable changes during these observations, except for the seeming

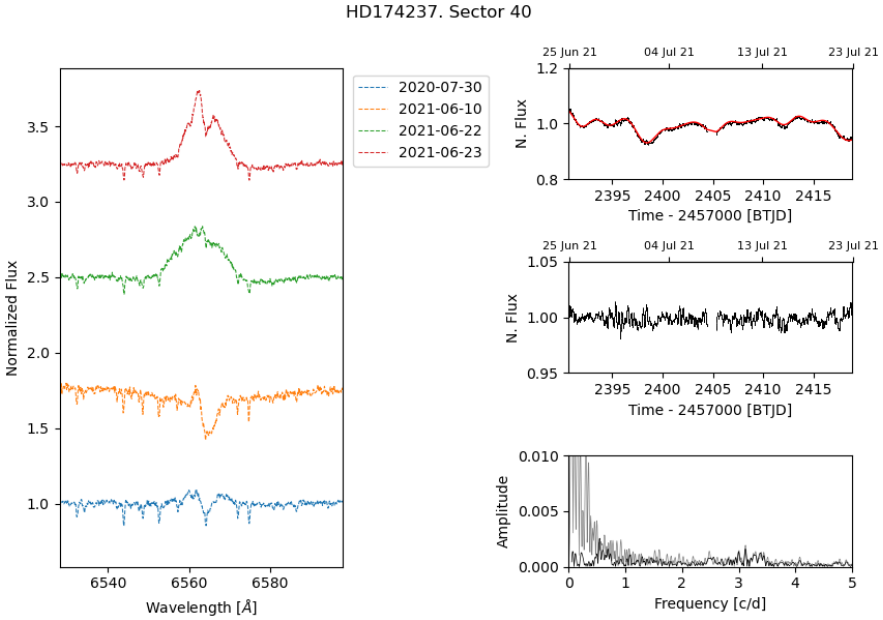

Figure 5.25: Results for the TESS sector 40 for the Be star HD 174237. The light curve was taken from Jun to Jul 2021. No spectra coincide with the TESS observations window (solid colours).

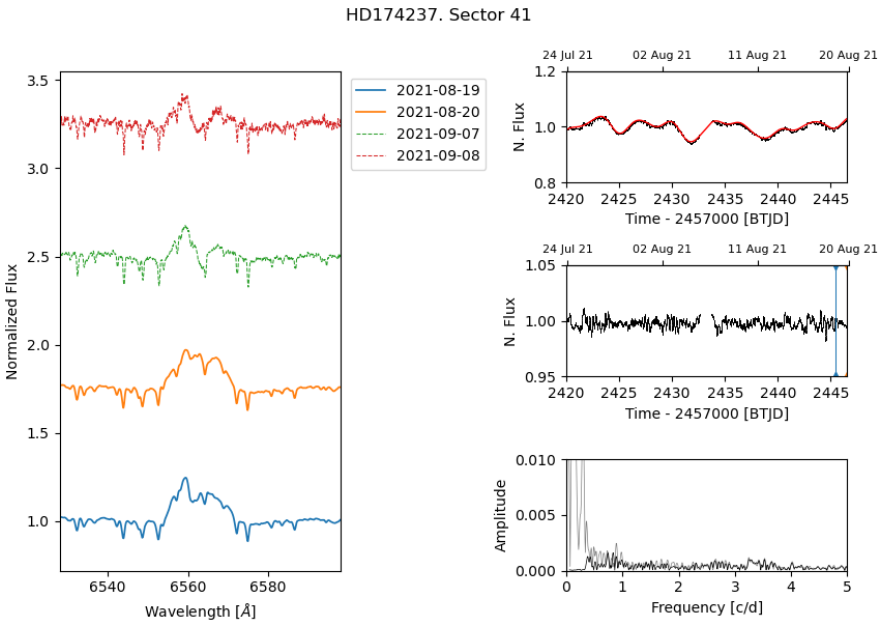

Figure 5.26: Results for the TESS sector 41 for the Be star HD 174237. The light curve was taken from Jul to Aug 2021. Two spectra coincide with the TESS observations window (solid colours).

change in V/R during days 29 and 30 May 2020.

During June 2020, in sector 26, Hα re-enters the instability stage of its DPS. The two peaks (2020-Jun-10) combine into one (2020-Jun-11 & 12), which then separates again (2020-Jun-21)

and then merges back together again (2020-Jun-24 & 25).

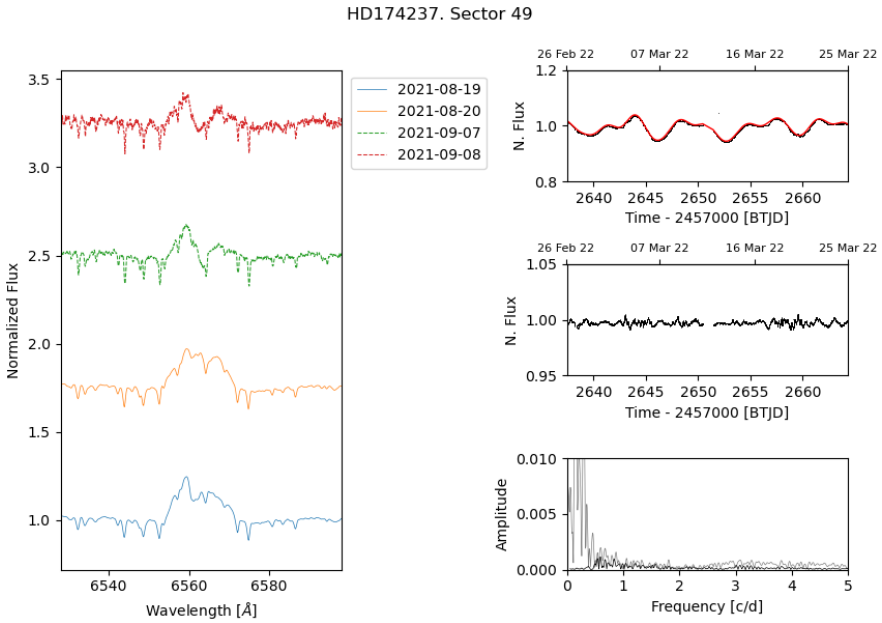

Figure 5.27: Results for the TESS sector 49 for the Be star HD 174237. The light curve was taken from Feb to Mar 2022. No spectra coincide with the TESS observations window (solid colours).

Sector 40 marks a new stage. In June 2021, Hα changes from absorption to emission with a DPS, with a red peak in higher intensity. In sector 41, this DPS starts to lower its intensity.

Finally, in sectors 52, 53, and 55, the DPS disappears completely, and then, on 22 July 26, a new emission starts that will become absorption (2022 August 27).

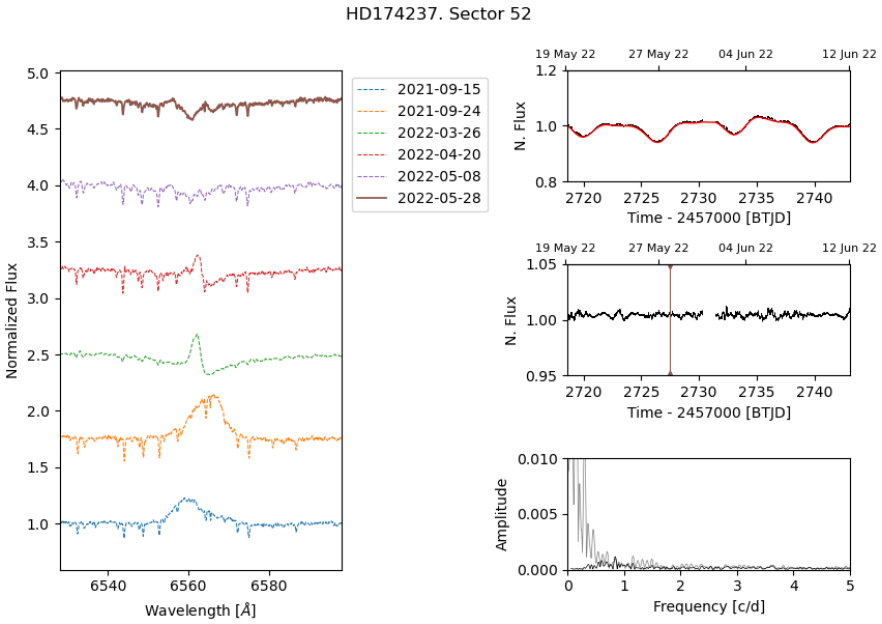

Figure 5.28: Results for the TESS sector 52 for the Be star HD 174237. The light curve was taken from May to Jun 2022. One spectra coincide with the TESS observations window (solid colours).

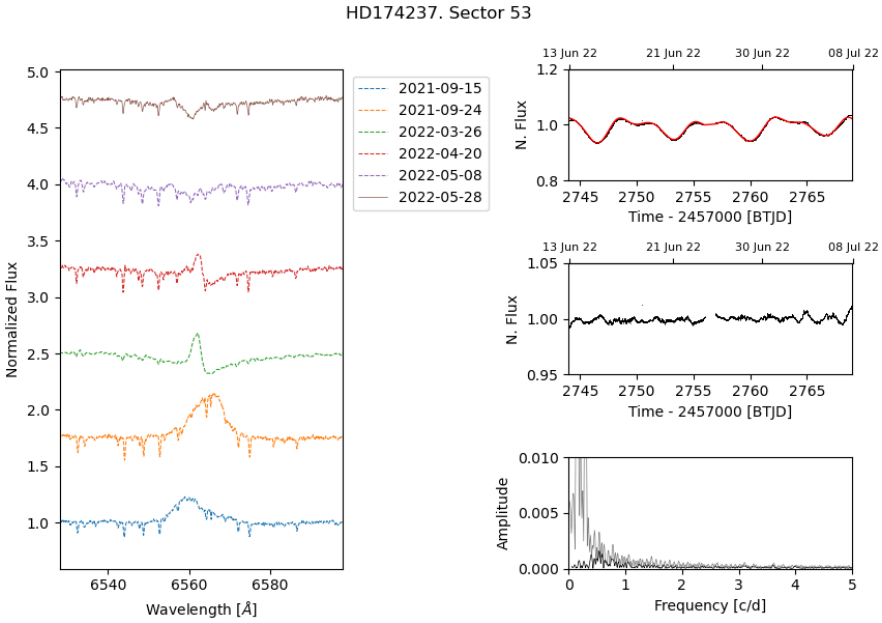

Figure 5.29: Results for the TESS sector 53 for the Be star HD 174237. The light curve was taken from Jun to Jul 2022. No spectra coincide with the TESS observations window (solid colours).

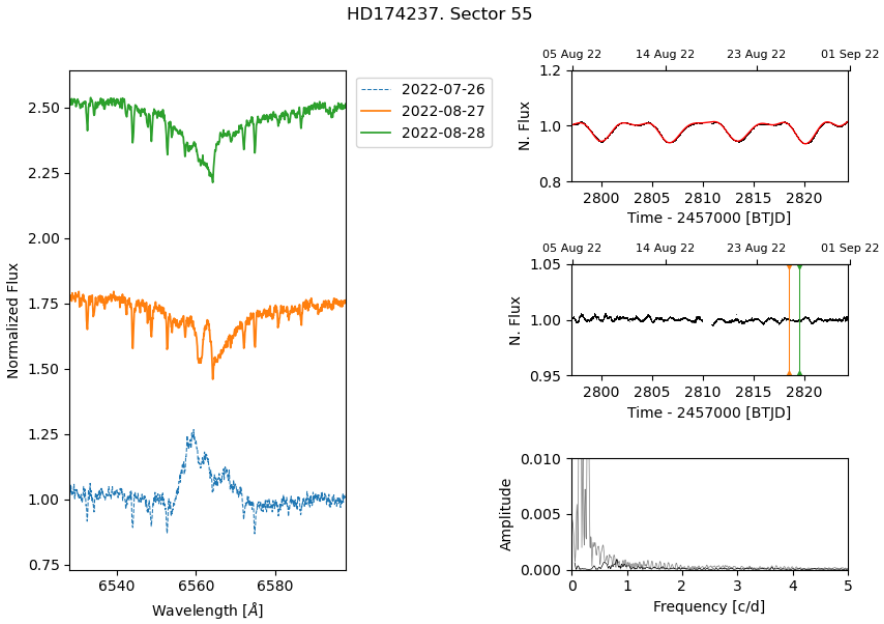

Figure 5.30: Results for the TESS sector 55 for the Be star HD 174237. The light curve was taken from Aug to Sep 2022. Two spectra coincide with the TESS observations window (solid colours).

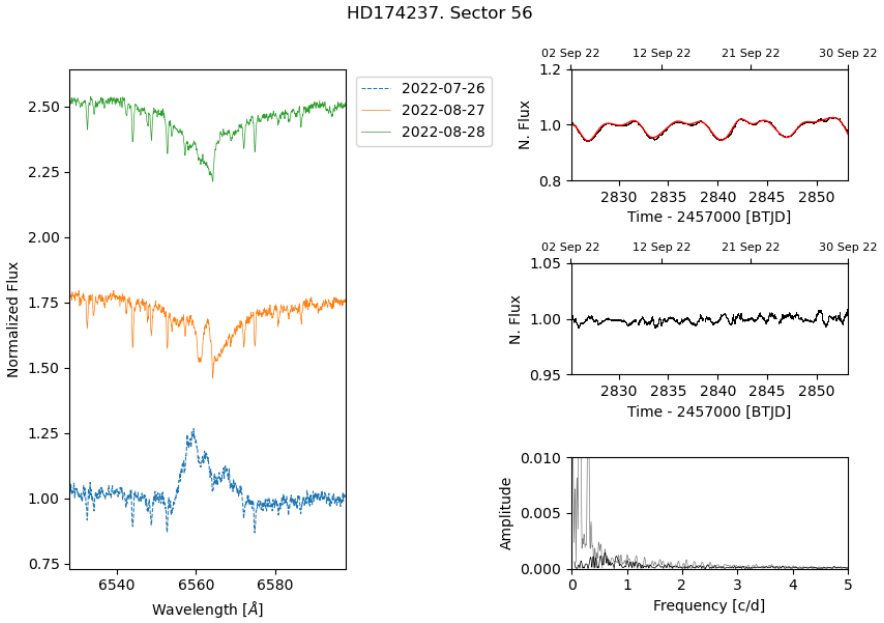

Figure 5.31: Results for the TESS sector 56 for the Be star HD 174237. The light curve was taken during Sep 2022. No spectra coincide with the TESS observations window (solid colours).

Sector 14	Sector 15	Sector 19
0.062362	0.046037	0.038257
0.063299	0.077591	0.075400
0.079342	0.112656	0.096421
0.106510	0.135299	0.201333
0.137336	0.170851	0.275289
0.169958	0.189411	0.299051
0.208414	0.297220	0.441080
0.244429	0.447153	0.848111
0.298048	0.609675	1.028749
0.321777	0.665702	3.041862
	3.693568	

Table 5.5: List of frequencies [d^{-1}] found in the periodograms of HD 174237 in Sectors 14, 15 and 19. Bold numbers represent the highest amplitude frequency in each sector. Above the horizontal line are the frequencies $< 0.5 d^{-1}$ (SLF).

Sector 22	Sector 25	Sector 26
0.040700	0.023910	0.053653
0.086912	0.053060	0.151489
0.110625	0.149439	0.244229
0.139290	0.229586	0.296610
0.167706	0.287060	0.322336
0.199851	0.320793	0.475064
0.291267	0.422600	0.516112
0.306022	0.707444	0.667479
0.376503	0.766400	0.732240
0.571926	0.841321	0.935845

Table 5.6: List of frequencies [d^{-1}] found in the periodograms of HD 174237 in Sectors 22, 25 and 26. Bold numbers represent the highest amplitude frequency in each sector. Above the horizontal line are the frequencies $< 0.5 d^{-1}$ (SLF).

Sector 40	Sector 41	Sector 49
0.049666	0.045393	0.061326
0.094961	0.099033	0.078674
0.156641	0.138508	0.150864
0.189290	0.160014	0.207065
0.285555	0.237287	0.230431
0.303220	0.297124	0.295893
0.343609	0.320298	0.419624
0.396933	0.484820	0.438488
0.441333	0.739121	0.592919
0.545893	0.833368	0.838935

Table 5.7: List of frequencies [d^{-1}] found in the periodograms of HD 174237 in Sectors 40, 41 and 49. Bold numbers represent the highest amplitude frequency in each sector. Above the horizontal line are the frequencies $< 0.5 d^{-1}$ (SLF).

Sector 52	Sector 53	Sector 55	Sector 56
0.051617	0.059539	0.065308	0.084338
0.081594	0.107687	0.083718	0.147562
0.105992	0.150360	0.120363	0.168928
0.144753	0.188107	0.151266	0.253478
0.196339	0.274870	0.210920	0.300820
0.223026	0.302252	0.241148	0.327080
0.298447	0.456530	0.295347	0.346751
0.366897	0.603836	0.347376	0.459496
0.483183	0.695144	0.432205	0.588751
0.603664	0.841552	0.538586	0.816181
		3.607475	3.626194
		3.992844	5.471928

Table 5.8: List of frequencies [d^{-1}] found in the periodograms of HD 174237 in Sectors 52, 53, 55 and 56. Bold numbers represent the highest amplitude frequency in each sector. Above the horizontal line are the frequencies $< 0.5 d^{-1}$ (SLF).

5.6 ζ Tauri

ζ Tauri (ζ Tau, HD 37202) is a B1IVe type star. It is very bright in magnitude, V 3.03. It is one of the most well-known Be stars, thanks to its brightness, with several data that spans interferometric techniques, photometry, spectroscopy and polarimetry observations.

ζ Tau is a spectroscopic binary star with a period of 133 days Harmanec (1984) but no identified companion. The nature of ζ Tau as a γ Cas type star was recently discovered by Nazé et al. (2022b). As mentioned, the γ Cas-type stars are thought to be in binary systems.

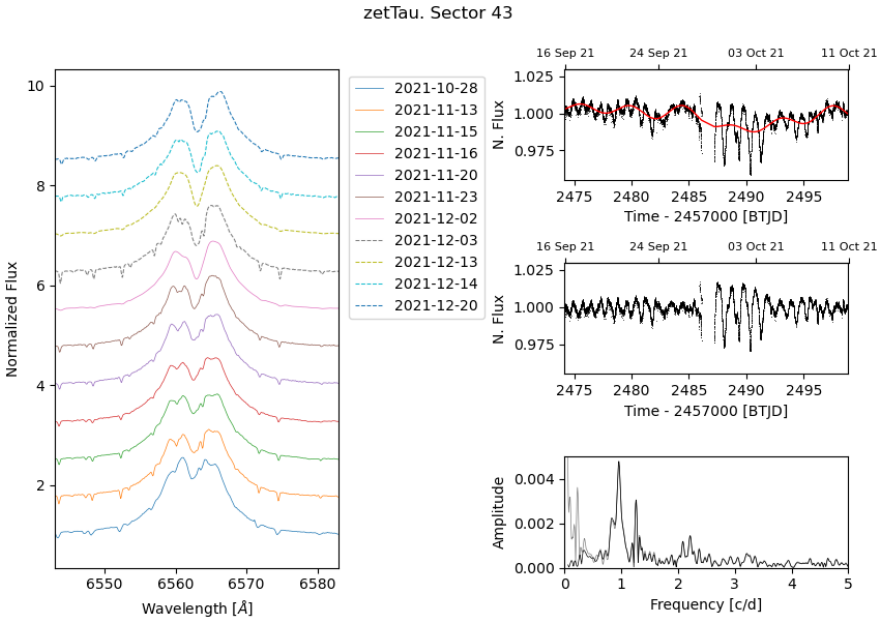

Figure 5.32: Results for the TESS sector 43 for the Be star ζ Tau. The light curve was taken from Sep to Oct 2021. No spectra coincide with the TESS observations window (solid colours).

Spectroscopic observations focused on variation in Hα, covering 1997–2008, revealed a cyclic behaviour of duration ∼1400 days (Štefl et al., 2009). This variation in the line profile suggests that the disc around ζ Tau is tilted and is precessing (Schaefer et al., 2010). Also, the precession in the disc is possibly due to the companion, which could be a main-sequence star or a white dwarf.

It appears in The General Catalogue of Be stars Jaschek & Egret (1982) with a $v \sin i = 310$ km s^{-1}. Posterior studies expanded the range of projected velocities from 225 km s^{-1} to 320 km s^{-1} (see Glebocki & Gnacinski (2005) for catalogue review).

The light curves of ζ Tau are presented in Figures 5.32, 5.33 and 5.34. The TESS telescope took the observations from sectors 43 - 45 (September - November 2021). As with all the Be stars in this study, ζ Tau also shows variability in its light curve. In sector 43, for example, a

saw-tooth pattern can be seen. The mean brightness in this sector is mostly constant, except around 2487 BTJD - 2490 BTJD, where the pattern breaks to give rise to a series of deep decreases in brightness and then returns to its initial position. This pattern repeats during sector 44; however, the light curve starts with the aforementioned deep changes in brightness and then resumes its average brightness. The period of this phenomenon is about ∼10 days.

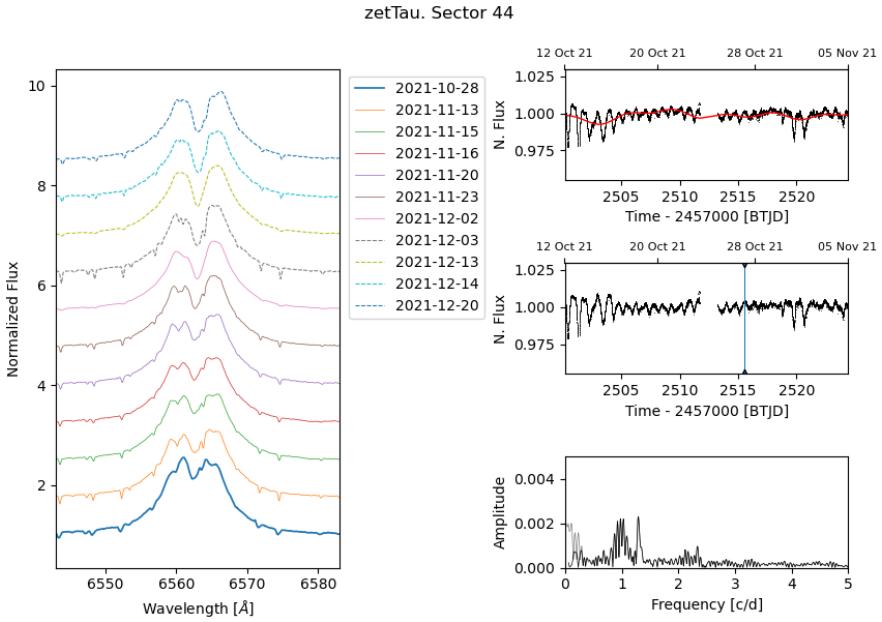

Figure 5.33: Results for the TESS sector 44 for the Be star ζ Tau. The light curve was taken from Oct to Nov 2021. One spectra coincide with the TESS observations window (solid colours).

The majority of our spectra fall in Sector 45. The light curve shows no noticeable changes. Short oscillations with durations of approximately one day are present again.

The periodograms, as well as the light curves, are shown in Figures 5.32, 5.33 and 5.34. A quick inspection of the periodograms shows that they are similar. They present clusters of repeated frequencies across the sectors, indicating that they are significant frequencies of possibly stellar origin. After the SLF fit, the light curve does not change much

In each periodogram, there are three well-determined frequency groups: ∼0.95 d^{-1}, ∼1.01 d^{-1} and ∼2.26 d^{-1}. These frequencies were found during the pre-whitening of the periodograms and listed in Table 5.9.

The spectra of ζ Tau from BeSS were obtained, covering the dates from October to December of 2021, coinciding with TESS observations. A total of 11 spectra were downloaded, 7 of which coincide with the TESS light curves.

ζ Tau shows the Hα double-peak profile, indicative of a disc in Keplerian rotation. The spectra show consistency in all the dates we have in this study. There are little changes in shapes,

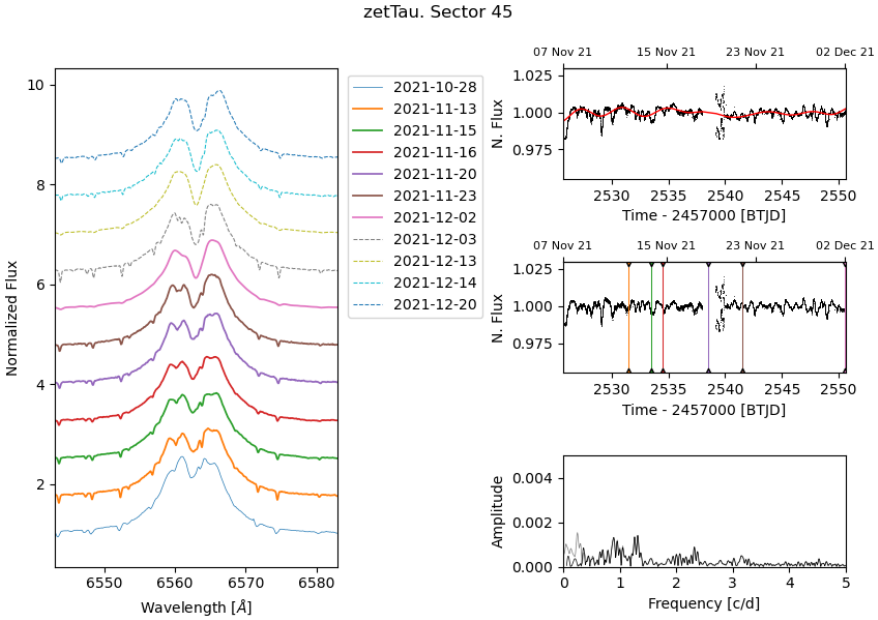

Figure 5.34: Results for the TESS sector 45 for the Be star ζ Tau. The light curve was taken from Nov to Dec 2021. Six spectra coincide with the TESS observations window (solid colours).

equivalent widths or line intensity. On close inspection, we can see a small movement of the central valley to the right, indicating a change in radial velocity. Also, with this variation, from 2021-12-02 until 2021-12-20, a subtle but constant increase in the left peak magnitude can be seen.

Sector 43	Sector 44	Sector 45
0.038884	0.078622	0.057993
0.091683	0.096629	0.135174
0.157298	0.236478	0.258565
0.228509		0.273663
	0.805677	0.790603
0.837299		0.888423
0.895920		
0.950760	0.927206	0.955151
0.998889	0.994003	
	1.018547	
	1.096368	
1.258637		**1.267138**
	1.292271	1.309538
2.212499	2.337140	2.318874

Table 5.9: List of frequencies [d^{-1}] found in the periodograms of ζ Tau in Sectors 43, 44 and 45. Bold numbers represent the highest amplitude frequency in each sector. Above the horizontal line are the frequencies $< 0.5 d^{-1}$ (SLF).

CHAPTER 6

Discussion

In this section, we thoroughly examine the observational and theoretical results obtained for the six Be stars: f01 Cyg, HD 45314, HD 110432, HD 120991, HD 174237, and ζ Tauri. We discuss the general results for the six stars, and then we go through each star in detail.

The table 6.1 summarises all the results found for the stars in this section. It lists the frequencies found as well as their corresponding pulsation mechanisms and also details whether the star is a confirmed or unconfirmed binary star along with its orbital period.

Each star presents unique aspects that reflect the diversity within the Be star population, yet they also share several common traits that allow for a meaningful comparative analysis. For instance, ζ Tauri and f01 Cyg, both classical Be stars, exhibit significant variability in their emission lines and photometric profiles, indicative of changes in their circumstellar disks. These variations are likely driven by the dynamical processes within the disc, such as density waves or interactions with a possible companion star. In contrast, HD 110432, often cited as an archetype of the γ Cas analogues, displays X-ray emissions that are unusually strong for a Be star, suggesting a different interaction mechanism, possibly involving magnetic fields or accretion processes by a companion that are not as prominent in the other stars in this study.

HD 174237 (B2 IIIe), provides insights into the early main-sequence evolution of Be stars. Its projected rotational velocity is estimated to be in the range of 150-200 km s^{-1}. This star also shows signs of variability in its disc structure, as evidenced by changes in its spectral lines over time. The presence of emission lines, coupled with the observed variability, suggests that its disc is not a stable structure but also a dynamic environment subject to continual change,

possibly influenced by the star's companion.

HD 120991, while similar in many respects to the other stars, stands out as one of the most variable cases in this study (along with HD 174237). Its strong variability, compared to other Be stars like ζ Tauri, provides an opportunity to explore the conditions necessary for disc formation and the role of stellar mass and rotational velocity in this process. Comparing HD 120991 with less variable stars may offer insights into how disc stability and the onset of the Be phenomenon contribute to the diverse observational characteristics seen across the Be star population.

Finally, this discussion will explore the broader implications of these findings for our understanding of the study of these six stars, with their varying degrees of disc activity and stellar parameters, which allows us to piece together a more comprehensive picture of how Be stars evolve, lose mass, and interact with their environments. By comparing our results, observational data, and theoretical models, we aim to learn more about the factors that drive the formation and evolution of Be stars' discs.

Star	Spec. Type	$v \sin i$ kms s^{-1}	Incl deg	Precessing	Binarity	Outburst	f d^{-1}	Group Range
f01 Cyg	B1.5Vnne	387	33.2	Yes	Yes[a] (28.2 d)	-	**1.66, 1.90, 2.05, 3.84**	g-mode
HD 45314	O9:npe	291	40.6	-	-	?	**1.11, 1.22, 1.75, 3.36**	g-mode
HD 110432	B0.5IVpe	419	85.4	?	?	?	**1.37, 1.57, 2.95**, 9.60	g-mode + p-mode
HD 120991	B2IIIe	75	13.0	-	-	Yes	SLF, 0.87, 1.80, 3.5	g-mode
HD 174237	B3+F5III	173	73.2	Yes	Yes[b] (6.69 d)	?	SLF	-
ζ Tau	B1IVe	326	66.0	-	Yes[c] (133 d)	Yes	**0.95, 1.01, 1.26**, 2.3	g-mode

Table 6.1: Summary of the results for the six stars. Bold frequencies are taken from each star's result table and mean the highest amplitude frequency in each sector. SLF stands for Stochastics Low Frequencies ($< 0.5\,d^{-1}$). The others are representative of a group of frequencies observed in the light curve but with low amplitude. The "Yes" convention appears in the columns Precessing, Binarity and Outburst. If no reference is given, the result is from this thesis, and for those results that are not conclusive, a question mark is added. The hyphen stands for no information in the literature or this thesis. In the Binarity column, the orbital period is given in units of days. The group range classification is a convention from Labadie-Bartz et al. (2022). $v \sin i$ and inclinations angles from Frémat et al. (2005). References: [a] Maintz et al. (2005), [b] Koubsky (1978) and [c] Ruždjak et al. (2009).

6.1 f01 Cygni

f01 Cyg, also known as 59 Cyg, is a Be-type star with a spectral classification of B1.5Vnne. This star is part of a binary system with an orbital period of 28.2 days, confirmed through spectral observations of the He II 4686 line by (Maintz et al., 2005; Peters et al., 2013). For this star, we found frequency clusters centred around 0.90 d^{-1}, 2.05 d^{-1}, and 3.84 d^{-1}. In addition to these clusters, we also found a frequency related to the orbital period of the binary system of 0.036400 d^{-1} or 27.7 d, being most prominent in sector 55. Nearby frequencies were found in the different sectors observed for f01 Cyg. All these frequencies are in the range of non-radial g-mode pulsations ($0.5\ d^{-1} < f < 5\ d^{-1}$).

Non-radial pulsations in Be stars often manifest as frequency clusters in frequency spectra. non-radial g-mode pulsations naturally form frequency groups that will oscillate at slightly different frequencies, generating the ”pulsating beats” visible in Sector 55 and, more notably, in Sector 56. The ”pulsating beats” seem to have a periodic repetition with no clear frequency in the periodograms but are identified visually at around ~ 10 d. The frequency groups, hence, the non-radial pulsations, can generate periodic changes in the spectrum (Osaki, 1971).

The companion of f01 Cyg has been observed through its ultraviolet spectrum, revealing it is a subdwarf O star (sdO), contributing approximately 4% of the total flux of the system (Peters et al., 2013). The influence of this companion extends beyond its UV contribution, as it heats the outer regions of the Be star’s circumstellar disc, particularly affecting the emission observed in the He I λ 6678 line, which varies in phase with the binary’s orbital period (Maintz et al., 2005; Peters et al., 2013). This suggests a direct correlation between the position of the sdO companion and the variable emission from the disc.

Although the exact rotational velocity of f01 Cyg remains uncertain, it ranges from 260 km s^{-1} (Slettebak, 1982) to recent estimates at 379 ± 22 km s^{-1} (Chauville et al., 2001). With different values for $v \sin i$ observed in different wavelengths, it is possible that it could be affected by stellar winds or the disc itself. During August and September 2019, from Sector 15 to 16 observations, we noted an increase in the deep of the variations. The observed photometric variations follow the orbital period, consistent with slow changes in brightness. These variations may be influenced by $m = 2$ waves in the disc, induced by tidal forces from the binary companion.

A major episode of high activity was observed in 1971, marked by a notable increase in the star’s emission, described as an ‘explosion’. After this, f01 Cyg experienced shell phases (Baade et al., 2023). The first documented shell phase occurred in June 1973, characterized by changes in H lines and He I emission (Doazan et al., 1975). A second shell phase followed in

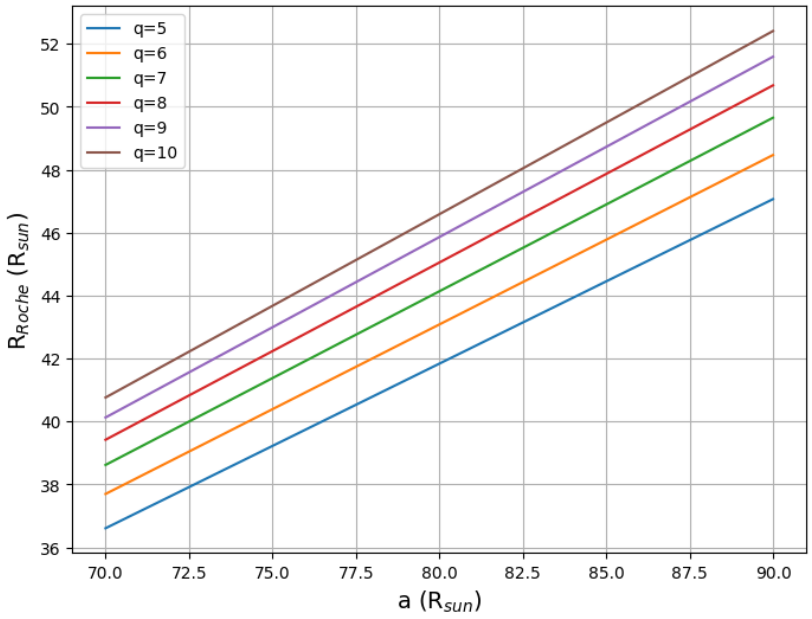

Figure 6.1: Roche radii for different mass ratios $q = M1/M2$

October 1974, peaking two months later and lasting approximately 160 days (Barker, 1982). The star's emission diminished drastically, reaching a minimum by late 1977 when the circumstellar disc almost disappeared. These phases are significant markers of variability in Be stars, often signalling changes in the structure of the circumstellar disc.

The presence of the sdO companion plays a crucial role in shaping the behaviour and configuration of f01 Cyg's disc. This system shares similarities with other Be binary systems such as FY Canis Majoris and ϕ Per, where the sdO companion also heats and potentially truncates the circumstellar disc (Peters et al., 2013). These similarities reinforce the theory that the sdO companion in f01 Cyg has been integral in spinning up the Be star through mass transfer, a process suggested by Peters et al. (2013).

Following this relation, we can estimate the flux ratio of the Be star and its companion, the sdO:

$$\frac{f_2}{f_1} = \frac{F_2}{F_1}\left(\frac{R_2}{R_1}\right)^2, \tag{6.1}$$

where $F2/F1$ is the monochromatic flux ratio per unit area. From Peters et al. (2013), the stellar parameters for this star and its companion are: $T_{eff,1} = 21800$ K $T_{eff,2} = 52100$ K; and $5.5 < R_1/R_\odot < 7.0$, $0.34 < R_2/R_\odot < 0.43$. Taking the average of the radii and computing the stellar luminosities, we found that the flux ratio f_2/f_1 between the sdO and the Be star in the f01 Cyg system is approximately 0.124. This means that the flux of the secondary star is about

12.4% of the flux of the primary star. Therefore the flux from the Be star is dominating the spectrum.

According to the sector model proposed by Štefl et al. (2000), a sector of the Be star's circumstellar disc, which faces the hot, low-mass companion, is partially ionized by the UV radiation from the sdO star. This interaction between the companion's radiation and the Be star's disc can explain the observed variability in f01 Cyg.

The Be stars are thought to be formed in mass transfer from close binary interactions, leaving a stripped star. A second mass transfer is possible if the disc of the Be star reaches the Roche radius. We want to know if f01 Cyg is near this event. If we estimate the Roche radius following Eggleton (1983), then we obtained a Roche radius of approximately 42.56 $R_\odot$ for f01 Cyg, assuming a separation between the stars of 73.3 $R_\odot$, and the mass ratio of $q = M1/M2 = 10.31$ (Values from Peters et al. (2013)). To support our estimation, a range of values was calculated and plotted in Figure 6.1. Our estimate falls within the range of values for the Roche radius, calculated using orbital parameters compiled by Peters et al. (2013).

The next step was to calculate the radius of the Be star's disc. We used an empirical relation $R_h/R_* \sim (v\sin i/DPS)^2$, given by Huang (1972), which links the projected rotational velocity $v\sin i$ and the DPS being the separation between the violet and red peaks of the Hα emission line. With estimated values of $v\sin i = 379$ km s^{-1} and a $DPS \sim 246.94$ km s^{-1} (from the 2022-07-16 spectrum), we calculate the radius of the circumstellar disc to be approximately 2.62 times the radius of the star, which correspond to $\sim 15R_\odot$. However, this value may be underestimated due to the influence of the secondary, which can disturb the Be disc and affect the direct mapping of peak separation to disc radius.

If we compare both radii, we observe that the disc radius is much smaller than the Roche radius. This implies that the circumstellar disc of f01 Cyg lies completely within the stability limit defined by the Roche radius. As a result, the forces of the companion star do not significantly affect the disc structure, suggesting that the material in the disc is in a stable region.

Recent studies have analyzed the photometric variability of f01 Cyg, identifying frequency variations as reported by Labadie-Bartz et al. (2021). Their study identified four distinct frequency groups in γ Cas: $g1 = 0.998$ d^{-1}, g2 $= 2.380$ d^{-1}, $g3 = 5.070$ d^{-1}, and $g4 = 7.571$ d^{-1}, a pattern that is also observed in f01 Cyg. This behaviour suggests that f01 Cyg is a non-radial pulsator. Baade et al. (2023) mentions that a study to be published by J. Labadie-Bartz and T. Rivinius found the strongest two frequency groups are centred near 1 d^{-1} and 2 d^{-1}, the third frequency group is centred around 3.9 d^{-1}, and like many other Be stars are due to non-radial pulsations. As mentioned before we found frequency clusters centred around 1 d^{-1}, 2.05 d^{-1}, and 3.84 d^{-1}.

Throughout all spectral observations, the equivalent width remained constant during the 2019 measurements, experiencing only a slight variation in 2022, attributable to the transient appearance of a variation in the V/R ratio.

In addition, no changes in shape, line intensity, or line profile (except as mentioned above) are observed. However, the spectra in 2019-08-18 and 2019-08-30 present a slight cut-like at the tip, possibly the disc being truncated by the companion. The spectra's visually constant intensity (and also no visible increase in the flux of the light curves) means that there was no outburst or the mass loss rate remained constant.

6.2 HD 45314

HD 45314 is classified as an O9:npe star, a massive analogue to Be stars. HD 45314 displays emission lines in the Balmer series, with variability in both its brightness and spectra. Moreover, HD 45314 has been characterized as a γ Cas analogue, largely due to its bright and hard X-ray emissions, as reported by Rauw et al. (2013).

Twenty-five spectra of HD 45314, obtained from the BeSS database, span the time range from 2019 to 2021. Of these, seventeen align with TESS observations, with eleven spectra recorded during Sector 44 and six during Sector 45. From October 16 to November 21, 2021 (Sector 44), no significant variations in the enclosed flux in the line profile are observed, but a rapid V/R variation of about 5 days can be seen.

Simultaneously, during Sector 43, an increase in flux is observed, which could be attributed to the ejection of mass during an outburst event. Subsequently, in Sector 44, the flux stabilizes and remains consistent compared to the previous sector. Finally, in Sector 45, the flux begins to decrease, likely due to the redistribution of the ejected material around the star. This process leads to the formation of a single-peaked structure in the spectrum.

From November 21, 2021, onwards, the shape of the line profile changes, going from a DPS profile to a one-peak broad emission line. Following Marr et al. (2018), this is an indication of a precessing disc, more probably because of the presence of a companion.

The periodogram of HD 45314 aligns with the typical profile observed in Be stars, characterized by frequency groups that vary in amplitude over time. During TESS Sectors 43, 44, and 45, increases and decreases in brightness were detected, indicative of significant variability in its light curve. Several dominant frequency groups were identified around 1.11, 1.22, 1.75, and 3.36 d^{-1}, with 3.36 d^{-1} being the most prominent during Sectors 43, 44 and 45. These frequencies are consistent with non-radial g-mode pulsations.

A closer examination of the light curve reveals a low-frequency range ($f < 5$ d^{-1}), with no

significant high frequencies detected ($f > 5$ d^{-1}). This low-frequency variability, along with observed amplitude changes, implies a pattern of fluctuating frequency groups. Interestingly, the amplitude of these variations does not exceed 0.01 mmag, indicating relatively subtle fluctuations in brightness.

Despite its variability, HD 45314 does not fall within the rotational modulation range typical of stars with magnetic spots or stellar winds. Instead, it is likely influenced by coherent or non-coherent g-mode pulsations, possibly linking it to the Oe/Be phenomenon. Research by Burssens et al. (2020) suggests a connection between the presence of frequency groups and the behaviour characteristic of γ Cas stars. Lanthermann et al. (2023) studies the multiplicity of O-type stars using optical long baseline interferometry (OLBI). Their results were analysed using the CANDID software, which allows the detection of potential companions. They noted HD 45314 as a candidate for binarity based on marginally significant criteria ($3 < n\sigma < 4$). However, it is not yet a confirmed binary system.

Studies of γ Cas stars Nazé et al. (2020b) reveal a broad structure peaking at 0.288 d^{-1} for HD 45314, with considerable frequency and amplitude variability in the observed spectra. Burssens et al. (2020) also found a similar dominant frequency at 0.287 d^{-1} in their observations, suggesting that the 0.28 d^{-1} signal in HD 45314 may result from the difference between two close frequencies, 1.184 d^{-1} and 1.460 d^{-1}, these are frequency combinations that can be interpreted as interactions between multiple modes (Semaan et al., 2018). We only found this frequency in Sector 43 hidden under the stochastic low-frequency. Furthermore, Burssens et al. (2020) highlighted stochastic low-frequency behaviour in HD 45314, along with coherent signals within the frequency range of 1.5 to 4.5 d^{-1}.

Its variable light curve, coupled with significant spectral changes and X-ray emissions, suggests a dynamic interplay between pulsations and circumstellar activity. Future observations, particularly those involving high-resolution spectroscopy and X-ray monitoring, will be essential for a more comprehensive understanding of this star's complex behaviour.

6.3 HD 110432

HD 110432 (BZ Cru, HR 4830) is a peculiar Be star (B0.5IVpe) that has garnered significant attention due to its distinctive optical and X-ray spectra features. Classified as a B0.5IVpe star, HD 110432 stands out from typical O-B stars, generally characterized by soft X-ray emissions of moderate luminosity (de Oliveira et al., 2007b; Smith et al., 2012; Torrejón et al., 2012). Instead, HD 110432 exhibits hard X-ray emissions and high luminosity, placing it as a γ Cas analogue (Smith & Balona, 2006), like the other stars in this Section. These characteristics

make it an intriguing object for studying high-energy astrophysical phenomena.

The spectrum of HD 110432 displays several emission lines, particularly from Fe II and He I, which often exhibit double-peak profiles. This line shape suggests that the circumstellar disc is observed nearly edge-on (Smith & Balona, 2006). The size and structure of the disc were analyzed in detail, revealing an extensive disc spanning over 1 AU and a projected area of 100 stellar radii, significantly larger than the disc typically observed in γ Cas itself. The mean disc temperature, derived from the fitting of Fe and He lines, is estimated to be 9800 K, and the column density, inferred from the equivalent width ratios of He lines, is approximately 3×10^{22} cm^{-2} (Smith & Balona, 2006).

Initial X-ray observations of HD 110432 suggested a periodic signal of 14 ks, which could hint at the presence of a white dwarf companion, potentially causing partial occultation of a hot spot on its surface (Torrejón & Orr, 2001). However, subsequent studies found no consistent evidence of this periodicity, demonstrating its spurious nature (de Oliveira et al., 2007b; Torrejón et al., 2012). Despite this, HD 110432 is highly variable in X-rays, with long-term cycles observed, including a notable 226-day cycle Smith et al. (2012). The absence of coherent pulsations, especially the 14 ks signal, challenges the hypothesis of a compact companion and suggests that the variability is intrinsic to the star disc system.

Detailed interferometric studies by Stee et al. (2013) provided valuable insights into the geometry and kinematics of the disc surrounding HD 110432. Using observations in the H- and K-bands, they modelled the shape and size of the disc, finding that the disc diameter measured through the Brγ emission line was $5.1 \pm 0.25 R_*$, while the estimation from He I lines yielded $3.9 \pm 0.5 R_*$. The smaller size inferred from He I suggests that this emission originates from a more internal region of the disc, closer to the star.

Analysis of the rotational velocity indicates that HD 110432 is near its critical velocity, with a ratio of $V_{rot}/V_c \sim 1.0 \pm 0.2$. This rapid rotation, coupled with the observed "S" shape in the differential phase diagram—reminiscent of the pattern seen in ζ Tauri—provides strong evidence of a one-armed spiral structure in the disc (Stee et al., 2013).

HD 110432 exhibits notable variability in its photometric observations, as highlighted in studies using ground-based instruments and space telescopes such as TESS. Frequencies detected in prior analyses, such as a signal at 1.77 days (Barrera et al., 1991), were supplemented by more recent findings. A prominent frequency of 9.6 d^{-1} was consistently detected across various observing periods (2003-2011, 2016, and 2019), suggesting a non-radial pulsation mode with an estimated degree of $l \sim 3 \pm 2$ (Nazé et al., 2020a). Additional signals around 1.6 d^{-1} were identified by multiple instruments (SMEI, BRITE, and TESS), revealing a complex pattern of pulsations.

Instrument	f (d^{-1})
SMEI	1.0343, 1.5758, 2.9458, 9.5880
BRITE	1.039, 1.573, 2.918, 9.584
TESS	1.032, 1.576, 2.952, 9.588

Table 6.2: Table from Nazé et al. (2020a) highlighting the most remarkable frequencies of HD 110432 with the different instruments used in their study.

The high-frequency signals detected in HD 110432 are interpreted as non-radial p-mode pulsations, which are uncommon in Be stars. This indicates a unique aspect of the star's internal structure. The mix of low- and high-frequency signals suggests the coexistence of several g-modes along with a single p-mode.

The spectroscopic data from the BeSS database, covering 2019 to 2023, reveal that the Hα line consistently appears in emission, with a nearly symmetrical profile throughout the observations. However, a subtle change in the orientation of the emission tip—from pointing right (2019-2021) to left (2021-2023)—hints at possible asymmetries induced by a companion. HD 110432 has no confirmed companion, a situation that mirrors other γ Cas analogues where binarity, if present, is inferred only through indirect signatures, e.g. RV variations.

The intensity of the Hα emission line remained quasi-constant, with a slight increase observed from 2019 to 2021. Notably, during Sector 64 (April 2023), a "wine-bottle profile" emerged, suggesting a precessing disc structure. However, this interpretation remains uncertain.

Our photometric observations from TESS during Sectors 11, 37-38, and 64-65 reveal several groups of frequencies, including signals at 1.03, 1.3, 1.5, 2.9, 6.5, 7.8, and 9.5 d^{-1}. These frequencies align with those detected in previous studies using SMEI, BRITE, and TESS from 2003 to 2019 by Nazé et al. (2020a). HD 110432 is distinct as the only star in this Section showing high-frequency p-mode pulsations at 9.5 d^{-1}, while the other detected frequencies are attributed to g-modes.

Amplitude variations are common, with the 9.5 d^{-1} signal decreasing over four years, while the 1.3 d^{-1} and 1.5 d^{-1} signals are steadily increasing. However, if we compare Sector 11 with Sector 37, the light curve shows small variations, which are reflected as an increase in the amplitude of the small frequencies. A similar frequency shift was noted by (Huat et al., 2009) during a minor outburst in V739 Mon, where p-modes weakened, and g-modes emerged at lower frequencies. A comparable pattern was observed in HD 110432 during Sectors 38 and 65. It can be concluded that there is no relation between the changes seen at the tip with low frequencies.

HD 110432 is a remarkable example of a γ Cas analogue, distinguished by its strong X-ray

emissions, rapid rotation, and complex disc dynamics. It required more observations, especially in the visual range, to study the changes in the disc through Hα. Its unique combination of non-radial pulsations, disc asymmetries, and evolving photometric signals provides a valuable case study for understanding the interplay between stellar rotation, pulsational behaviour, and circumstellar environment in Be stars.

6.4 HD 120991

HD 120991, also known as V767 Centauri or HR 5223, is a B2IIIe-type star. It is classified as a Be star by Jaschek & Egret (1982). It has an estimated $v \sin i = 70$ km s^{-1} (Frémat et al., 2005). It is characterized by prominent emission lines in its spectrum, particularly in the Hα line.

As a γ Cassiopeiae (γ Cas) analogue, HD 120991 displays peculiar X-ray properties. Nazé et al. (2022b) conclude a high X-ray luminosity, ~ -5.4, which is unusually elevated for a B-type star. The X-ray plasma temperature is measured at approximately 6.4 keV, indicative of a very hot environment. This temperature suggests that the X-rays originate from a high-energy process in or around the circumstellar disc. Finally, the hard-to-soft flux X-ray ratio is around 2, which signifies that a large portion of its X-ray emission is from high-energy photons. This hard X-ray spectrum is characteristic of γ Cas stars and is atypical of other Be stars, where softer X-rays are more common. X-ray emissions may result from star-disc interactions or shock heating within the circumstellar material.

Our results show that HD 120991 is a highly photometric variable star. We analysed Sectors 11, 38, 64 and 65 of TESS, all exposed in Figures 5.15, 5.16, 5.17, 5.18.

Regarding light curves, they are highly variable. Sector 11 drops its brightness while Sector 65 increases it. This is unusual but possible in a star where the inner disc rapidly dissipates (Labadie-Bartz et al., 2022).

Regarding spectra, 11 of 21 coincide with our TESS observations, during Sector 11 (2), 38 (2) 64 (3) and 65 (4). The Hα emission line presented strong emissions in 2019 that later diminished, implying the disc did not disappear.

The changes observed in the emission of the Hα line coincide with the variations of the light curves. During Sector 11, the spectrum of 20 May 2019 has the highest intensity one month before seen in the light. The same happens during Sector 65, where the spectra and the starting of an outburst coincide, and a double peak appears in the Hα emission.

We propose that if a change is observed in the light curve, it is likely to influence the spectroscopic features. In this case, however, the process occurs in reverse, where changes in spectroscopic features manifest over approximately five days.

If the high intensity observed in the emission line originates from an outburst, the reaction is not instantaneous. For such a delayed response, the circumstellar disc must be significantly large, affecting the propagation of the outburst's influence. The TESS photometry varies dramatically, which can lead to apparent changes in the Hα EW. This suggests that the discrepancies between the spectroscopic and photometric variations may be primarily due to the influence of the varying continuum on the EW measurements. Stellar winds also play a significant role, as some Be stars, such as Achernar, display enhanced polar winds. These winds can impact the line profiles by adding complexity to the observed variability.

Furthermore, the variability in the V/R ratio is particularly notable. At the peak of the emission line, a periodic change over approximately five days has been detected, suggesting that these dynamic processes are more likely associated with the inner disc, where shorter timescales prevail, rather than the outer disc, which would be expected to vary on much longer timescales.

Regarding the periodograms, we found that all of them present stochastic low-frequency noise, which dominated the entire spectrum making it difficult to identify signals, an uncommon feature in low inclination angle stars. Above the low-frequency level, we found 0.87 d^{-1}, 1.80 d^{-1} and 3.5 d^{-1}.Labadie-Bartz et al. (2022) found the same frequency groups.

Nazé et al. (2020b) searched for variability in several datasets, including TESS; The Hipparcos data suggest recurrent bursts with a time scale of 300 days, which is consistent with the strong long-term variations observed in the TESS light curves; notable in this work observations of Sectors 11 - 65.

We did not find any high-frequency signal, coinciding with the study of γ Cas stars by Nazé et al. (2020b) where HD 120991 shows significant variability at low frequencies ($f < 5$ d^{-1}), but no significant signals are detected at high frequencies.

6.5 HD 174237

HD 174237 (CX Draconis) is an interacting Be binary located in the constellation of Draco. The system consists of a B3V primary component and an F5III secondary, which fills its Roche lobe. The orbit was determined for both components (Horn et al., 1992; Simon, 1996). HD 174237 has long-term fluctuations of its brightness found by Koubskỳ et al. (1980).

This star stands out within our sample because it is not a classical Be star, nor does it fit the γ Cas classification. Instead, it is an interacting binary system consisting of a B-type primary star and an accretion disk (as previously stated) formed through mass transfer rather than rapid rotation. This distinction is crucial because, while classical Be stars exhibit disks generated by their own decretion, CX Dra's disk originates from binary interactions, fundamentally altering

its evolutionary context and observational properties.

This is the star with the most spectra in the group. It has 99 spectra downloaded from the BeSS, 57 of which coincide with TESS observations. The spectra are characterised by a low intensity of Hα, a subtle V/R in some Sectors, a "shell" profile and abrupt changes in the line (absorption to emission and vice versa).

In some Sectors, such as Sectors 40, 41 and 55, we can see rapid variations in the emission and shape of Hα. During Sector 40 we can appreciate the transition from absorption to emission within 8 days. In Sector 55, from July 2022 to August 2022 the same behaviour is spotted. However, we can not say if there were more changes in between since we have a one-month gap during observations.

The majority of Hα lines are shallow in intensity, with wide wings. They present variations in a time scale of days. During the 70s, light variations on a time scale of 7 to 12 days and the Hα cyclic variations with a characteristic time scale of 5 to 7 days were present. The fact that the period of the binary $P = 6.696$ days and Hα variations were on the same time scale led to the conclusion that HD 174237 was an interacting binary (Koubsky, 1978).

In 2000, Richards et al. (2000) compiled a collection of multiple spectra at different wavelengths. They focused on the lines Hα HeI λ6678, Si II λ6347 and Hβ. The observations of Hα were composed of two components. They suggest that the origin of this emission is multiple, proposing a gas stream, an accretion disc and a partial ring structure (annulus).

Models indicate that the main source of the Hα emission is located mid-way between the two stars, with other emission lines originating from an accretion disc orbiting the primary circumstellar environment changing in cycles lasting hundreds of days (Richards et al., 2000).

Accompanying the rapid variations in Hα is the TESS photometry. A total of 13 sectors were obtained. During these observations, the light curve of HD 174237 undergoes flux changes, increases and decreases in flux with no apparent periodicity. Outbursts (no associated frequencies) or a slow perturbation of the disc caused by the binary may be the possible source of these variations. From Sector 41 onwards, the normalized light curve goes from showing large variations in flux to being centred around 1, since then the ellipsoidal variations are more evident. At the same time as this occurs, the Hα is in absorption.

No primary frequency or group of frequencies was correctly identified above 1 d^{-1} in any Sector (Tables 5.5, 5.6, 5.7, and 5.8). All the periodograms are full of low frequencies. The most repeated signal during all sectors is around 0.30 d^{-1} (3.33 days), which corresponds to approximately half the period of the binary (6.6 days). It is not possible to distinguish clearly whether the other frequencies are of stellar or circumstellar origins, such as the stochastic low frequency, instrumental origin, or noise.

HD 174237 is a complex binary system, showing high variations in its Hα spectrum and light curve. The disc around the primary star is precessing, and all the highly variable observations are due to the secondary perturbation of the disc. Studies of this star have been scarce in recent years. Most of the investigations were conducted before the year 2000. Most of them focused on the binarity of the star. A greater emphasis on this binary system could offer us a glimpse of the ongoing mass transfer instants that would give rise to already fairly well-met Be+stripped core stars (or possible γ Cas analogues).

6.6 ζ Tauri

ζ Tauri is one of the brightest Be stars. It is a spectroscopic binary (B4IIIpe) with a period of 133 days (Ruždjak et al., 2009). We note this period was not found during this study because it covers a much longer period than the observations. The secondary component has not yet been observed. It has a $v \sin i = 310$ km s^{-1}, and an orbital inclination plane between $60^\circ < i_{orb} < 90^\circ$ obtained from radial velocities curves (Floquet et al., 1989). Recently ζ Tauri has been promoted to the γ Cas type stars due to its X-ray emissions (Nazé et al., 2022b); the emission is composed of a soft and bright hard component. The exact origin of this X-ray emission remains debatable, with some models suggesting it could arise from interactions between the star and its disc or disc winds.

Although the secondary is hard to observe directly, it has been studied. For example, Jarad (1987) assuming a $i_{orb} = 70^\circ$ obtained that the binary system has a separation of 254 ± 20 R$_\odot$ and a Roche radius for the primary star of 144 ± 12 R$_\odot$. With this inference, it is possible to say that the secondary component is outside the limits of the tidal forces of the primary component, following several models, e.g., Ruždjak et al. (2009)

In Ruždjak et al. (2009) the authors mentioned that Abt & Cardona (1984) and Floquet et al. (1989) found that ζ Tauri consist of a primary component of 11 M$_\odot$ and a secondary of 1.3 M$_\odot$. Ruždjak et al. (2009) also states that during 1981 Pavlovski & Bozic (1982) and Bozic & Pavlovski (1988) carried observations of ζ Tauri at the Hvar Observatory, and it classified the light variability as long-term changes, and 0.8 days (or 1.6 days) rapid variations with periods and amplitudes varying in time.

ζ Tauri presents V/R cyclic variations with a period of ~ 1429 days (Ruždjak et al., 2009; Štefl et al., 2009). Some studies suggest that these variations could be explained by the global one-armed oscillation model Okazaki (1997), manifested in density waves in the disc.

Schaefer et al. (2010) adds that the companion of ζ Tauri is several magnitudes fainter than the primary. In Hutter et al. (2021), the magnitude difference (visual) between the primary and

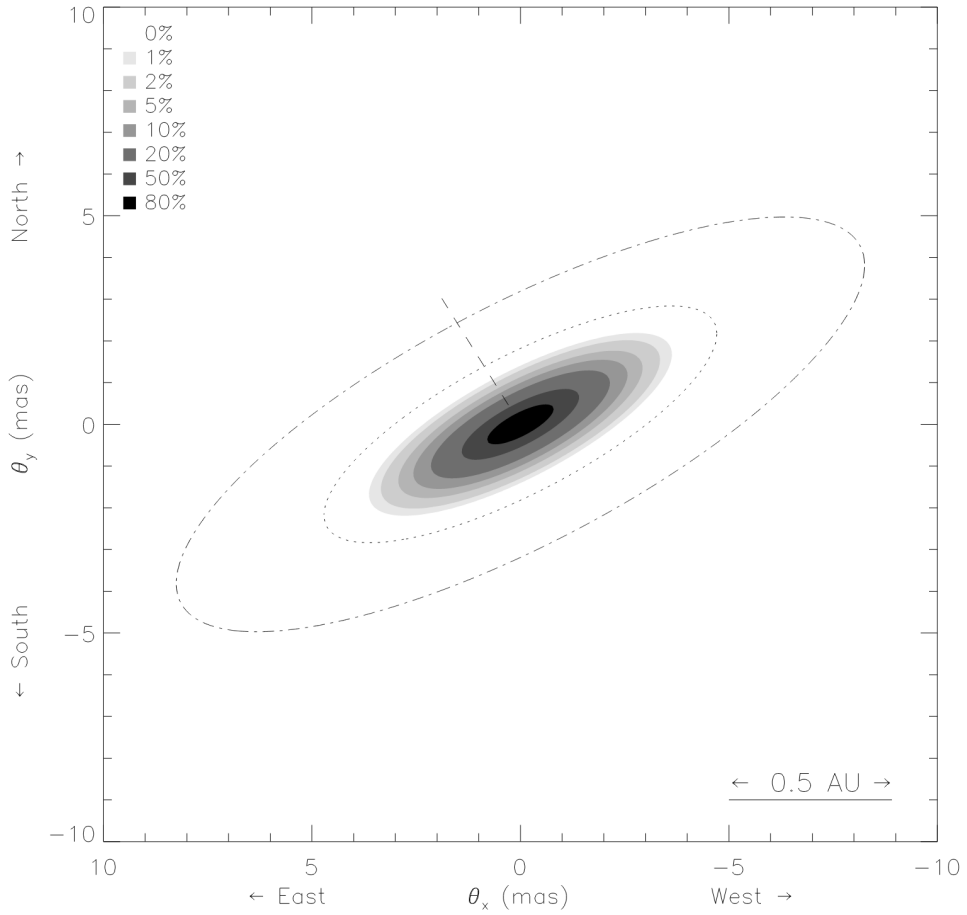

Figure 6.2: Schematic of the disc of ζ Tauri from the best-fit elliptical Gaussian model (taken from Tycner et al. (2004)). The dotted line represents the Roche radius, while the dashed line represents the orbit of the companion (in the outermost part).

secondary components is clarified. Townsend et al. (2004) and Landolt-Bornstein (1982) predict an absolute visual magnitude of $M_V \sim -3.1$ (for the primary) and $M_V \sim +5.0$ (for the secondary with a spectral type of G5) respectively, resulting in a magnitude difference of $\Delta m \sim 8$. Klement et al. (2022) suggests that although there are no confirmed main sequence companions to Be stars, some of these stars, such as ζ Tauri, may have a late-type main sequence companion, putting the hypothesis that Be stars come from binary systems at a crossroads.

Regarding the light curves, TESS observed this star during Sectors 43, 44, and 45, showing that the shape and contour of the light curve are not constant. There are intervals where the brightness oscillates sinusoidally abruptly, with a sudden change from one state to the other.

Its periodogram is a typical amplitude spectrum of a Be star, showing frequency groups. Here three frequency groups are visible around 0.95 d^{-1}, 1.01 d^{-1} and 2.26 d^{-1}. No high-

frequencies (> 10 d^{-1}) were found significant. These results are in agreement with the previous observations of Pavlovski & Bozic (1982) and Bozic & Pavlovski (1988), and a more recent study of X-ray in ζ Tauri (Nazé et al., 2024).

Concerning the frequencies, their amplitudes as mentioned in Pavlovski & Bozic (1982) and Bozic & Pavlovski (1988) change in time, as noted in Figures 5.32, 5.33, and 5.34. Observing the periodogram's behaviour, we note that the ~ 0.95 d^{-1} frequency group is related to the abrupt change in amplitude, as can be seen decreasing its amplitude and throughout the TESS observations its disappearance. Although Nazé et al. (2024) also notes and emphasizes these light curve features, they still do not explain their origin. All the frequency groups are located in the g-mode pulsation (0.5 d$^{-1} < f < 5$ d^{-1}, see Labadie-Bartz et al. (2022)) Subtle photometric drops —potentially linked to outbursts, since this is a shell star— can be seen in the middle of sector 43 and the beginning of sector 44, suggesting a possible connection to mass loss, though the effect remains modest. The abrupt and fast changes in amplitude in the light curves are not an overdensity in the disc since these start to be seen in Sector 45 when the light curve looks 'normal', so we cannot conclude their origin.

Regarding the BeSS data, we have 11 spectra, 7 of which fall within the light curves observation time (one in Sector 44 and six in Sector 45). The spectra show a typical "shell" shape characteristic of Be stars seen edge-on. The Hα emission in ζ Tauri passes through a cyclic variation of V/R of 1429 days. We can observe the profile slightly changing during our observation data; it starts with a small shell profile on 2021-10-28 and increases its absorption depth the following month, reaching its deepest on 2021-12-20. Also, during December 2021, a slight V/R < 1 is starting to appear.

The variation in the absorption depth is produced by density waves along the disc. Klement et al. (2022) state that there are two scenarios for "shell" absortions originating in 60 Cyg, similar to ζ Tau. The first case (the disc is edge-on, but it does not seem like it) is similar to the ζ Tau scenario. In this, the disc has density instabilities that are visible in the Hα line through the changes in depth of the absorption part of the line ("shell" line). When the high-density regions pass in front of the observer, Hα increases its EW and vice versa. This is supported by the global disc oscillation model, which applied to ζ Tauri perfectly explains observation in Hα for this star (Ruždjak et al., 2009; Carciofi et al., 2009; Štefl et al., 2009; Tycner et al., 2004). The same occurs for the V/R variation, which is not phase-locked with the companion (Štefl et al., 2009).

CHAPTER 7

Conclusions

This study conducted a photometric and spectroscopic analysis of Be stars, focusing on the relationship between non-radial pulsations (NRPs) and the formation and variability of circumstellar disks. NRPs are believed to play a significant role in mass ejection through outbursts, influencing disc formation and modulating variability in emission lines such as Hα, as well as photometric behaviour. The primary objective of this study was to establish correlations between NRPs and disc formation using simultaneous data from TESS photometry and BeSS spectroscopy, aiming to enlighten the connection between stellar pulsations and disc behaviour.

A total of 135 Be stars were analyzed. Photometric data were obtained from the TESS space telescope, while spectroscopic data were sourced from the BeSS database. The spectroscopic data were carefully selected to align with the observation dates of each TESS sector, ensuring simultaneous observations of Hα emission lines and light curves. This synchronization allowed for the correlation of variability observed in the light curves with changes in the spectra. From the 135 stars, approximately 220 photometric observations and 560 Hα spectra were compiled.

The stellar sample was catalogued in a table, including stellar parameters such as effective temperature (T_{eff}), surface gravity ($\log g$), and projected rotational velocity ($v \sin i$) and astrometric parameters like parallax and position were also documented following a thorough literature review. Additionally, critical rotational velocities and associated frequencies were calculated for each star.

Light curves were extracted and processed using the Python package `lightkurve`, developed for TESS data analysis. The pipeline involved downloading raw pixel data, performing

aperture photometry to extract the light curves, and subsequently normalizing and cleaning the data by removing outliers and corrupted points. Spectroscopic data were normalized and corrected for barycentric velocity using a code provided by Yanina López from the Universidad de Valparaíso, Chile.

The analysis began with an examination of each light curve and its frequency content using the Lomb-Scargle method. A periodogram was generated for each TESS sector, identifying the corresponding frequencies. Comprehensive graphical analyses were performed for all 135 stars, including plots of cleaned light curves, comparisons of spectra, associations of spectra with light curves, and frequency spectra (periodograms).

In this study, we analyzed a subsample of six Be stars, f01 Cyg, HD 45314, HD 110432, HD 120991, HD 174237, and ζ Tauri. These stars were chosen based on their prominent Be star characteristics, such as well-defined circumstellar disks, significant variations in light curves and spectra, and the availability of a substantial number of spectra associated with each light curve. Three of these six stars are also classified as γ Cassiopeiae (or γ Cas) analogues due to their X-ray emission.

These selected stars, predominantly early-type Be stars (B0-B2), exhibit distinct frequency groupings indicative of non-radial g-mode pulsations. Notably, HD 110432 demonstrates a single p-mode pulsation, while the others display more complex pulsational behaviour. HD 45314 is exceptional primarily because, as an Oe star, it represents an earlier spectral type than the typical Be stars in the sample.

Among these, we successfully recovered the orbital periods of the binary systems associated with f01 Cyg and HD 174237. We concluded that all Be stars in this sample exhibit g-mode pulsations, with frequencies ranging between 0.8 and 4 d^{-1}, except for HD 110432, which also presents a single p-mode pulsation. For f01 Cyg, we estimated the disc's radial extent to be $\sim 15 R_{\odot}$, concluding that it resides well within the Roche limit ($\sim 40 R_{\odot}$). Additionally, for HD 120991, we proposed that the observed high intensity in the emission line originates from an outburst. A periodic variation in the V/R ratio over approximately five days was detected at the peak of the emission line. For HD 110432, we observed amplitude changes in the detected frequencies, which we interpret as the initial signatures of a future outburst, consistent with previous studies.

In our investigation of this subsample, no clear correlation was found between non-radial pulsation and the variations observed in the Hα emission line. Future work will require high-resolution spectroscopic observations with increased cadence to capture rapid variations in the Hα emission line. This research contributes to a broader effort to reconstruct the short-term variability patterns of Be stars by combining photometric and spectroscopic data, providing new

insights into disc formation and dissipation processes.

APPENDIX A

LCExtrac.py

- `query_lc`
  - `ID`: ID of the source to query.
  - `method`: Method used to query the lightcurve. There are three methods: `'simple'` which uses the `search_lightcurve` method to find available observations (Default), `'tpf'` uses the `search_targetpixelfile` method and finally, `'tesscut'` uses the `search_tesscut` method. The `'simple'` method was used for all stars.
  - `mission`: `'Kepler'`, `'K2'` (Kepler 2nd mission), or `'TESS'`.
  - `author`: Author of the data product (`'Kepler'`, `'K2'`, and `'SPOC'`). `'SPOC'` was used for all stars.
  - `cadence`: Exposure time. Could be: `'short'` (1 min), `'long'` (10 min), `'fast'` (20 sec). Long exposure time was used, i.e., `'long'`.
  - `sec`: TESS Sector number. The input sectors depended of the target.
  - `cutout_size`: Side length of cutout in pixels. None was used as default
  - `quarter`: Kepler Quarter. None was used as default
  - `campaign`: K2 Campaign. None was used as default
- `change_aperture`
  - `tpf`: The input TargetPixelFile from TESS

  - `ini_mask`: Initial mask for the aperture:
    1. `'pipeline'` takes the default pipeline mask (Default).
    2. `'new'` takes the `mask_new` if created before.
    3. `'manual'` input array of values for the initial mask.
  - `method`: Method used to select the aperture mask.
    1. `'threshold'` uses a threshold value to cut the pixels. (Default)
    2. `'basic'` manually change the True/False values of the mask.
  - `star_cut`: If `'threshold'` method is selected, input cut value to select the star. Default was 8.
  - `sky_cut`: If 'threshold' method is selected, input cut value to select the background. Default was 0.01
  - `ref_pixel`: Pixel column and row (`col, row`) coordinate closest to the desired region.

- `contaminants`
  - `tpf`: The input TargetPixelFile from TESS
  - `mask`: Mask created before with the `change_aperture` function
    1. `'pipeline'` takes the default pipeline mask. (Default)
    2. `'new'` takes the new mask if created before.
    3. `None` if no mask is used.
  - `dmag`: Gaia G magnitude difference used to limit the contaminants. The default was 5.
  - `dist_cont`: Maximum distance in arsecs of the contaminant sources to be exported to a `txt` file.

- `tpf_to_lc`
  - `tpf`: The input TargetPixelFile from TESS
  - `mask`: Mask for the aperture. Input values are the same as the previous function.
  - `flux_err_cut`: Threshold value for the flux error to remove bad data. The default was 0.

- `detrended_tpf_to_lc`

  - `lc`: Input lightcurve from TESS created with the previous function
  - `tpf`: Input TargetPixelFile from TESS
  - `mask_background`: Mask used to consider the background. The mask created with `change_aperture` was used.
  - `npcs`: Define the initial number of principal components to inspect. The default was 5.

- `sig_clip_lc`
  - `lc`: The input lightcurve object from either TESS or Kepler.
  - `sigma`: Sigma clipping factor applied to the lightcurve. The standard deviation from the light curve was used.

Bibliography

Abt H. A., Cardona O., 1984, Astrophysical Journal, Part 1 (ISSN 0004-637X), vol. 285, Oct. 1, 1984, p. 190-194., 285, 190

Abt H. A., Levato H., Grosso M., 2002, The Astrophysical Journal, 573, 359

Apparao K. M., Tarafdar S., 1989, Astrophysics and space science, 153, 61

Arcos C., Jones C., Sigut T., Kanaan S., Curé M., 2017, The Astrophysical Journal, 842, 48

Arcos C., Kanaan S., Chávez J., Vanzi L., Araya I., Curé M., 2018, Monthly Notices of the Royal Astronomical Society, 474, 5287

Arias M. L., Zorec J., Cidale L., Ringuelet A. E., Morrell N. I., Ballereau D., 2006, Astronomy & Astrophysics, 460, 821

Baade D., 1982a, Astronomy and Astrophysics, vol. 105, no. 1, Jan. 1982, p. 65-75., 105, 65

Baade D., 1982b, Astronomy and Astrophysics, vol. 110, no. 2, June 1982, p. L15-L17., 110, L15

Baade D., Labadie-Bartz J., Rivinius T., Carciofi A., 2023, Astronomy & Astrophysics, 678, A47

Balona L., 2012, in , Stellar Pulsations: Impact of New Instrumentation and New Insights. Springer, pp 247–252

Barker P. K., 1982, Astrophysical Journal Supplement Series, vol. 49, May 1982, p. 89-109. Research supported by the Natural Sciences and Engineering Research Council of Canada, 49, 89

Barrera L., Mennickent R., Vogt N., 1991, Astrophysics and space science, 185, 79

Bjorkman J., Cassinelli J., 1993, Astrophysical Journal, Part 1 (ISSN 0004-637X), vol. 409, no. 1, p. 429-449., 409, 429

Bozic H., Pavlovski K., 1988, Hvar Observatory Bulletin, Volume 12, Issue 1, p. 15, 12, 15

Burssens S., et al., 2020, Astronomy & Astrophysics, 639, A81

Carciofi A. C., 2010, Proceedings of the International Astronomical Union, 6, 325

Carciofi A., Bjorkman J. E., 2008, The Astrophysical Journal, 684, 1374

Carciofi A. C., Okazaki A., Le Bouquin J.-B., Štefl S., Rivinius T., Baade D., Bjorkman J., Hummel C., 2009, Astronomy & Astrophysics, 504, 915

Castor J. I., Abbott D. C., Klein R. I., 1975, Astrophysical Journal, vol. 195, Jan. 1, 1975, pt. 1, p. 157-174., 195, 157

Chauville J., Zorec J., Ballereau D., Morrell N., Cidale L., Garcia A., 2001, Astronomy & Astrophysics, 378, 861

Dachs J., Hummel W., Hanuschik R., 1992, Astronomy and Astrophysics Supplement Series, 95, 437

Delaa O., et al., 2011, Astronomy & Astrophysics, 529, A87

Doazan V., Briot D., Bourdonneau B., 1975, Astronomy and Astrophysics, Vol. 42, p. 161-162, 42, 161

Ducati J., 2002, Catalogue of Stellar Photometry in Johnsons 11-Colour System, CDS/ADC Collection of Electronic Catalogues

Eggleton P. P., 1983, Astrophysical Journal, Part 1 (ISSN 0004-637X), vol. 268, May 1, 1983, p. 368, 369., 268, 368

Floquet M., Hubert A., Maillard J., Chauville J., Chatzichristou H., 1989, Astronomy and Astrophysics (ISSN 0004-6361), vol. 214, no. 1-2, April 1989, p. 295-303., 214, 295

Friend D. B., Abbott D. C., 1986, Astrophysical Journal, Part 1 (ISSN 0004-637X), vol. 311, Dec. 15, 1986, p. 701-707., 311, 701

Frémat Y., Zorec J., Hubert A.-M., Floquet M., 2005, Astronomy & Astrophysics, 440, 305

Gies D., Josephs T., Wallace D., McSwain M., Huang W., 2000, NOAO Proposal, p. 234

Glebocki R., Gnacinski P., 2005, VizieR online data catalog, pp III–244

Golden-Marx J. B., Oey M., Lamb J., Graus A. S., White A. S., 2016, The Astrophysical Journal, 819, 55

Grady C., Bjorkman K., Snow T., 1987, Astrophysical Journal, Part 1 (ISSN 0004-637X), vol. 320, Sept. 1, 1987, p. 376-397., 320, 376

Grady C., Bjorkman K., Snow T., Sonneborn G., Shore S. N., Barker P. K., 1989, Astrophysical Journal, Part 1 (ISSN 0004-637X), vol. 339, April 1, 1989, p. 403-419., 339, 403

Grunhut J., et al., 2022, Monthly Notices of the Royal Astronomical Society, 512, 1944

Guinan E. F., Koch R. H., Plavec M. J., 1984, Astrophysical Journal, Part 1 (ISSN 0004-637X), vol. 282, July 15, 1984, p. 667-674., 282, 667

Harmanec P., 1984, Astronomical Institutes of Czechoslovakia, Bulletin (ISSN 0004-6248), vol. 35, no. 3, 1984, p. 164-179., 35, 164

Harmanec P., et al., 2002, Astronomy & astrophysics, 387, 580

Horn J., Hubert A., Hubert H., Koubsky P., Bailloux N., 1992, Astronomy and Astrophysics (ISSN 0004-6361), vol. 259, no. 1, p. L5-L8., 259, L5

Huang S.-S., 1972, Astrophysical Journal, vol. 171, p. 549, 171, 549

Huat A.-L., et al., 2009, Astronomy & Astrophysics, 506, 95

Hummel W., 1994, Astronomy and Astrophysics (ISSN 0004-6361), vol. 289, no. 2, p. 458-468, 289, 458

Hummel W., Dachs J., 1992, Astronomy and Astrophysics (ISSN 0004-6361), vol. 262, no. 2, p. L17-L20., 262, L17

Hutter D., Tycner C., Zavala R., Benson J., Hummel C., Zirm H., 2021, The Astrophysical Journal Supplement Series, 257, 69

Jagadeesh M. K., Mathew B., Paul K., Banerjee G., Subramaniam A., Arun R., 2021, Journal of Astrophysics and Astronomy, 42, 109

Jarad M., 1987, Astrophysics and space science, 139, 83

Jaschek M., Egret D., 1982, in Symposium-International Astronomical Union. pp 261–263

Juza K., Harmanec P., Hill G., Tarasov A., Matthews J., Tuominen I., Yang S., 1991, Astronomical Institutes of Czechoslovakia, Bulletin (ISSN 0004-6248), vol. 42, Feb. 1991, p. 39-61., 42, 39

Kervella P., de Souza A. D., 2006, Astronomy & Astrophysics, 453, 1059

Kervella P., Arenou F., Mignard F., Thévenin F., 2019, Astronomy & Astrophysics, 623, A72

Kervella P., Arenou F., Thévenin F., 2022, Astronomy & Astrophysics, 657, A7

Klement R., et al., 2017, Astronomy & Astrophysics, 601, A74

Klement R., et al., 2019, The Astrophysical Journal, 885, 147

Klement R., et al., 2022, The Astrophysical Journal, 926, 213

Koubsky P., 1978, Astronomical Institutes of Czechoslovakia, Bulletin, vol. 29, no. 5, 1978, p. 288-298., 29, 288

Koubskỳ P., Harmanec P., Horn J., Jerzykiewicz M., Papousek S., Pavlovski K., Zdárskỳ F., et al., 1980, Astronomical Institutes of Czechoslovakia, Bulletin, vol. 31, no. 2, 1980, p. 75-84., 31, 75

Koubskỳ P., et al., 2000, Astronomy and Astrophysics, v. 356, p. 913-928 (2000), 356, 913

Koubskỳ P., et al., 2010, Astronomy & astrophysics, 517, A24

Labadie-Bartz J., Baade D., Carciofi A. C., Rubio A., Rivinius T., Borre C. C., Martayan C., Siverd R. J., 2021, Monthly Notices of the Royal Astronomical Society, 502, 242

Labadie-Bartz J., Carciofi A. C., de Amorim T. H., Rubio A., Figueiredo A. L., dos Santos P. T., Thomson-Paressant K., 2022, The Astronomical Journal, 163, 226

Lailey B., Sigut T., 2024, Monthly Notices of the Royal Astronomical Society, 527, 2585

Landolt-Bornstein N. D., 1982, Functional Relationship in Science and Technology, edited by K. Hellwege

Lanthermann C., et al., 2023, Astronomy & Astrophysics, 672, A6

Lee U., Saio H., Osaki Y., 1991, Monthly Notices of the Royal Astronomical Society, 250, 432

Lesh J. R., 1968, Astrophysical Journal Supplement, vol. 17, p. 371 (1968), 17, 371

Levenhagen R. S., Leister N. V., 2006, Monthly Notices of the Royal Astronomical Society, 371, 252

Linder N., Rauw G., Martins F., Sana H., De Becker M., Gosset E., 2008, Astronomy & Astrophysics, 489, 713

Lomb N. R., 1976, Astrophysics and space science, 39, 447

Maintz M., Rivinius T., Stahl O., Stefl S., Appenzeller I., 2005, Publications of the Astronomical Institute of the Czechoslovak Academy of Sciences, 93, 21

Marr K., Jones C., Halonen R., 2018, The Astrophysical Journal, 852, 103

Meilland A., et al., 2007, Astronomy & Astrophysics, 464, 59

Miroshnichenko A. S., et al., 2023, Galaxies, 11, 83

Nazé Y., 2009, Astronomy & Astrophysics, 506, 1055

Naze Y., Robrade J., 2023, arXiv preprint arXiv:2307.13308

Nazé Y., Pigulski A., Rauw G., Smith M. A., 2020a, Monthly Notices of the Royal Astronomical Society, 494, 958

Nazé Y., Rauw G., Pigulski A., 2020b, Monthly Notices of the Royal Astronomical Society, 498, 3171

Nazé Y., Rauw G., Czesla S., Smith M. A., Robrade J., 2022a, Monthly Notices of the Royal Astronomical Society, 510, 2286

Nazé Y., Rauw G., Bohlsen T., Heathcote B., Mc Gee P., Cacella P., Motch C., 2022b, Monthly Notices of the Royal Astronomical Society, 512, 1648

Nazé Y., Motch C., Rauw G., Smith M. A., Robrade J., 2024, Astronomy & Astrophysics, 688, A181

Neiner C., de Batz B., Cochard F., Floquet M., Mekkas A., Desnoux V., 2011, The Astronomical Journal, 142, 149

Okazaki A. T., 1997, A&A, 318, 548

Osaki Y., 1971, Publications of the Astronomical Society of Japan, vol. 23, p. 485 (1971)., 23, 485

Oudmaijer R. D., Parr A. M., 2010, Monthly Notices of the Royal Astronomical Society, 405, 2439

Owocki S., Cranmer S., Gayley K., 1996, The Astrophysical Journal, 472, L115

Pavlovski K., Bozic H., 1982, Hvar Observatory Bulletin, Volume 6, Issue 1, p. 45, 6, 45

Peters G. J., Pewett T. D., Gies D. R., Touhami Y. N., Grundstrom E. D., 2013, The Astrophysical Journal, 765, 2

Plaskett J., 1922, Monthly Notices of the Royal Astronomical Society, Vol. 82, p. 447, 82, 447

Quirrenbach A., et al., 1997, The Astrophysical Journal, 479, 477

Rauw G., Nazé Y., Spano M., Morel T., et al., 2013, Astronomy & Astrophysics, 555, L9

Richards M. T., Kobuskỳ P., Šimon V., Peters G. J., Hirata R., Škoda P., Masuda S., 2000, The Astrophysical Journal, 531, 1003

Ricker G. R., et al., 2015, Journal of Astronomical Telescopes, Instruments, and Systems, 1, 014003

Rivinius T., Baade D., Štefl S., Townsend R., Stahl O., Wolf B., Kaufer A., 2001, Astronomy & Astrophysics, 369, 1058

Rivinius T., Baade D., Štefl S., 2003, Astronomy & Astrophysics, 411, 229

Rivinius T., Carciofi A. C., Martayan C., 2013, The Astronomy and Astrophysics Review, 21, 1

Ruždjak D., et al., 2009, Astronomy & astrophysics, 506, 1319

Samus' N., Kazarovets E., Durlevich O., Kireeva N., Pastukhova E., 2017, Astronomy Reports, 61, 80

Scargle J. D., 1982, Astrophysical Journal, Part 1, vol. 263, Dec. 15, 1982, p. 835-853., 263, 835

Schaefer G., et al., 2010, The Astronomical Journal, 140, 1838

Secchi A., 1866, Astronomische Nachrichten, volume 68, p. 63, 68, 63

Semaan T., Hubert A., Zorec J., Gutiérrez-Soto J., Frémat Y., Martayan C., Fabregat J., Eggenberger P., 2018, Astronomy & Astrophysics, 613, A70

Sigut T., 2018, in Workshop on Astrophysical Opacities. p. 213

Sigut T., Mahjour A., Tycner C., 2020, The Astrophysical Journal, 894, 18

Silaj J., Jones C., Tycner C., Sigut T., Smith A., 2010, The Astrophysical Journal Supplement Series, 187, 228

Silaj J., Jones C., Sigut T., Tycner C., 2014, The Astrophysical Journal, 795, 82

Simon V., 1996, Astronomy and Astrophysics, v. 308, p. 799-808, 308, 799

Slettebak A., 1982, Astrophysical Journal Supplement Series, vol. 50, Sept. 1982, p. 55-83., 50, 55

Slettebak A., Collins G., Boyce P., White N. M., Parkinson T., 1975, Astrophysical Journal Supplement Series (Supplement no. 281), vol. 29, May 1975, p. 137-159. Research supported by the Ohio State University, 29, 137

Smith M. A., Balona L., 2006, The Astrophysical Journal, 640, 491

Smith M. A., de Oliveira R. L., Motch C., 2012, The Astrophysical Journal, 755, 64

Stacey E., 2022, Master's thesis, Royal Military College of Canada

Stee P., et al., 2013, Astronomy & Astrophysics, 550, A65

Štefl S., Hummel W., Rivinius T., 2000, Astron. Astrophys, 358, 208

Štefl S., et al., 2009, Astronomy & Astrophysics, 504, 929

Struve O., 1931, Astrophysical Journal, vol. 73, p. 94, 73, 94

TESS Website 2023, TESS Observations, `https://tess.mit.edu/observations/`

Torrejón J., Orr A., 2001, Astronomy & Astrophysics, 377, 148

Torrejón J. M., Schulz N. S., Nowak M. A., 2012, The Astrophysical Journal, 750, 75

Touhami Y., et al., 2010, Publications of the Astronomical Society of the Pacific, 122, 379

Touhami Y., Gies D., Schaefer G., 2011, The Astrophysical Journal, 729, 17

Touhami Y., et al., 2013, The Astrophysical Journal, 768, 128

Townsend R. H., Owocki S. P., Howarth I. D., 2004, Monthly Notices of the Royal Astronomical Society, 350, 189

Tycner C., et al., 2004, The Astronomical Journal, 127, 1194

Tycner C., et al., 2005, The Astrophysical Journal, 624, 359

Tycner C., et al., 2006, The Astronomical Journal, 131, 2710

Tycner C., Jones C., Sigut T., Schmitt H., Benson J., Hutter D., Zavala R., 2008, The Astrophysical Journal, 689, 461

VanderPlas J. T., 2018, The Astrophysical Journal Supplement Series, 236, 16

Vieira R. G., Carciofi A. C., Bjorkman J. E., Rivinius T., Baade D., Rímulo L. R., 2017, Monthly Notices of the Royal Astronomical Society, 464, 3071

Yudin R., 2001, Astronomy & Astrophysics, 368, 912

de Oliveira R. L., Motch C., Smith M. A., Negueruela I., Torrejon J. M., 2007a, Astronomy & Astrophysics, 474, 983

de Oliveira R. L., Motch C., Smith M. A., Negueruela I., Torrejón J. M., 2007b, Astronomy & Astrophysics, 474, 983